RNG140 (caprin2)-mediated translational regulation implicated in mouse eye lens differentiation

Nakazawa, Kaori

Department of Basic Biology

School of Life Science

The Graduate University for Advanced Studies,

SOKENDAI

Laboratory of Neuronal Cell Biology

National Institute for Basic Biology

Contents

Introduction

Gene expression is an essential process in development, cell differentiation, and other diverse processes in organisms and is regulated in multiple steps. Although transcriptional control has received much attention, post-transcriptional steps such as mRNA splicing, polyadenylation, stabilization, transport, and translation are also important layers of gene expression control (Mata et al., 2005; Keene, 2007; Hieronymus & Silver, 2004; Teixeira & Lehmann, 2019; Tahmasebi et al., 2019). Apparently, RNA-binding proteins play a central role in the post-transcriptional gene regulation (Glisovic et al., 2008; Kishore et al., 2010).

RNA granule protein 140 (RNG140, also known as caprin2) is such an RNA binding protein that regulates cell differentiation and various functional processes. For example, RNG140 functions in embryonic development through facilitating canonical Wnt/β-catenin signaling (Ding et al., 2008). In erythroid cells, RNG140 expression increases during the cells shift from a proliferative state to a differentiated state (Aerbajinai et al., 2004). Indeed, RNG140 expression level negatively correlates with cell growth in Chinese hamster ovary (CHO) cells (Aerbajinai et al., 2004), confirming its role in inhibiting cell proliferation. In addition to the regulation of cell proliferation and differentiation, RNG140 is highly expressed in the brain and is involved in processes such as the formation and maintenance of dendrites and synapses (Shiina & Tokunaga, 2010) and the osmotic stress response in the hypothalamus (Konopacka et al., 2015).

Since RNG140 has two RNA-binding coiled-coil and RGG box domains (Fig. 1A) (Shiina & Tokunaga, 2010), its function may be attributed to the RNA-binding activity. For example, RNG140 has been reported to bind to arginine vasopressin (*AVP*) mRNA and stabilize the mRNA by increasing poly(A) tail length in response to osmotic stress in

the hypothalamus (Konopacka et al., 2015). Alternatively, RNG140 may function as a hub of protein interaction through a C-terminal C1q domain, which often undergoes trimerization (Tang et al., 2005): it interacts with low-density lipoprotein receptor-related protein 5/6 (LRP5/6) and Cpn1027 via the C1q domain and enhances phosphorylation of LRP5/6 to mediate Wnt/β-catenin signaling (Miao et al., 2014; Flores & Zhong, 2015).

Like many other developmental processes, gene expression during the eye lens development is highly controlled. In this context, transcriptional regulation has been studied well: transcription factors such as Pax6, Six3, and Sox2 drive the progression of lens development, and those including Pax6 directly regulate the transcription of the lens-specific proteins such as crystallins (Cvekl & Zhang, 2017; Cvekl & Ashery-Padan, 2014). In contrast, understanding of the post-transcriptional control during lens development is still limited (Cvekl & Zhang, 2017; Dash et al., 2016), except for the involvement of RNA-binding proteins as follows: Tudor domain containing 7 (TDRD7) deficiency in mice reduced the level of target transcripts such as the heat shock protein *Hspb1* mRNA and the crystallin *Crybb3* mRNA, and caused cataract and glaucoma (Lachke et al., 2011). In zebrafish, the loss of the eukaryotic translation initiation factor *eif3ha* gene reduced translation of crystallin *crygm2d7* mRNA and caused brain and eye development defects (Choudhuri et al., 2013). As a post-transcriptional gene regulator, RNG140 is one of such an example in lens development. During lens differentiation, RNG140 expression is increased by fibroblast growth factor (FGF) (Dash et al., 2015; Lorén et al, 2009). Indeed, RNG140 conditional knockout in mice caused lens compaction defects and features of Peters anomaly (Dash et al., 2015).

RNG140 has been shown to inhibit translation in rabbit reticulocyte lysates (Fig. 1B) (Shiina & Tokunaga, 2010). However, it is not known how RNG140 blocks translation

and how the translational regulation is relevant to the *in vivo* function of RNG140 such as lens differentiation. Here, I show that RNG140 represses translation in an mRNA-selective manner. Protein interaction and internal ribosome entry site (IRES)-based reporter assays suggested that RNG140 blocks eIF3 in translation initiation. Moreover, genome-wide ribosome profiling in RNG140-overexpressing CHO cells and RNG140 knockout mouse eyes indicated that RNG140-mediated translational repression is biased toward long mRNAs. Thus, short mRNAs including crystallin mRNAs, which are important for lens differentiation, escape RNG140-mediated translational repression. These results suggested that RNG140 shifts the translational balance of gene expression from a proliferative state to a differentiated state.

Material and methods

Ethics statement

All animal care and experiments were approved by the Institutional Animal Care and Use Committee of the National Institutes of Natural Sciences and performed in accordance with the guideline from the National Institutes of Natural Sciences.

Cell culture and transfection

CHO-K1 cells (RCB0285, RIKEN BRC, Tsukuba, Japan) were cultured in HAM's F-12 medium (FUJIFILM Wako Pure Chemical Corporation, Osaka, Japan) containing 5% fetal bovine serum (FBS). SRA 01/04 (RCB1591, RIKEN BRC) were cultured in low-glucose D-MEM medium (FUJIFILM Wako Pure Chemical Corporation) containing 20% FBS. Cells were placed at 37°C in a 5% CO_2 incubator. For transfection, cells were grown to approximately 90% confluence and transfected with plasmids using Lipofectamine 2000 (Thermo Fisher Scientific, Waltham, MA) in accordance with the manufacturer's protocol. Stable transfectants were selected in the presence of 1 mg/ml geneticin (Thermo Fisher Scientific) in the medium and then obtained by picking up fluorescent colonies with the use of a CKX41 microscope equipped with an epifluorescence module (Olympus, Tokyo, Japan).

Plasmid construction

Plasmids for the expression of RNG140 tagged with GFP and glutathione S-transferase (GST) were constructed previously (Shiina & Tokunaga, 2010). To construct a plasmid for the expression of RNG140 untagged with GFP, a portion of RNG140 CDS was amplified by PCR using primers 5′-CTGTTCTAGATTTTGACAAACCC-3′ and 5′-

GGGGGTACCTTAATCTTGATAAAGAAGATAGCCTGAAA-3′, which introduced a stop codon at the 3′ end of the RNG140 CDS. The fragment was cloned into the *Xba*I/*Kpn*I sites of the RNG140-GFP plasmid. To construct a control plasmid for the RNG140 expression plasmid, GFP CDS was deleted from pEGFP-N1 (Clontech, Mountain View, CA) with *Bsp120*I/*Not*I and the vector was self-ligated.

To construct plasmids for luciferase reporter assays, DNA fragments of EIF2S3 5′ UTR, HCV IRES, and CrPV IRES were inserted between T7 promoter and ORF of Renilla luciferase (hRluc) in psiCHECK2 vector (Promega, Madison, WI). Plasmids containing EIF2S3 5′ UTR and HCV IRES were constructed previously (Iwasaki et al., 2016). To construct the plasmid containing the CrPV IRES, the following sequence was inserted:

AAAGCAAAAATGTGATCTTGCTTGTAAATACAATTTTGAGAGGTTAATAAATT
ACAAGTAGTGCTATTTTTGTATTTAGGTTAGCTATTTAGCTTTACGTTCCAGGA
TGCCTAGTGGCAGCCCCACAATATCCAGGAAGCCCTCTCTGCGGTTTTTCAG
ATTAGGTAGTCGAAAAACCTAAGAAATTTACCTGCTACATTTCAAGATA.

To construct a plasmid for Cas9 mRNA preparation, hCas9 gene was excised with *Age*I/*EcoR*I from pX330 vector (Addgene, Watertown, MA). The fragment was inserted downstream of the SP6 promoter in the pSP64 vector (Promega) and used for *in vitro* transcription. To clone RNG140 guide RNA (gRNA), a pair of oligonucleotides targeting the *Rng140* gene (5′-TAGGGGAAGGTAGTGAAAAAACAG-3′ and 5′-AAACCTGTTTTTTCACTACCTTCC-3′) was annealed and inserted into the *Bsa*I site of the pDR274 vector (Addgene).

Ribopuromycilation assay

Ribopuromycilation assay was performed as previously described (Shiina, 2019). Briefly, cells were pulse labeled with 50 μg/ml puromycin in the medium containing 100 μg/ml cycloheximide for 10 min at 37°C and washed with phosphate-buffered saline (PBS; 137 mM NaCl, 8.1 mM Na_2HPO_4, 1.5 mM KH_2PO_4, and 2.7 mM KCl, pH 7.4) containing 100 μg/ml cycloheximide for 3 min on ice. The cells were permeabilized and fixed with 50 mM Tris-HCl (pH 7.5), 5 mM $MgCl_2$, 25 mM KCl, 100 μg/ml cycloheximide, 0.015% digitonin, and 3.7% formaldehyde for 5 min on ice. After post-fixation with 3.7% formaldehyde in PBS for 10 min at room temperature, the cells were immunofluorescent-stained with an anti-puromycin antibody (3RH11, KeraFAST Inc., Boston, MA) and cyanine 3-conjugated anti-mouse IgG (Jackson ImmunoResearch, West Grove, PA). Cycloheximide was included in the buffers to maintain the association of puromycin-labeled nascent polypeptides with ribosomes, which prevents the labeled polypeptides from being lost from the cells during the permeabilization process with digitonin and enables the detection of translation sites at the sub-cellular level.

To compare the fluorescence intensity of puromycin staining between GFP-expressing cells and RNG140-GFP-expressing cells, they were co-cultured on the same coverslips. GFP-expressing cells and RNG140-GFP-expressing cells were clearly distinguished by the predominant localization of GFP fluorescence in the nucleus and cytoplasm, respectively. Fluorescence images were acquired using an A1 confocal laser microscope equipped with a Ti-E inverted microscope (Nikon, Tokyo, Japan) with a PlanApo VC60× water objective. For transient transfectants, the average fluorescence intensity of GFP and puromycin staining in the whole cell area was measured using Fiji software. In the case of stable transfectants, because the cell morphology of each clone was different, total fluorescence intensity (mean fluorescence intensity × cell area) of

puromycin staining in the whole cell area was measured.

Western blotting SUnSET

Puromycin incorporation into nascent polypeptides was quantitatively analyzed by Western blotting SUnSET with modifications to the ribopuromycilation assay. Briefly, cells were pulse labeled with 20 μM puromycin in cycloheximide-free medium for 30 min at 37°C. Cells were washed with ice-cold PBS and lysed with 20 mM Tris-HCl, pH 7.5, 150 mM NaCl, 5 mM $MgCl_2$, and 1% Triton X-100. After centrifugation at 20,000 g for 10 min at 4°C, the supernatant was subjected to Western blotting with the anti-puromycin antibody (KeraFAST Inc.). The total band intensity of puromycin was normalized with tubulin band intensity in the same cell extract probed with anti-α-tubulin antibody (T9026, Sigma-Aldrich, St.Louis, MO). Quantification of band intensity was performed as previously described using a standard curve generated from a standard dilution series of cell extracts on the same membrane (Ohashi et al., 2013).

Sucrose density gradient centrifugation

Cells were incubated with 100 μg/ml cycloheximide in the medium for 15 min, washed with ice-cold PBS, and lysed with cell lysis buffer (20 mM Hepes-KOH pH 7.4, 15 mM $MgCl_2$, 200 mM KCl, 1% Triton X-100, 100 μg/ml cycloheximide, 2 mM DTT, 1 mg/ml heparin, 10 μg/ml leupeptin, 10 μg/ml pepstatin, and 1 mM PMSF). After centrifugation at 14,000 g for 5 min at 4°C, the supernatant was overlaid onto a 15–45% w/w linear sucrose density gradient in the cell lysis buffer lacking Triton X-100 and heparin, which had been prepared using a gradient gel-making device (ATTO, Tokyo, Japan), and then centrifuged at 100,000 g for 4 h at 4°C in an SW41Ti swing rotor

(Beckman Coulter, Brea, CA). In experiments without cycloheximide, the drug was removed during the procedures. In EDTA-adding experiments, 0.1 M EDTA was added to the cell lysis buffer and the sucrose density gradient, omitting cycloheximide. After centrifugation, cell lysates remaining on the top of the sucrose gradient were removed and then the sucrose gradient was fractionated into 22 fractions. RNA was isolated from each fraction using ISOGEN (Nippon Gene, Tokyo, Japan) and the absorbance was measured at 254 nm using NanoDrop (Thermo Fisher Scientific, Waltham, MA). Relative amount of RNA in each fraction was calculated so that the total amount of RNA in the 22 fractions was 1.00.

Ribosome pelleting through a sucrose cushion

Ribosome pellets were prepared as described previously (Liu & Qian, 2016). Briefly, cells were incubated with 100 μg/ml cycloheximide in the medium for 15 min, washed with ice-cold PBS, and then lysed with polysome lysis buffer (10 mM Hepes-KOH pH 7.4, 5 mM $MgCl_2$, 100 mM KCl, 2% Triton X-100, and 100 μg/ml cycloheximide). After centrifugation at 14,000 g for 10 min at 4°C, 300 μl lysate was overlaid onto 900 μl of a 1 M sucrose cushion and centrifuged at 78,000 rpm for 120 min at 4°C in a TLA-110 rotor (Beckman Coulter). After removing the supernatant, ribosome pellets were rinsed once with polysome lysis buffer and resuspended in Laemmli sample buffer for Western blotting.

Generation of a polyclonal antibody against RNG140

RNG140 tagged with GST (Shiina & Tokunaga, 2010) was expressed in *E. coli* (BL21) and purified using Glutathione Sepharose 4B columns (GE Healthcare, Chicago,

IL). The GST tag was removed by factor Xa cleavage, and the RNG140 protein was purified in accordance with the manufacturer's protocol. The purified protein was used as an antigen to generate a polyclonal antibody in a rabbit. An anti-RNG140 antibody was affinity purified from rabbit serum using Affi-Gel 10 gel (Bio-Rad, Hercules, CA) conjugated with purified RNG140.

Western blotting

Western blotting was performed on polyvinylidene difluoride membranes using the following primary antibodies: anti-RNG140 polyclonal antibody, anti-GFP antibody (GF200, Nacalai Tesque, Kyoto, Japan), anti-eIF3b antibodies (sc-163777 and sc-137214, Santa Cruz Biotechnology, Dallas, TX), anti-eIF3e antibody (A302-985A, Bethyl Laboratories, Montgomery, TX), anti-eIF3k antibody (NB100-93304, Novus Biologicals, Centennial, CO), anti-eIF3l antibody (GTX120119, GeneTex, Irvine, CA), anti-eEF2 antibody (#2332, Cell Signaling Technology), and anti-S6 ribosomal protein antibody (#2317, Cell Signaling Technology), anti-ATR antibody (#2790, Cell Signaling Technology), anti-POLA antibody (ab31777, Abcam, Cambridge, UK), anti-RPS18 antibody (ab91293, Abcam), anti-FBL antibody (ab4566, Abcam). Biotinylated secondary antibodies (GE Healthcare) and alkaline phosphatase-conjugated streptavidin (GE Healthcare) were used to detect the reacted proteins with a solution with bromochloroindolyl phosphate and nitro blue tetrazolium. Quantification of band intensity was performed as previously described using a standard curve generated from a standard dilution series of cell extracts on the same membrane (Ohashi et al., 2013).

Immunoprecipitation

Immunoprecipitation was performed as described previously (Shiina & Nakayama, 2014). Cells were homogenized in 0.25 M sucrose, 0.7% Triton X-100, 0.1 mM DTT, protease inhibitors (10 μg/ml leupeptin, 10 μg/ml pepstatin, 10 μg/ml aprotinin, and 1 mM PMSF), and 1,000 units/ml RNase inhibitor (Takara Bio, Shiga, Japan), and then centrifuged at 10,000 g for 10 min at 4°C. The lysate was added to 1:10 volume of 10× PBS followed by 1:20 volume of anti-GFP-agarose beads (Medical and Biological Laboratories, Nagoya, Japan) or protein A sepharose (GE Healthcare) that had been conjugated with the anti-eIF3b antibody or control mouse IgG. After rocking for 2 h at 4°C, the beads were washed three times with PBS containing 0.1 mM DTT, the protease inhibitors, and 100 units/ml RNase inhibitor. For RNase treatment, 0.2 mg/ml RNase A (FUJIFILM Wako Pure Chemical Corporation) was added, omitting RNase inhibitor in the lysis buffer and the wash buffer.

Mass spectrometry

Proteins in immunoprecipitates with the anti-GFP antibody were separated by SDS-PAGE and stained with Coomassie Brilliant Blue. Gel slices with corresponding protein bands were excised and then destained with 30% acetonitrile in 25 mM NH_4HCO_3 for 10 min. The gel slices were dehydrated with 50% acetonitrile in 25 mM NH_4HCO_3 for 10 min and dried in a vacuum desiccator. After rehydrating the gel slices with 10 μg/ml trypsin in 50 mM NH_4HCO_3 for 30 min on ice, excess solution was removed, and the gel slices were incubated for 12 h at 37°C for in-gel digestion. Digested peptides were extracted with 50% acetonitrile and 5% CF_3COOH for 1 h at room temperature and then analyzed with Orbitrap Elite mass spectrometer (Thermo Fisher Scientific). The peptides were eluted using a 20 min acetonitrile gradient (10 minute 0%-30% acetonitrile gradient,

followed by a 2 minute 30%-80% gradient, with a final 8 minute isocratic step at 80% acetonitrile) at a flow rate of 300 nl/min. Singly charged ions (and unassigned charge states) were excluded.

Peak lists were generated from raw data using Proteome Discoverer 2.2 software (Thermo Fisher Scientific). The peak-list files were searched against the NCBIprot (20200204; 257,100,649 sequences) (National Center for Biotechnology Information, Bethesda, MD) using Mascot software (version 2.6.1) (Matrix Science, London, UK). Trypsin was selected as the enzyme, with two potential missed cleavage. Fragment ion mass tolerance was set to 0.8 Da and precursor ion mass tolerance was set to 10 ppm. Variable amino acid modification was oxidized methionine and no fixed amino acid modification. Peptide spectral matches were filtered to a 1% false discovery rate (FDR) using the target-decoy strategy combined with linear discriminant analysis. Proteins with only a single peptide identified were removed from the list. If proteins were contained in the control GFP immunoprecipitates in an amount comparable to those in the RNG140-GFP immunoprecipitates, as judged by the mascot score ratio of the protein in the RNG140-GFP immunoprecipitates to the GFP immunoprecipitates being less than 2.5, those proteins were also removed from the list.

Two biological replicates were acquired. One was a pilot experiment and the other was a large-scale experiment. The results acquired from the latter are shown as Table S1 and are deposited in PRIDE repository. The results of the two experiments were reproducible except that the pilot experiment detected only major proteins including eIF3 subunits and ribosomal small subunit proteins.

Translation reporter assay

Stable cell lines of GFP and GFP-RNG140 were transfected with plasmids encoding CrPV IRES-hRluc, HCV IRES-hRluc, or EIF2S3 5′ UTR-hRluc in 96-well dishes. hRluc luciferase assays were performed using the Renilla-Glo Luciferase Assay System (Promega) in accordance with the manufacturer's protocol. The luminescence was quantified using a Corona SH-9000Lab (HITACHI, Tokyo, Japan) and normalized by the amount of the hRluc transcripts measured by qRT-PCR as described below.

Quantitative reverse transcription PCR

Total RNA was extracted from cell lysates or mouse tissues using ISOGEN (Nippon Gene) in accordance with the manufacturer's protocol. RT was performed with M-MLV-Reverse Transcriptase (Thermo Fisher Scientific), and quantitative PCR was performed with SYBR Premix Ex Taq II (Tli RNaseH Plus) (Takara Bio) using a 7500 real-time PCR system (Applied Biosystems, Carlsbad, CA) in accordance with the manufacturer's protocol. The primers used for qPCR are listed below:

hRluc: 5′-ACGCAAACGCATGATCACTG-3′ and 5′-GCAGAAAAATCACGGCGTTC-3′,

GAPDH: 5′-AACGACCCCTTCATTGACCT -3′ and 5′-TGGAAGATGGTGATGGGCTT -3′, and

RNG140: 5′-AGAGCAGCTTAACCCAGACCAGTTG-3′ and 5′-GGGCCTTTTTCTGCGCTTTCAGC-3′.

Ribosome profiling and RNA-seq

Ribosome profiling was performed as previously reported (McGlincy & Ingolia, 2017) with modifications. Cultured CHO cells or eyes excised from P0.5 mice were

washed with ice-cold PBS, lysed with ice-cold lysis buffer (20 mM Tris-HCl, pH 7.5, 150 mM NaCl, 5 mM $MgCl_2$, 1 mM DTT, 100 μg/ml cycloheximide, and 1% Triton X-100), treated with TURBO DNase (25 U/ml at final concentration, Thermo Fisher Scientific), and centrifuged at 20,000 g for 10 min at 4°C. For eyes, beads shocker (Yasui Kikai, Osaka, Japan) was used for lysis. The RNA concentration of this lysate was measured using a Qubit RNA HS Assay Kit (Thermo Fisher Scientific). CHO cell lysate containing 10 μg RNA and mouse eye lysate containing 3 μg RNA were treated with 20 U and 6 U of RNase I (Lucigen, Middleton, WI) at 25°C for 45 min. The sample was overlaid on a 1 M sucrose cushion and the ribosomes were pelleted by centrifugation for 1 h at 100,000 rpm at 4°C in a TLA-110 rotor. Ribosome-bound RNA was isolated using a Direct-zol RNA MicroPrep kit (Zymo Research, Irvine, CA). After gel electrophoresis, RNA fragments corresponding to 26 nt-34 nt were excised and subjected to library construction as described previously (McGlincy & Ingolia, 2017).

RNA-seq analysis was performed on total RNA extracted from the exact same lysate used for ribosome profiling, using TRIzol reagent (Thermo Fisher Scientific). rRNAs were removed from the total RNA using Ribo-Zero Gold rRNA Removal Kit (Human/Mouse/Rat) (Illumina, San Diego, CA), and cDNA libraries were prepared using TruSeq Stranded mRNA Library Prep Kit (Illumina).

The libraries were sequenced on a HiSeq4000 (Illumina), and the reads were aligned to the Chinese hamster genome (criGri1) and the mouse genome (GRCm38/mm10). For ribosome profiling, the offsets of the A-site from the 5′ end of ribosome footprints were determined to be 12 for 25 nt, 13 for 26 nt, 14 for 27 nt, 15 for 28 nt and 16 for 29–30 nt in cultured CHO cells, and 15 for 26-29 nt and 16 for 30-31 nt in mouse eyes. For RNA-seq analysis, offset 15 was used for all mRNA fragments. To count the number of

footprints in the CDS, footprints corresponding to the first and the last 5 codons of the CDS were excluded. To calculate the translation efficiency, ribosome profiling counts were normalized by RNA-seq counts using the DESeq package (Anders & Huber, 2010). Two and three independent experiments were conducted for CHO cells and mouse eyes, respectively, and the data were analyzed statistically. All custom scripts used in this study are available upon request.

Gene ontology analysis

Gene ontology (GO) enrichment analysis was performed using PANTHER gene list analysis tools and DAVID functional annotation tools. Significance of overrepresentation of GO terms was assessed using the Benjamini–Hochberg false discovery rate (FDR) criterion at $q < 0.05$.

Transcript length and exon numbers

The length of UTR and CDS, and the number of coding exons of transcripts were obtained from Ensembl data base.

Cell proliferation assay

CHO cells stably expressing RNG140-GFP or GFP were seeded in 6-well cell culture plates (1×10^4 cells/well) and incubated at 37°C with 5% CO_2. After washing with saline, the cells were detached from the plate with 0.25% trypsin-EDTA (Thermo Fisher Scientific) and counted using a hemocytometer. Cells were counted daily for 5 days after seeding.

Preparation of Cas9 mRNA and guide RNA (gRNA)

The pSP64-hCas9 plasmid was linearized by digestion with *Sal*I, and used for *hCas9* mRNA preparation by an mMESSAGE mMACHINE SP6 Transcription Kit (Thermo Fisher Scientific) in accordance with the manufacturer's protocol. For RNG140 gRNA preparation, the plasmids were digested with *Dra*I and used for *in vitro* transcription by a MEGAshortscript T7 Transcription Kit (Thermo Fisher Scientific). The synthesized mRNA and gRNA were purified using phenol-chloroform-isoamyl alcohol extraction and isopropanol precipitation. The precipitated RNA was dissolved in Opti-MEM I (Thermo Fisher Scientific) at 2–4 μg/μl.

Generation of RNG140 knockout mice

RNG140 knockout mice were generated using CRISPR/Cas9 system with modifications to a previous report (Hashimoto & Takemoto, 2015). *In vitro* fertilized eggs from C57BL/6J strain mice were cultured in modified Whitten's medium (mWM) for 2 h, washed three times with Opti-MEM I, and then aligned in an electrode gap (LF501PT1-10, BEX, Tokyo, Japan), which had been filled with 5 μl of Opti-MEM I containing 750 ng/μl Cas9 mRNA and 400 ng/μl gRNA. Electroporation was performed using SEN-3401 (NIHON KOHDEN, Tokyo, Japan) with 35 V (3 msec ON + 97 msec OFF) × 6 times, changing the current direction alternately. After electroporation, the eggs were washed four times with M2 medium and two times with mWM medium, and cultured in mWM medium at 37°C in a 5% CO_2 incubator. On the next day, surviving 2-cell stage zygotes were transferred to the oviducts of pseudopregnant females.

To analyze CRISPR/Cas9-mediated mutations in the *Rng140* gene, the genome region flanking the gRNA target was amplified by PCR using primers 5′-

TTCCTTTTCACTTCAGTTGGTTTAG-3′ (RNG140-F1) and 5′-ATGTAAGTTCTGATGGACTGACACA-3′, and then sequenced using the RNG140-F1 primer. For genotyping of wild-type mice and the 5-bp deleted RNG140 knockout mice, primers RNG140-F1 and 5′- CTCACATGTTGTTCCTACCACTG-3′ were used to detect the wild-type allele and primers RNG140-F1 and 5′-CACATGTTGTTCCTACTTTTTTC-3′ were used to detect the RNG140 knockout allele.

Immunofluorescence and WGA staining

To immunostain sections of mouse eyes, P0.5 mouse heads were embedded in Tissue-Tek (Sakura Finetek, Tokyo, Japan), frozen in liquid nitrogen, and horizontally sectioned at 12 μm thickness using a cryostat (Leica CM1950, Leica, Wetzlar, Germany).

The sections attached to coverslips were fixed with 3.7% formaldehyde in PBS for 10 min at room temperature. After washing with PBS, the specimens were treated with 0.5% Triton X-100 in PBS, washed with PBS, and blocked with 10% FBS. For immunostaining, the specimens were incubated with the anti-RNG140 antibody and then labeled with an Alexa 488-conjugated anti-rabbit IgG antibody (Thermo Fisher Scientific). For WGA staining, they were incubated with WGA conjugated with Alexa 594 (Thermo Fisher Scientific). Fluorescence images were acquired using an A1 confocal laser microscope equipped with a Ti-E inverted microscope (Nikon) with a 10× objective.

The images from the WGA staining were used to measure the size of the lens nucleus region compared to the entire lens region using Fiji software. From the serial sections of a mouse head, 2-3 sections with the largest lens diameter were selected. WGA fluorescence intensity was measured along the diameter, perpendicular to the cornea, of the lens nucleus region and the entire lens region. To reduce the noise in the fluorescence

intensity waveform along the diameter, the fluorescence intensity of a pixel (position X) was converted to the average of 31 adjacent pixels (position X ± 15). The diameter of the entire lens region corresponded to 500-600 pixels. The average of the maximum and minimum fluorescence intensity was calculated and defined as the boundary value between the lens nucleus and the lens cortex: the region with less fluorescence than that value was considered to be the lens nucleus region. The ratio of the diameter of the lens nucleus to that of the entire lens was calculated from 2-3 replicates from 3 mice for each genotype.

Statistical analysis

Data are represented as box plots or as the mean with dot plots of individual values. Two samples were compared using unpaired t-test. Statistical analysis was performed with R. The GO term enrichment was analyzed using PANTHER gene list analysis tools (http://pantherdb.org/) and DAVID functional annotation tools (https://david.ncifcrf.gov/).

Accession numbers

The results of mass spectrometry of CHO cells have been deposited to ProteomeXchange Consortium via PRIDE partner repository with the dataset identifier PXD019040.

The results of ribosome profiling and RNA-seq of CHO cells (GSE141840) and mouse eyes (GSE141842) used in this study were deposited in the National Center for Biotechnology Information (NCBI).

Results

RNG140 reduces translation in CHO cells

I examined the effect of RNG140 on translation in cells. To this end, we set out to perform ribopuromycilation of nascent polypeptides in CHO cells that expressed RNG140-GFP (Fig. 2A-D). First, RNG140-GFP or GFP was transiently expressed in CHO cells, and puromycin staining intensity of those cells was compared with that of nearby untransfected control cells. RNG140-GFP expression, but not GFP expression, significantly reduced puromycin staining compared with control cells, especially at higher doses, suggesting that global translation was suppressed by RNG140 expression (Fig. 2A and B). This effect of RNG140-GFP expression on translation was independent of cell type, as essentially the same results were obtained with another cell line, SRA 01/04, a human lens epithelial cell line (Fig. 2C and D).

I examined whether native RNG140 exerts translational repression independent of the GFP tag. Transient overexpression of RNG140 in CHO cells was confirmed by Western blotting with anti-RNG140 antibody (Fig. 2E). In the ribopuromycilation assay, RNG140-transfected cells were distinguished from untransfected cells by co-transfection of mRFP1. It was estimated that about 96% of the mRFP1-positive cells expressed exogenous RNG140, judging from experiments in which CHO cells co-transfected with two plasmids encoding GFP and mRFP1 showed co-expression of the proteins in 96.4 ± 6.9% of mRFP1-positive cells. Puromycin staining was significantly reduced in mRFP1-positive cells co-transfected with RNG140, but not in mRFP1-positive cells not transfected with RNG140, compared with nearby untransfected cells (Fig. 2F and G). These results validated that RNG140 represses translation.

Next, I generated CHO cell clones that stably expressed RNG140-GFP. The

expression levels of RNG140-GFP were about 1.9 times higher than that of endogenous RNG140 in mouse eyes (Fig. 2H). However, RNG140-GFP did not form RNA granules in those clones, suggesting that RNG140-GFP levels were below the critical concentration for granule formation and not toxic levels (Shiina & Tokunaga, 2010). In addition, because expression of RNG140 in the eye is restricted to the lens region, the expression level of RNG140 in the lens is higher than the average expression level in the whole eye and may be comparable to the RNG140-GFP levels in the CHO clones.

To compare puromycin staining between cells expressing RNG140-GFP and GFP in the same specimen, the CHO cell clones were co-cultured on the same coverslips (Fig. 2I and J). RNG140-GFP- and GFP-expressing cells were distinguishable by predominant localization of the GFP signal in the cytoplasm and nucleus, respectively. These different distribution patterns may be due to the following reasons: GFP was distributed in both the cytoplasm and nucleus of living cells. However, in the ribopuromycilation assay, cytoplasmic GFP, but not nuclear GFP, was effluxed from the cells because the cell membrane, but not the nuclear membrane, was permeabilized with digitonin before fixation. As a result, GFP localization appeared to be prominent in the nucleus. In contrast, RNG140-GFP was localized only to the cytoplasm and may be anchored to certain scaffolds in the cytoplasm, which may be the reason why the RNG140-GFP signal remained in the cytoplasm after digitonin treatment. Cells stably expressing RNG140-GFP significantly reduced the staining for puromycin compared with GFP, supporting that global translation was suppressed by RNG140 expression (Fig. 2I and J).

These results were further complemented by quantitative analysis of the stable clones by Western blotting for puromycin (SUnSET method). Total puromycin incorporation into nascent polypeptides was lower in RNG140-GFP-expressing cells than in GFP-

expressing cells, confirming global translational suppression by RNG140 expression (Fig. 2K and L).

I further analyzed the effect of RNG140 expression on the polysome profile using sucrose density gradient centrifugation (Fig. 3A-C). After centrifugation, the sample was fractionated into 22 fractions, the amount of RNA in each fraction was measured at an absorbance of 254 nm, and relative amount of RNA in each fraction was calculated. This analysis detected a fraction with a slightly higher RNA peak in RNG140-GFP-expressing cells than in GFP-expressing cells (Fig. 3A, Fraction No. 7, an arrowhead). EDTA treatment is known to release 80S ribosomes from polysomes and increase the amount of 60S and 40S subunits. This treatment reduced the relative RNA amount in fractions 11-19 and increased the amount in fractions 3-5, suggesting that these fractions corresponded to polysomes and 40-60S, respectively (Fig. 3B). Therefore, we reasoned that the fraction 7, sedimented between the polysomes and 40-60S, corresponded to the 80S peak. Although the difference in the polysome profile between the 2 groups was modest in the presence of cycloheximide (Fig. 3A), removing cycloheximide from the buffers, which increases ribosome drop-off from mRNA, enhanced the difference between the two groups: the 80S peak did not increase in GFP-expressing cells, but did increase in RNG140-GFP-expressing cells (Fig. 3C, an arrowhead). This suggested that ribosomes formed 80S after drop-off from mRNA and/or ribosomes did not initially bind to mRNA at the 80S peak in RNG140-GFP-expressing cells. Thus, RNG140 appeared to increase 80S ribosomes that are not engaged on mRNAs.

To have more evidence of translational repression, I probed eukaryotic elongation factor 2 (eEF2) on ribosomes, which is a hallmark of inactive 80S (Liu & Qian, 2016). Ribosome pellets collected through a sucrose cushion showed that RNG140-GFP

increased the recovery of eEF2, whereas an equivalent amount of ribosomes (S6 small subunit protein) and initiation factor eIF3b was found, compared to GFP expression (Fig. 3D). These results further supported the notion that RNG140 increases free 80S ribosomes, which was relevant to global translational suppression by RNG140.

RNG140 binds with eIF3 and reduces eIF3-dependent translation

Given that RNG140 was also found in sucrose cushion pellet (Fig. 3D), I reasoned that RNG140 associates with ribosome proteins or translation initiation factors that are typically co-sedimented in sucrose cushion. To identify RNG140-associated proteins, I performed immunoprecipitation (IP) with RNG140-GFP followed by mass spectrometry. I found about 150 proteins specifically co-immunoprecipitated with RNG140-GFP but not with GFP (Fig. 4A) (Supplementary Table 1). Gene ontology (GO) enrichment analysis revealed that eIF3 subunit proteins and small ribosomal subunit proteins were significantly enriched in the RNG140-associated complex (Fig. 4B).

Western blotting of the immunoprecipitates confirmed the association of RNG140 to eIF3 subunits and S6 ribosomal protein (Fig. 4C and E). This association of RNG140 to eIF3 was independent of cell type, as reproduced in SRA 01/04 cells (Fig. 4D). Reciprocally, immunoprecipitation with anti-eIF3 antibody co-precipitated RNG140-GFP from CHO cells and RNG140 from mouse eyes, supporting the interaction between RNG140 and eIF3 (Fig. 4F). Furthermore, treatment of the immunoprecipitates with RNase A sustained the association of eIF3b with RNG140 (Fig. 4E), showing RNA-independent interaction of these proteins. I observed that S6 ribosomal protein was lost from the RNG140-associated complex by RNase A treatment, which may be because ribosomal small subunits bound to RNG140 through mRNA, or alternatively ribosome

integrity was lost by RNase A treatment. These results suggested that RNG140 forms a complex with eIF3 through protein–protein interactions.

The RNG140-eIF3 interaction led us to hypothesize that RNG140 inhibits the function of eIF3 for translational repression. To examine this, I monitored translation driven by eIF3-dependent and independent mechanisms using reporters. In the designed reporters, three different sequences were placed in front of *Renilla* luciferase: endogenous 5′ UTR (*EIF2S3*), hepatitis C virus (HCV) internal ribosome entry site (IRES), and cricket paralysis virus (CrPV) IRES. Former two require eIF3 and eIF2 for translation, while the last one does not (Kieft, 2008). In CHO cells, RNG140 expression did not affect CrPV IRES-mediated translation, but repressed HCV IRES- and *EIF2S3* 5′ UTR-mediated translation (Fig. 4G). These results further supported the idea that RNG140 represses eIF3-dependent translation but not eIF3-independent translation. , although they did not rule out the possibilities that RNG140 also represses eIF2-dependent translation and other translation mechanisms.

RNG140 reduces translation of a set of mRNAs in CHO cells

Since translation of endogenous mRNAs is thought to be driven by eIF3, I wondered which mRNAs are affected by RNG140 in cells. Here, I performed ribosome profiling (Iwasaki et al., 2016, Ingolia, 2016, Ingolia et al., 2009) upon RNG140 overexpression in CHO cells (Supplementary Table 2). I identified 1,113 transcripts decreased in translation efficiency, which is calculated by over- or under-representation of footprint reads over RNA-seq reads, by RNG140-GFP expression (Fig. 5A and B; Supplementary Table 3). I designated these as “more likely target transcripts (more-T)”. Ribosome profiling also identified 860 transcripts with increased translation efficiency (Fig. 5A and

B; Supplementary Table 4). I designated them as “less likely target transcripts (less-T)”.

To validate the effect of RNG140 expression on translation efficiency, we analyzed the expression levels of proteins encoded by representative transcripts in the more-T (*Atr* and *Pola1*) and less-T (*Rps18* and *Fbl*) groups by Western blotting. RNG140-GFP reduced the expression levels of ATR and POLA, but not RPS18 or FBL in CHO cells (Fig. 5C). These results confirmed that RNG140 reduces the translation efficiency of more-T group transcripts.

In most cases, translation efficiency of redundant transcripts from the same gene was changed in a similar manner, i.e., increased or decreased, by RNG140 expression. However, some redundant transcripts, such as splicing isoforms from *Rbm39*, *Tcp1*, and *Dars* genes, were separated into the more-T and less-T groups. Of note, the splicing isoforms of these genes classified into the more-T group were longer and had more exons than those classified into the less-T group (Fig. 6A). This finding led me to compare the length and the number of exons between the more-T and less-T groups. Thus, the length of the 5′ UTR, 3′ UTR, and coding sequence (CDS), and the number of coding exons of transcripts were compared between the top 100 in the more-T and less-T groups (Fig. 6B; Supplementary Tables 3 and 4). As a result, the length of CDS and the number of coding exons for the more-T group were markedly larger than those of the less-T group (Fig. 6B), suggesting that RNG140 preferentially targets transcripts with longer CDS and more coding exons to repress translation.

Next, to identify the biological categories in which the more-T and less-T groups are involved, GO enrichment analysis was conducted (Fig. 6C; Supplementary Tables 5 and 6). Major categories with high fold enrichment in the more-T group were "HECT (a domain found in ubiquitin ligases)", "chaperonin Cpn60/TCP-1", "PI3K/PI4K

(Phosphoinositide 3/4-kinase)", "membrane coat", "DNA replication initiation", etc. (Fig. 6C; Supplementary Table 5). These categories contained a number of factors involved in cell proliferation, for example, ubiquitin ligases [UBE3A (Mishra et al., 2009), UBE3C (Okada et al., 2015), and NEDD4 (Li et al., 2015)], PI3K (Yu & Cui, 2016), PI3K-related kinases such as TRRAP (Herceg et al., 2001), DNA replication initiators, and mitotic regulatory proteins.

These gene categories were reminiscent of the function of RNG140 in inhibiting cell proliferation (Aerbajinai et al., 2004). Therefore, I tested whether overexpression of RNG140 affected the proliferation of CHO cells. Compared with GFP, RNG140-GFP expression decreased the rate of cell growth (Fig. 6D). Taken ribosome profiling data together, the results suggested that RNG140-mediated translational repression of cell proliferation-associated mRNAs slows the cell growth.

Generation of RNG140 knockout mice

To investigate whether the RNG140-mediated translational regulation operates *in vivo*, I generated RNG140 knockout mice by CRISPR/Cas9-mediated genome editing. I first obtained a heterozygous mutant, which had a 5-bp deletion in exon 6 of the *Rng140* genome (Fig. 7A). This deletion caused a frame-shift in the *Rng140* open reading frame (ORF) and generated a downstream premature stop codon in exon 7 (Fig. 7A). If the truncated protein were synthesized, it would contain the N-terminal basic helix domain that binds to mRNA and inhibits translation *in vitro* (Shiina & Tokunaga, 2010). However, the premature stop codon in the 7th exon of a total of 19 exons was expected to cause nonsense-mediated decay of mRNA, resulting in much less expression of the truncated form. This was indeed the case as analyzed below. By crossing heterozygous ($Rng140^{+/-}$)

mice, I obtained RNG140 knockout (*Rng140*$^{-/-}$) mice (Fig. 7B and C), which grew into adult and were fertile, and used them in the analysis below.

As RNG140 is highly expressed in embryonic and postnatal eye lens in mice and RNG140 deficiency causes developmental defect in lens (Dash et al., 2015), I checked the expression level of RNG140 in the eye of *Rng140*$^{-/-}$ mice at postnatal day 0.5 (P0.5). Quantitative reverse transcription PCR (qRT-PCR) showed that RNG140 transcripts were markedly decreased in the eye of *Rng140*$^{-/-}$ mice, as expected (Fig. 7D). This may be due to destabilization of *Rng140* mRNA through nonsense-mediated decay caused by the premature stop codon. Western blotting analysis showed that RNG140 protein was also decreased in the eye of *Rng140*$^{-/-}$ mice (Fig. 7E). Immunostaining of eye slices with the anti-RNG140 antibody revealed a decrease in lens fiber cell staining in *Rng140*$^{-/-}$ mice (Fig. 7F). I noted that the antibody I raised may also recognizes other non-specific proteins, because of high staining intensity outside of the lens was indistinguishable between *Rng140*$^{-/-}$ mice and *Rng140*$^{+/+}$ mice and many bands detected in Western blotting. Together, these results indicated that RNG140 expression was decreased in the eye lens of *Rng140*$^{-/-}$ mice.

The effect of RNG140 knockout on lens development was analyzed by staining of eye slices with wheat germ agglutinin (WGA), which stains lens nucleus regions with less intensity compared with high intensity staining of lens cortex regions (Dash et al., 2015). Measuring the diameter of the nucleus region compared with the entire lens region revealed that *Rng140*$^{-/-}$ mice had a significantly reduced size of the lens nucleus compared with *Rng140*$^{+/+}$ mice (Fig. 7G and H). These results were consistent with the previous report that RNG140 (caprin2) deficiency showed a defect in lens fiber cell nuclear compaction and reduced the size of the lens nucleus (Dash et al., 2015).

In vivo relevance of RNG140-mediated translational repression in mouse eyes

Next, I conducted ribosome profiling of *Rng140*$^{-/-}$ mouse eyes at P0.5 and compared with that of *Rng140*$^{+/+}$ mice (Fig. 8A-D; Supplementary Table 7). For technical feasibility, I isolated whole eyes instead of lens. This may underestimate differences in translation efficiency between the genotypes, due to non-lens tissues that express low levels of RNG140 and may be less sensitive to RNG140 knockout. However, even underestimated, the results were expected to reflect the impact of RNG140 knockout on the lens. If RNG140-mediated translational repression operates *in vivo*, the effect of RNG140 knockout on translation efficiency is expected to be opposite to that of RNG140 overexpression in CHO cells. Indeed, RNG140 deficiency significantly increased the translation efficiency of the transcripts corresponding to the more-T group in the CHO ribosome profiling, but in contrast, decreased that of the less-T group (Fig. 8B). I further examined transcripts that were enriched in the major GO categories in the CHO ribosome profiling: more-T enriched in "HECT" and "PI3K/PI4K", and less-T enriched in "Histone core" and "Ribosomal protein" (Fig. 8C; Supplementary Table 8). Changes in the translation efficiency of these mRNAs in the eyes of RNG140 knockout mice were opposite to that of RNG140 overexpression in CHO cells. These results suggested that the targets of RNG140 were similar between CHO cells and mouse eyes, and that changes in translation efficiency correlated with RNG140 dose.

RNG140 was highly expressed during lens differentiation; therefore, a question was raised whether key factors that regulate lens differentiation escape RNG140-mediated translational repression. I thus examined transcripts encoding lens differentiation factors such as α-, β-, and γ-crystallins, lens major intrinsic protein (Mip), CP115, and CP49 (De

Longh et al., 2001) (Fig. 8D; Supplementary Table 8). Translation efficiency of these transcripts was reduced by RNG140 deficiency, suggesting that the loss of RNG140 had an effect on global translation, which reduced the relative translation of lens differentiation-related transcripts compared with transcripts that RNG140 would normally repress.

The correspondence between the short CDS in crystallin mRNAs and the length-dependent effect of RNG140 found in CHO cells led me to hypothesize that shortness is the basis for escaping translational repression by RNG140. In fact, in differentiating lenses, shorter CDSs and fewer coding exons were found in translationally decreased transcripts by RNG140 deficiency (Fig. 8E; Supplementary Tables 9 and 10). Taken together, these results suggested that RNG140-mediated translational repression operates in mouse eyes *in vivo*, which reduces the translation of a set of mRNAs, whereas it allows other mRNAs, including those associated with lens differentiation, to escape repression and be translated during lens differentiation.

Discussion

In this study, I characterized RNG140-mediated translational regulation. Several lines of evidence revealed that RNG140 inhibits translation through mechanisms including suppression of eIF3-dependent translation initiation. RNG140 preferentially inhibited the translation of long mRNAs, which can be a way to regulate a specific set of mRNAs. Taken together with the fact that FGF activity drives both RNG140 expression and cell cycle exit during lens differentiation (Cvekl & Zhang, 2017, Lorén et al., 2009), I argue that RNG140 selectively inhibits the translation of long mRNAs involved in cell proliferation, leaving the short mRNAs involved in lens differentiation translated. This mRNA-selective mechanism is likely to underlie the reduction in the size of the lens nucleus, which may be caused by impaired cell cycle exit and delayed lens differentiation by RNG140 (caprin2) deficiency in moue eyes (Dash et al., 2015).

A possible mechanism underlying the long mRNA selectivity is that RNG140 binds preferentially to long mRNAs and inhibits their translation through mechanisms such as binding with eIF3 (Fig. 9A). However, the mechanism by which RNG140 prefers long mRNAs remains unclear, except for the hypothesis that the low sequence selectivity of RNG140 increases stochastic interactions with longer mRNAs. RNG140 and its paralog RNG105 (caprin1) share the conserved N-terminal basic helix domains, which have low sequence specificity for binding to mRNAs. This low-specificity binding is essential for the ability of RNG140 to suppress translation *in vitro* (Shiina & Tokunaga, 2010, Shiina et al., 2005). Given this property, RNG140 could preferentially bind to longer mRNAs that may provide multiple binding sites for RNG140. A similar idea has been suggested for mRNAs in stress granules, where mRNA length correlates with targeting to the granules (Khong et al., 2017). Longer mRNAs stretch out long strands in crowded spaces

within the cell. In addition, due to the low sequence specificity of RNG140, longer mRNAs provide multiple binding sites for RNG140. Thus, the entire length of the long mRNA may behave like a large antenna, increasing the probability of receiving RNG140 in the crowded space of the cell. Once RNG140 binds to an mRNA, the RNG140-eIF3-ribosome-mRNA complex may be more easily formed in a cis-acting than a trans-acting manner. This mechanism may not preclude another possibility that the selectivity depends on the properties of eIF3, as discussed below.

eIF3 is the largest and most complicated translation initiation factor, composed of 13 subunits, and it binds to the eIF4F complex and promotes m^7G cap-dependent translation (Valášek et al., 2017). Besides this general role in translation initiation, eIF3 has been reported to alternatively regulate protein synthesis in a selective and mRNA-specific manner. For example, eIF3 specifically associates with mRNAs such as c-Jun and BTG1, and regulates cell growth in human 293T cells (Lee et al., 2015). In yeast, eIF3e and eIF3d upregulates the translation for mitochondrial electron transport chains and ribosome biogenesis (Shah et al., 2016). In mice, eIF3 is involved in terminal erythroid differentiation by binding to cytoplasmic polyadenylation element binding protein 4 (CPEB4) and suppressing translation of a set of mRNAs (Hu et al., 2014). In addition, in zebrafish, eIF3h is required for the translation of certain mRNAs, including crystallin mRNAs, for brain and eye development (Choudhuri et al., 2013). These studies suggested that eIF3 selectively upregulates the translation of mRNAs for mitochondrial function, ribosome function, and eye differentiation.

These functional categories are reminiscent of RNG140 non-targeted short mRNAs, which led to the idea that the selective mode of eIF3 works on relatively short mRNAs. In that case, if RNG140 inhibits only the general mode and not the selective mode of eIF3,

short mRNAs could selectively escape translational repression by RNG140 (Fig. 9B). In the eIF3h-deficient zebrafish, transcripts that are selectively translated through an eIF3h-dependent mechanism were identified (Choudhuri et al., 2013). Of these, 19 transcripts corresponded to the orthologs analyzed in the mouse eyes in the current study (*Atp2a1*, *Capn3*, *Col15a1*, *Cox4i1*, *Cox6b1*, *Cryba1*, *Cryba2*, *Crybb1*, *Crygn*, *Dusp26*, *Emc4*, *Lim2*, *Mip*, *Mylpf*, *Nefm*, *Pkm*, *Slc25A4*, *Tnnt3*, and *Tyrp1*). The average change in translation efficiency of these 19 transcripts by RNG140 knockout was −0.31±0.24, suggesting that they tend not to be targeted by RNG140. They included the lens differentiation-related transcripts (*Cryba1*, *Cryba2, Crybb1*, *Crygn*, and *Mip*), all of which escaped translational repression by RNG140. These results supported the notion that RNG140 has a less effect on the selective mode of eIF3. Thus, another possible mechanism is that RNG140 exerts mRNA selectivity through regulating eIF3. Alternatively, RNG140 could specifically upregulates the selective mode of eIF3. However, the expression levels of lens proteins such as γ-crystallin and lens MIP/Aqp0 were not altered by RNG140 (caprin2) knockout (Dash et al., 2015), which may support the explanation that RNG140 suppresses the general mode of eIF3.

In contrast to short mRNAs, including those associated with lens differentiation, long mRNAs corresponding to more-T enriched in "HECT" and "PI3K/PI4K" were de-repressed in translation in RNG140 knockout eyes. Ubiquitin ligases such as UBE3A, UBE3C, and NEDD4 contained in "HECT" promote cell proliferation (Mishra et al., 2009; Okada et al., 2015; Li et al., 2015), and PI3K and PI3K-related kinases such as TRRAP contained in "PI3K/PI4K" also upregulate cell proliferation (Yu & Cui, 2016; Herceg et al., 2001). Consequently, RNG140 deficiency, which increases translation of these proliferation-related proteins, may delay cell cycle exit, thereby delaying lens

differentiation and reducing in the size of the lens nucleus, where terminally differentiated fiber cells are compacted within the lens.

A reduction in the size of lens nucleus has also been reported in knockout mice of Bfsp2 (CP49), encoding a lens-specific intermediate filament (IF) protein (Fudge et al., 2011), whose relative translation efficiency in the eye was reduced by RNG140 knockout (Fig. 8D; Supplementary Table 8). Since lens-specific IFs make significant contributions to lens stiffness and morphology (Fudge et al., 2011), the relative reduction in the IF protein concentration by RNG140 deficiency could cause the reduction in the size of lens nucleus.

RNG140 has been reported to form RNA granules that are neither rich in ribosomes nor G3BP (Shiina & Tokunaga, 2010). Cells containing such granules stop cell division and are more susceptible to cell death than those expressing lower levels of RNG140 without granule formation (Shiina & Tokunaga, 2010). In general, excessive and prolonged formation of RNA-containing granules is toxic to cells (Reineke & Neilson, 2019). This may be due to the transition of the granules formed by liquid-liquid phase separation to the solid state by excessive and prolonged formation, which could lead to sequestration of proteins essential for translation into such granules and/or toxicity of the solid aggregation itself. This aggregation-dependent toxicity is well known in neurodegenerative diseases such as amyotrophic lateral sclerosis (ALS) and frontotemporal lobar degeneration (FTLD) (Ling et al., 2013; Ramaswami et al., 2013), and could be common with RNG140-induced RNA granules. The CHO cell clones used in the current study did not form granules, and RNG140 interacted with G3BP and ribosomes in these cells. Together, these suggest that at low concentrations, RNG140 binds to G3BP and ribosomes without forming granules, whereas above the critical

concentration, RNG140 undergoes phase separation/transition to form granules and rearrange its binding partners.

The granule formation of RNG140 is stage-specific during mouse eye development: RNG140 transiently forms granular structures in lens pit cells at embryonic day 10.5 (E10.5), when the lens vesicle detaches from the surface ectoderm. Later, RNG140 granules disappear and RNG140 is abundantly expressed without forming granules in lens fiber cells from E12.5 to P4 (Dash et al., 2015). Thus, RNG140 granules are not static rather dynamic, by switching condensation-dissolution states and rearranging interaction partners at various stages of lens development. It is not known whether the switching is regulated by the expression level of RNG140 or by other mechanisms such as post-translational modifications of RNG140 granule components in the lens cell. In either case, CHO cells expressing RNG140-GFP used in the current study may resemble the physiological state of lens fiber cells in that they did not contain RNG140 granule structures.

Vertebrates have two RNG paralogs, RNG140 and RNG105, which both bind to mRNAs and inhibit translation *in vitro* (Shiina & Tokunaga, 2010). However, RNA granules they localize are different, and their functions in neurons are not redundant (Shiina & Tokunaga, 2010). RNG140 knockdown in neurons reduced dendrite length and spine density, which was not rescued by RNG105 expression. This result suggests a possibility that RNG140 plays roles in the maintenance of dendritic structure through different mechanisms from RNG105 (Shiina & Tokunaga, 2010). Furthermore, their effects on proliferation are opposite: RNG105, besides its function in mRNA localization and long-term memory formation in the brain, is highly expressed in proliferating cells and is responsible for proliferation of DT40 cells (Grill et al., 2004; Wang et al., 2005).

Thus, RNG105 and RNG140 are likely to be positive and negative regulators of cell proliferation, respectively. As for invertebrates, *Drosophila* has RNGI (also known as caprin) as an ortholog of RNG140 and RNG105 (Shiina & Tokunaga, 2010). RNGI acts to suppress eye growth (Baumgartner et al., 2013), which is similar to the RNG140 function in vertebrates.

Defects in the lens nucleus are associated with eye disfunction. For example, lens nuclear compaction increases with aging and the formation of nuclear cataract (Al-Ghoul et al., 2001). The lens nucleus is composed of lens fiber cells (Augusteyn, 2010; Augusteyn, 2018; Gangalum et al., 2018), in which RNG140 is highly expressed during development. Given that RNG140 deficiency reduces lens nuclear compaction (Dash et al., 2015), RNG140 and proteins whose translation is regulated by RNG140 could be therapeutic targets for certain types of eye dysfunction.

In summary, this study characterized RNG140-mediated translational regulation, providing a mechanistic insight into post-transcriptional regulation that downregulates proliferation-related factors without suppressing differentiation-related factors during lens development. This study also raised new questions about why and how mRNA length is distinguished by translational regulators in the coordination of proliferation and differentiation. The specific questions are: 1) Does RNG140 indeed bind preferentially to long mRNAs? To answer this question, an *in vitro* binding assay between RNG140 and mRNAs of various length will be required. In particularly, multivalent binding between intrinsically disordered regions (IDRs) of RNA-binding proteins and mRNAs is known as the basis for RNA granule formation and the recruitment of long mRNAs into the granules. With this in mind, analyzing the multivalent binding of RNG140 to mRNAs and/or the multivalent binding of RNG140 to proteins and mRNAs through its IDR would

be a way to understand the preference for long mRNAs. 2) How does eIF3 switch between the general mode and selective mode? In addition, does the selective mode actually prioritize shorter mRNAs? To answer this question, I need to look at the contribution of each eIF3 subunit to the translation modes. By revealing the binding of RNG140 to specific eIF3 subunits, it will be possible to clarify how RNG140 specifically suppress the general mode rather than the selective mode of eIF3-dependent translation. Furthermore, analyzing the multivalent binding of eIF3 to proteins and mRNAs through its IDR could understand the differences in the modes of eIF3-dependent translation regulation. 3) Are the length of mRNA and the number of exons related to the functional category of the protein encoded by the mRNA? Collaboration between developmental biology and bioimformatics will solve this problem. I hope that future research will resolve these questions, and in addition, whether these questions are limited to lens development or are common to other aspects of cell fate determination and function.

Acknowledgements

First of all, I would like to express my sincere gratitude to my supervisor Dr. Nobuyuki Shiina for sharing his wisdom and guiding me with limitless kindness and patience. His guidance helped me all the time of research and writing this thesis. Without his invaluable support, I would not have been where I am today. I would also like to specially thank Dr. Kei Nakayama with much appreciation. His stimulating suggestions and encouragement helped me to coordinate my path in science. Furthermore, I am deeply indebted to Dr. Shintaro Iwasaki for his extremely valuable experience, support, and insights. I would specially like to thank Dr. Yuichi Shichino for giving me technical advice and making important contributions to my project. I thank Dr. Masakazu Hashimoto for advice on CRISPR/Cas9 system; Ms. Sonoko Ohsawa for the generation of RNG140 knockout mice; Ms. Yumiko Makino for mass spectrometry; Ms. Mari Mito and Ms. Chisato Matsuda for technical assistance; Spectrography and Bioimaging Facility, Functional Genomics Facility, and Model Animal Research Facility in National Institute for Basic Biology for technical support. I extend my thanks to all my colleagues, Dr. Rie Ohashi, Mr. Akira Yamashita, Ms. Tomoyo Horio and Ms. Akiho Shiba for making every day brighter and happier. I also appreciate my Progress Committee members, Dr. Naoto Ueno, Dr. Eiji Watanabe, and Dr. Yuriko Komine, and a previous member, Dr. Yoshito Masamizu for fruitful discussions. I have always been pleased with the assistance of all the staffs in NIBB and SOKENDAI for their kind help and cooperation throughout my student life. Special thanks to Okashin research fellow for providing a scholarship. I also thank my friends at NIBB, Waseda, and Kichijo institutions. Finally, I owe a deep sense of gratitude to my loving family members, especially my husband Dr. Shingo Nakazawa. I am able to spend ordinary days at NIBB only because of the support and kindness of

my family. I would like to return my gratitude and love to them.

References

Aerbajinai, W., Lee, Y. T., Wojda, U., Barr, V. A., & Miller, J. L. (2004). Cloning and characterization of a gene expressed during terminal differentiation that encodes a novel Inhibitor of growth. *Journal of Biological Chemistry*, *279*(3), 1916–1921. https://doi.org/10.1074/jbc.M305634200

Al-Ghoul, K. J., Nordgren, R. K., Kuszak, A. J., Freel, C. D., Costello, M. J., & Kuszak, J. R. (2001). Structural evidence of human nuclear fiber compaction as a function of ageing and cataractogenesis. *Experimental Eye Research*, *72*(3), 199-214. https://doi.org/ 10.1006/exer.2000.0937

Anders, S., & Huber, W. (2010). Differential expression analysis for sequence count data. *Genome Biology*, *11*(10), R106. https://doi.org/10.1186/gb-2010-11-10-r106

Augusteyn, R. C. (2010). On the growth and internal structure of the human lens. *Experimental Eye Research*, *90*(6), 643-654. https://doi.org/10.1016/j.exer.2010.01.013

Augusteyn, R. C. (2018). On the contribution of the nucleus and cortex to human lens shape and size. *Clinical and Experimental Optometry*, *101*(1), 64-68. https://doi.org/10.1111/cxo.12539

Baumgartner, R., Stocker, H., & Hafen, E. (2013). The RNA-binding proteins FMR1, rasputin and caprin act together with the UBA protein lingerer to restrict tissue growth in Drosophila melanogaster. *PLoS Genetics*, *9*(7), e1003598. https://doi.org/10.1371/journal.pgen.1003598

Choudhuri, A., Maitra, U., & Evans, T. (2013). Translation initiation factor eIF3h targets specific transcripts to polysomes during embryogenesis. *Proceedings of the National Academy of Sciences of the United States of America*, *110*(24), 9818–

9823. https://doi.org/10.1073/pnas.1302934110

Cvekl, A., & Ashery-Padan, R. (2014). The cellular and molecular mechanisms of vertebrate lens development. *Development*, *141*(23), 4432–4447. https://doi.org/10.1242/dev.107953

Cvekl, A., & Zhang, X. (2017). Signaling and gene regulatory networks in mammalian lens development. *Trends in Genetics*, *33*(10), 677–702. https://doi.org/10.1016/j.tig.2017.08.001

Dash, S., Dang, C. A., Beebe, D. C., & Lachke, S. A. (2015). Deficiency of the RNA binding protein caprin2 causes lens defects and features of peters anomaly. *Developmental Dynamics*, *244*(10), 1313–1327. https://doi.org/10.1002/dvdy.24303

Dash, S., Siddam, A. D., Barnum, C. E., Janga, S. C., & Lachke, S. A. (2016). RNA-binding proteins in eye development and disease: implication of conserved RNA granule components. *Wiley Interdisciplinary Reviews: RNA*, *7*(4), 527–557. https://doi.org/10.1002/wrna.1355

De Longh, R. U., Lovicu, F. J., Overbeek, P. A., Schneider, M. D., Joya, J., Hardeman, E. D., & McAvoy, J. W. (2001). Requirement for TGFβ receptor signaling during terminal lens fiber differentiation. *Development*, *128*(20), 3995–4010.

Ding, Y., Xi, Y., Chen, T., Wang, J. Y., Tao, D. L., Wu, Z. L., Li, Y. P., Li, C., Zeng, R., & Li, L. (2008). Caprin-2 enhances canonical Wnt signaling through regulating LRP5/6 phosphorylation. *Journal of Cell Biology*, *182*(5), 865–872. https://doi.org/10.1083/jcb.200803147

Flores, R., & Zhong, G. (2015). The Chlamydia pneumoniae inclusion membrane protein Cpn1027 interacts with host cell Wnt signaling pathway regulator

cytoplasmic activation/ proliferation-associated protein 2 (Caprin2). *PLoS ONE*, *10*(5), e0127909. https://doi.org/10.1371/journal.pone.0127909

Gangalum, R. K., Kim, D., Kashyap, R. K., Mangul, S., Zhou, X., Elashoff, D., & Bhat, S. P. (2018). Spatial analysis of single fiber cells of the developing ocular lens reveals regulated heterogeneity of gene expression. *iScience*, *10*, 66-79. https://doi.org/10.1016/j.isci.2018.11.024

Glisovic, T., Bachorik, J. L., Yong, J., & Dreyfuss, G. (2008). RNA-binding proteins and post-transcriptional gene regulation. *FEBS Letters*, *582*(14), 1977–1986. https://doi.org/10.1016/j.febslet.2008.03.004

Grill, B., Wilson G. M., Zhang, K. W., Wang, B., Doyonnas, R., Quadroni, M., & Schrader, J. W. (2004). Activation/division of lymphocytes results in increased levels of cytoplasmicactivation/proliferation-associated protein-1: prototype of a new family of proteins. *Journal of Immunology*, *172*(4), 2389-2400. https://doi.org/10.4049/jimmunol.172.4.2389

Hashimoto, M., & Takemoto, T. (2015). Electroporation enables the efficient mRNA delivery into the mouse zygotes and facilitates CRISPR/Cas9-based genome editing. *Scientific Reports*, *5*, 11315. https://doi.org/10.1038/srep11315

Herceg, Z., Hulla, W., Gell, D., Cuenin, C., Lleonart, M., Jackson, S., & Wang, Z. Q. (2001). Disruption of Trrap causes early embryonic lethality and defects in cell cycle progression. *Nature Genetics*, *29*(2), 206–211. https://doi.org/10.1038/ng725

Hieronymus, H., & Silver, P. A. (2004). A systems view of mRNP biology. *Genes and Development*, *18*(23), 2845–2860. https://doi.org/10.1101/gad.1256904

Hu, W., Yuan, B., & Lodish, H. F. (2014). Cpeb4-mediated translational regulatory circuitry controls terminal erythroid differentiation. *Developmental Cell*, *30*(6),

660–672. https://doi.org/10.1016/j.devcel.2014.07.008

Ingolia, N. T. (2016). Ribosome footprint profiling of translation throughout the genome. *Cell*, *165*(1), 22-33. https://doi.org/ 10.1016/j.cell.2016.02.066

Ingolia, N. T., Ghaemmaghami, S., Newman, J. R., Weissman, J. S. (2009). Genome-wide analysis in vivo of translation with nucleotide resolution using ribosome profiling. *Science*, *324*(5924), 218-223. https://doi.org/ 10.1126/science.1168978

Iwasaki, S., Floor, S. N., & Ingolia, N. T. (2016). Rocaglates convert DEAD-box protein eIF4A into a sequence-selective translational repressor. *Nature*, *534*(7608), 558–561. https://doi.org/10.1038/nature17978

Keene, J. D. (2007). RNA regulons: coordination of post-transcriptional events. *Nature Reviews Genetics*, *8*(7), 533–543. https://doi.org/10.1038/nrg2111

Kieft, J. S. (2008). Viral IRES RNA structures and ribosome interactions. *Trends in Biochemical Sciences*, *33*(6), 274–283. https://doi.org/10.1016/j.tibs.2008.04.007

Kishore, S., Luber, S., & Zavolan, M. (2010). Deciphering the role of RNA-binding proteins in the post-transcriptional control of gene expression. *Briefings in Functional Genomics*, *9*(5–6), 391–404. https://doi.org/10.1093/bfgp/elq028

Khong, A., Matheny, T., Jain, S., Mitchell, S. F., Wheeler, J. R., & Parker, R. (2017). The stress granule transcriptome reveals principles of mRNA accumulation in stress granules. *Molecular Cell*, *68*(4), 808–820. https://doi.org/10.1016/j.molcel.2017.10.015

Konopacka, A., Greenwood, M., Loh, S. Y., Paton, J., & Murphy, D. (2015). RNA binding protein Caprin-2 is a pivotal regulator of the central osmotic defense response. *ELife*, *4*, e09656. https://doi.org/10.7554/eLife.09656.001

Lachke, S. A., Alkuraya, F. S., Kneeland, S. C., Ohn, T., Aboukhalil, A., Howell, G. R.,

Saadi, I., Cavallesco, R., Yue, Y., Tsai, A. C., Nair, K. S., Cosma, M. I, Smith, R. S., Hodges, E., Alfadhli, S. M., AI-Hajeri, A., Shamseldin, H. E., Behbehani, A., Hannon, G. J., Bulyk, M. L., Drack, A. V., Anderson, P. J., John, S. W., & Maas, R. L. (2011). Mutations in the RNA granule component TDRD7 cause cataract and glaucoma. *Science*, *331*(6024), 1571-1576. https://doi.org/10.1126/science.1195970

Lee, A. S. Y., Kranzusch, P. J., & Cate, J. H. D. (2015). eIF3 targets cell-proliferation messenger RNAs for translational activation or repression. *Nature*, *522*(7554), 111–114. https://doi.org/10.1038/nature14267

Li, Y., Zhang, L., Zhou, J., Luo, S., Huang, R., Zhao, C., & Diao, A. (2015). Nedd4 E3 ubiquitin ligase promotes cell proliferation and autophagy. *Cell Proliferation*, *48*(3), 338–347. https://doi.org/10.1111/cpr.12184

Ling, S. C., Polymenidou, M., & Cleveland, D. W. (2013). Converging mechanisms in ALS and FTD: disrupted RNA and protein homeostasis. *Neuron*, *79*(3), 416-438. http://doi.org/10.1016/j.neuron.2013.07.033

Liu, B., & Qian, SB. (2016). Characterizing inactive ribosomes in translational profiling. *Translation*, *4*(1), e1138018. https://doi.org/10.1080/21690731.2015.1138018

Lorén, C. E., Schrader, J. W., Ahlgren, U., & Gunhaga, L. (2009). FGF signals induce Caprin2 expression in the vertebrate lens. *Differentiation*, *77*(4), 386–394. https://doi.org/10.1016/j.diff.2008.11.003

Mata, J., Marguerat, S., & Bähler, J. (2005). Post-transcriptional control of gene expression: a genome-wide perspective. *Trends in Biochemical Sciences*, *30*(9), 506–514. https://doi.org/10.1016/j.tibs.2005.07.005

McGlincy, N. J., & Ingolia, N. T. (2017). Transcriptome-wide measurement of translation by ribosome profiling. *Methods*, *126*, 112–129. https://doi.org/10.1016/j.ymeth.2017.05.028

Miao, H., Jia, Y., Xie, S., Wang, X., Zhao, J., Chu, Y., Zhou, Z., Shi, Z., Song, X., & Li, L. (2014). Structural insights into the C1q domain of Caprin-2 in canonical Wnt signaling. *Journal of Biological Chemistry*, *289*(49), 34104–34113. https://doi.org/10.1074/jbc.M114.591636

Mishra, A., Godavarthi, S. K., & Jana, N. R. (2009). UBE3A/E6-AP regulates cell proliferation by promoting proteasomal degradation of p27. *Neurobiology of Disease*, *36*(1), 26–34. https://doi.org/10.1016/j.nbd.2009.06.010

Ohashi, R., Takao, K., Miyakawa, T., & Shiina, N. (2016). Comprehensive behavioral analysis of RNG105 (Caprin1) heterozygous mice: Reduced social interaction and attenuated response to novelty. Scientific Reports, 6, 20775. https://doi.org/10.1038/srep20775.

Okada, M., Ohtake, F., Nishikawa, H., Wu, W., Saeki, Y., Takana, K., & Ohta, T. (2015). Liganded ERα stimulates the E3 ubiquitin ligase activity of UBE3C to facilitate cell proliferation. *Molecular Endocrinology*, *29*(11), 1646–1657. https://doi.org/10.1210/me.2015-1125

Ramaswami, M., Taylor, J. P., & Parker, R. (2013). Altered Ribostasis : RNA-Protein Granules in Degenerative Disorders. *Cell*, *154*(4), 727-736. http://doi.org/10.1016/j.cell.2013.07.038

Reineke, L. C., & Neilson, J. R. (2019). Differences between acute and chronic stress granules, and how these differences may impact function in human disease. *Biochemical Pharmacology*, 162, 123-131.

https://doi.org/10.1016/j.bcp.2018.10.009

Shah, M., Su, D., Scheliga, J. S., Pluskal, T., Boronat, S., Motamedchaboki, K., Campos, A., R., Qi, F., Hidalgo, E., Yanagida, M., & Wolf, D. A. (2016). A transcript-specific eIF3 complex mediates global translational control of energy metabolism. *Cell Reports*, *16*(7), 1891–1902. https://doi.org/10.1016/j.celrep.2016.07.006

Shiina, N. (2019). Liquid- and solid-like RNA granules form through specific scaffold proteins and combine into biphasic granules. *Journal of Biological Chemistry*, *294*(10), 3532–3548. https://doi.org/10.1074/jbc.RA118.005423

Shiina, N., & Nakayama, K. (2014). RNA granule assembly and disassembly modulated by nuclear factor associated with double-stranded RNA 2 and nuclear factor 45. *Journal of Biological Chemistry*, *289*(30), 21163–21180. https://doi.org/10.1074/jbc.M114.556365

Shiina, N., & Tokunaga, M. (2010). RNA granule protein 140 (RNG140), a paralog of RNG105 localized to distinct RNA granules in neuronal dendrites in the adult vertebrate brain. *Journal of Biological Chemistry*, *285*(31), 24260–24269. https://doi.org/10.1074/jbc.M110.108944

Shiina, N., Shinkura, K., & Tokunaga, M. (2005). A novel RNA-binding protein in neuronal RNA granules: regulatory machinery for local translation. *Journal of Neuroscience*, 25(17), 4420–4434. https://doi.org/10.1523/JNEUROSCI.0382-05.2005

Tahmasebi, S., Amiri, M., & Sonenberg, N. (2019). Translational control in stem cells. *Frontiers in Genetics*, *9*, 709. https://doi.org/10.3389/fgene.2018.00709

Tang, Y. T., Hu, T., Arterburn, M., Boyle, B., Bright, J. M., Palencia, S., Emtage, P., C., & Funk, W. D. (2005). The complete complement of C1q-domain-containing

proteins in Homo sapiens. *Genomics*, *86*(1), 100–111. https://doi.org/10.1016/j.ygeno.2005.03.001

Teixeira, F. K., & Lehmann, R. (2019). Translational control during developmental transitions. *Cold Spring Harbor Perspectives in Medicine*, *11*(6), a032987. https://doi.org/10.1101/cshperspect.a032987

Valášek, L. S., Zeman, J., Wagner, S., Beznosková, P., Pavlíková, Z., Mohammad, M. P., Hronová, V., Herrmannová, A., Hashem, Y., & Gunišová, S. (2017). Embraced by eIF3: structural and functional insights into the roles of eIF3 across the translation cycle. *Nucleic Acids Research*, *45*(19), 10948–10968. https://doi.org/10.1093/nar/gkx805

Wang, B., & David, M. D., & Schrader, J. W. (2005). Absence of caprin-1 results in defects in cellular proliferation. *The Journal of Immunology*, *175*(7), 4274-4282. https://doi.org/10.4049/jimmunol.175.7.4274

Yu, J. S. L., & Cui, W. (2016). Proliferation, survival and metabolism: the role of PI3K/AKT/ mTOR signalling in pluripotency and cell fate determination. *Development*, *143*(17), 3050–3060. https://doi.org/10.1242/dev.137075

A

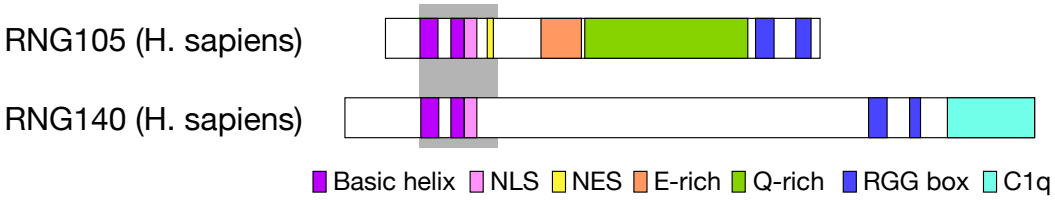
RNG105 (H. sapiens)
RNG140 (H. sapiens)
Basic helix
NLS
NES
E-rich
Q-rich
RGG box
C1q

B

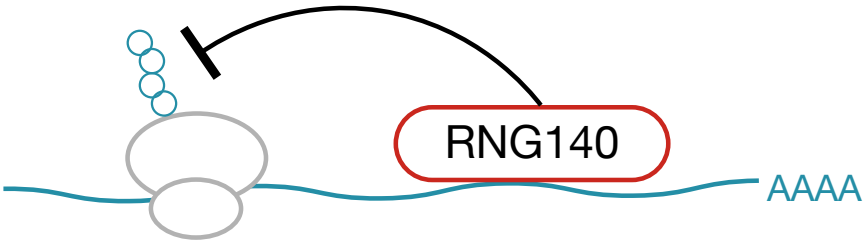
RNG140
AAAA

Fig. 1. RNG140 binds mRNA and inhibits its translation. *A*, shematic diagram showing the domain structures of RNG105 and RNG140 of *H. sapiens*. *Gray shadow* shows a highly conserved region between them. *B*, RNG140 binds to mRNA and repress translation, but the precise mechanism is unknown. Modified from Shiina & Tokunaga, 2010.

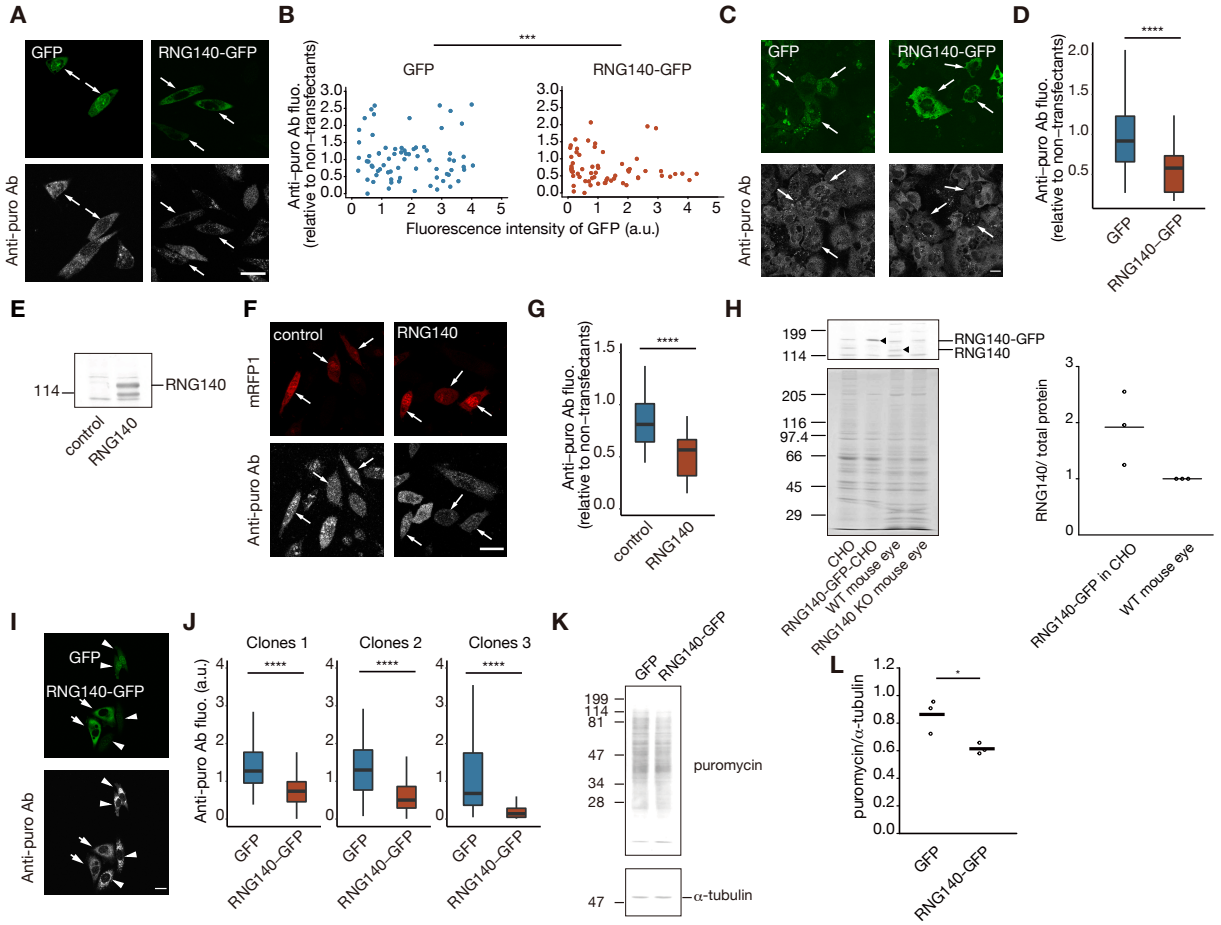
A
GFP
RNG140-GFP
Anti-puro Ab
B
***
GFP
RNG140-GFP
Anti−puro Ab fluo.
(relative to non−transfectants)
Fluorescence intensity of GFP (a.u.)
C
GFP
RNG140-GFP
Anti-puro Ab
D
****
Anti−puro Ab fluo.
(relative to non−transfectants)
GFP
RNG140-GFP
E
114
RNG140
control
RNG140
F
control
RNG140
mRFP1
Anti-puro Ab
G
****
Anti−puro Ab fluo.
(relative to non−transfectants)
control
RNG140
H
199
114
205
116
97.4
66
45
29
RNG140-GFP
RNG140
CHO
RNG140-GFP-CHO
WT mouse eye
RNG140 KO mouse eye
RNG140/ total protein
RNG140-GFP in CHO
WT mouse eye
I
GFP
RNG140-GFP
Anti-puro Ab
J
Clones 1
Clones 2
Clones 3
****
Anti-puro Ab fluo. (a.u.)
GFP
RNG140-GFP
K
GFP
RNG140-GFP
199
114
81
47
34
28
puromycin
47
α-tubulin
L
*
puromycin/α-tubulin
GFP
RNG140-GFP

Fig. 2. Decreased translation in RNG140-GFP-expressing CHO cells. *A*, CHO cells transiently transfected with GFP and RNG140-GFP were analyzed by ribopuromycilation assay to measure translation in cells. Arrows denote transfected cells. *Scale bars* in *A-I*, 20 μm. *B*, relationship between fluorescence intensities of GFP and puromycin staining in cells in *A*. Puromycin staining intensity of the transfected cells was compared with that of nearby untransfected control cells. GFP-expressing cells, n=72; RNG140-GFP-expressing cells, n=63; ***p=0.00123, main effect in ANCOVA. *C,* SRA 01/04 cells transiently transfected with GFP and RNG140-GFP were analyzed as in *A*. *D*, quantification of puromycin staining in cells in *C*. GFP-expressing cells, n=27; RNG140-GFP-expressing cells, n=39; **** p=0.000117, *t* test. *E*, Western blotting of CHO cells transiently transfected with RNG140 untagged with GFP with anti-RNG140 antibody. *F*, cells in *E* were analyzed by ribopuromycilation assay. Arrows denote transfected cells as judged by mRFP1 co-transfection. *G*, quantification of puromycin staining in cells in *F*. Control cells, n=17; RNG140-expressing cells, n=18 , ****p= 0.000680, t test. *H*, CHO cells stably transfected with RNG140-GFP (clone 1) and mouse eyes were analyzed by Western blotting with anti-RNG140 antibody (top) and Coomassie Brilliant Blue staining (bottom). RNG140-GFP expression levels, normalized to total protein levels, were compared to endogenous RNG140 expression levels in wild-type mouse eyes (right). Arrowheads indicate RNG140-GFP and endogenous RNG140 that was not detected in RNG140 knockout mice. See Fig. 7 for RNG140 knockout mice. *I*, CHO stable transfectants were analyzed by ribopuromycilation assay. Arrows and arrowheads indicate RNG140-GFP- and GFP-expressing cells, respectively. *J*, quantification of puromycin staining in cells in *I*. Results of 3 clones are shown. The numbers of cells

expressing GFP and RNG140-GFP are 132 and 101 (clones 1), 38 and 39 (clones 2), and 47 and 41 (clones 3), respectively. ****p<2.2e-16 (clones 1), ****p=1.23e-5 (clones 2), and ****p=3.78e-8 (clones 3), *t* test. *K*, the stable clones (clones 1) were analyzed by Western blotting for puromycin incorporation into nascent polypeptides and for α-tubulin as a control. *L*, Quantification of puromycin staining normalized to α-tubulin in *K*. n=3, *p= 0.0293, *t* test.

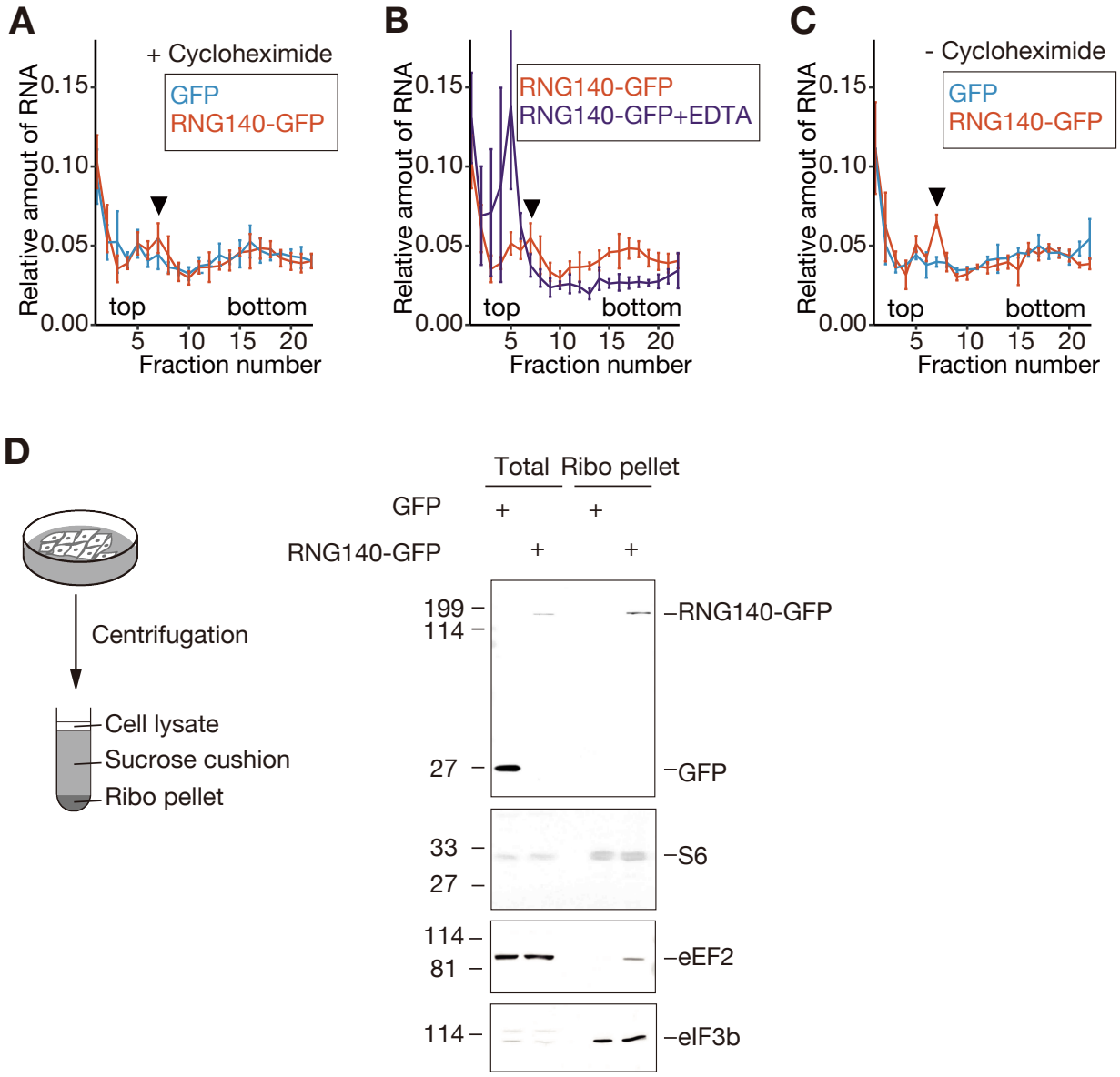
A
+ Cycloheximide
GFP
RNG140-GFP
Relative amout of RNA
0.15
0.10
0.05
0.00
top
bottom
5
10
15
20
Fraction number
B
RNG140-GFP
RNG140-GFP+EDTA
C
- Cycloheximide
D
Total
Ribo pellet
GFP
RNG140-GFP
Centrifugation
Cell lysate
Sucrose cushion
Ribo pellet
199
114
27
33
81
–RNG140-GFP
–GFP
–S6
–eEF2
–eIF3b

Fig. 3. Increased inactive ribosomes in RNG140-GFP-expressing CHO cells. *A-C* polysome profiles of CHO cells stably expressing GFP and RNG140-GFP analyzed by sucrose density gradient centrifugation. Shown are the relative amount of RNA in each fraction, normalized to the total amount of RNA in the 22 fractions. *A*, polysome profiling with cycloheximide. *B*, polysome profiling without or with EDTA, which dissociates polysome-associated ribosomes into 60S and 40S subunits. *C*, cycloheximide-free polysome profiling that allows ribosomes to drop-off from mRNA. Arrowheads denote the peak of 80S ribosomes. *D*, whole cell lysates (total) and ribosome pellets (Ribo pellet) from the CHO stable transfectants were immunoblotted with anti-RNG140, anti-ribosomal S6, anti-eEF2 and anti-eIF3b antibodies. Ribo pellet was prepared in the presence of cycloheximide through a sucrose cushion.

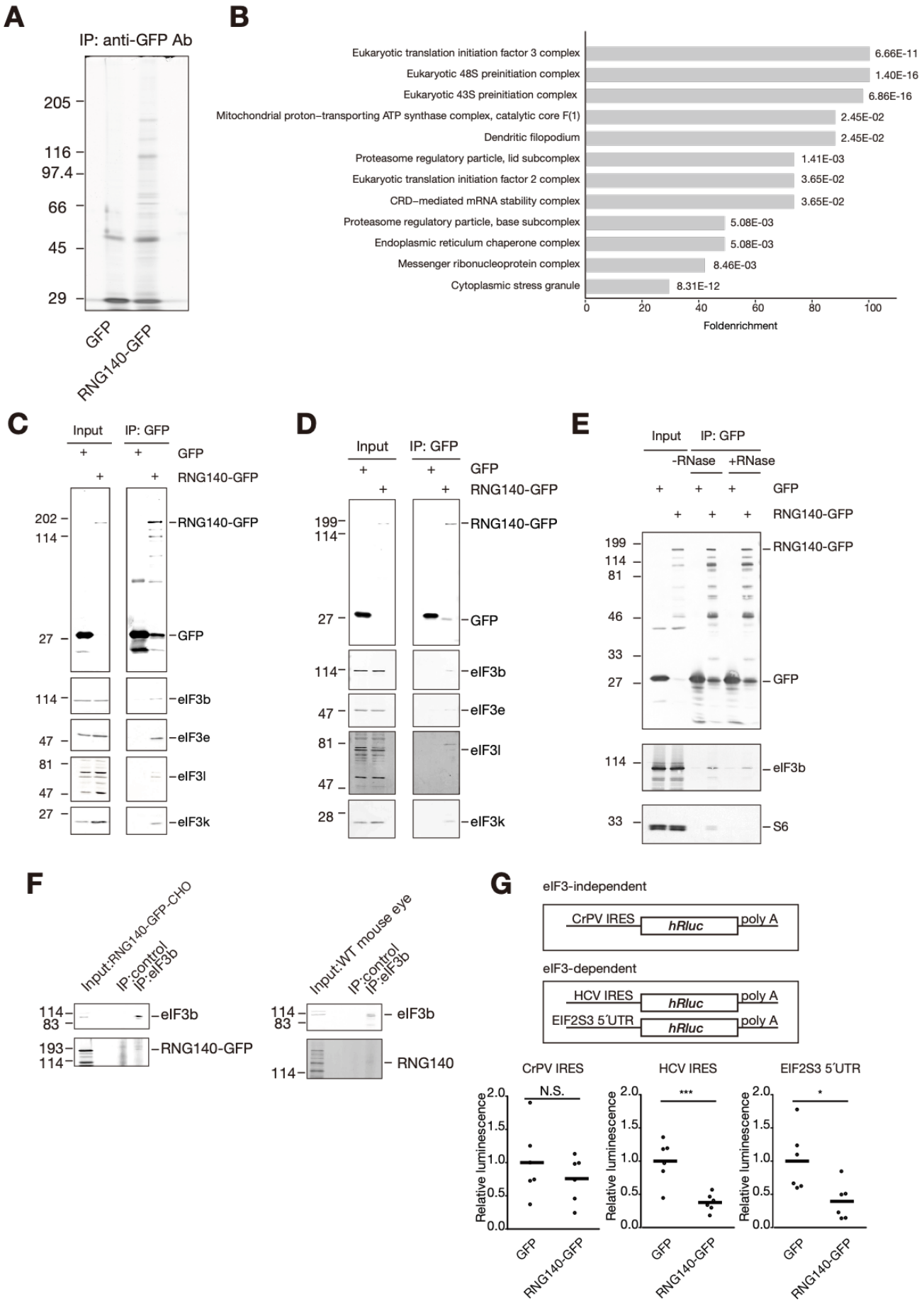
A
IP: anti-GFP Ab
205
116
97.4
66
45
29
GFP
RNG140-GFP
B
Eukaryotic translation initiation factor 3 complex
Eukaryotic 48S preinitiation complex
Eukaryotic 43S preinitiation complex
Mitochondrial proton−transporting ATP synthase complex, catalytic core F(1)
Dendritic filopodium
Proteasome regulatory particle, lid subcomplex
Eukaryotic translation initiation factor 2 complex
CRD−mediated mRNA stability complex
Proteasome regulatory particle, base subcomplex
Endoplasmic reticulum chaperone complex
Messenger ribonucleoprotein complex
Cytoplasmic stress granule
6.66E-11
1.40E-16
6.86E-16
2.45E-02
2.45E-02
1.41E-03
3.65E-02
3.65E-02
5.08E-03
5.08E-03
8.46E-03
8.31E-12
0
20
40
60
80
100
Foldenrichment
C
Input
IP: GFP
GFP
RNG140-GFP
202
114
27
114
47
81
47
27
RNG140-GFP
GFP
eIF3b
eIF3e
eIF3l
eIF3k
D
Input
IP: GFP
GFP
RNG140-GFP
199
114
27
114
47
81
47
28
RNG140-GFP
GFP
eIF3b
eIF3e
eIF3l
eIF3k
E
Input
IP: GFP
-RNase
+RNase
GFP
RNG140-GFP
199
114
81
46
33
27
114
33
RNG140-GFP
GFP
eIF3b
S6
F
Input:RNG140-GFP-CHO
IP:control
IP:eIF3b
114
83
193
114
eIF3b
RNG140-GFP
Input:WT mouse eye
IP:control
IP:eIF3b
114
83
114
eIF3b
RNG140
G
eIF3-independent
CrPV IRES
hRluc
poly A
eIF3-dependent
HCV IRES
hRluc
poly A
EIF2S3 5´UTR
hRluc
poly A
CrPV IRES
HCV IRES
EIF2S3 5´UTR
N.S.
***
*
Relative luminescence
2.0
1.5
1.0
0.5
0.0
GFP
RNG140-GFP

Fig. 4. RNG140 binds with eIF3 and reduces eIF3-dependent translation in CHO cells. *A*, immunoprecipitates with an anti-GFP antibody from CHO cells stably expressing GFP and RNG140-GFP were silver-stained after SDS-PAGE. *B*, Gene ontology enrichment analysis of RNG140-associated proteins. eIF3 subunit proteins and small ribosomal subunit proteins were included in the top categories. *C*, input extracts and the immunoprecipitates from the CHO stable transfectants were immunoblotted with anti-GFP and anti-eIF3 subunits antibodies. *D*, experiments similar to *C* using SRA 01/04 transient transfectants. *E*, immunoprecipitation from the CHO stable transfectants in the presence or absence of RNase A. Immunoprecipitates were immunoblotted with anti-GFP, anti-eIF3b, and anti-ribosomal S6 antibodies. *F*, input extracts and immunoprecipitates with anti-eIF3b antibody from CHO cells stably expressing RNG140-GFP were immunoblotted with anti-GFP antibody (top). Similar experiments using P0.5 wild-type mouse eyes were probed with anti-RNG140 antibody (bottom). *G*, CHO cells stably expressing GFP and RNG140-GFP were transfected with a reporter construct in which luciferase is translated under the control of CrPV IRES (left), HCV IRES (middle) or EIF2S3 5′UTR (right), and evaluated for luciferase activity. n=6, ***p=0.0015, *p=0.0209, N.S., p=0.373, *t* test.

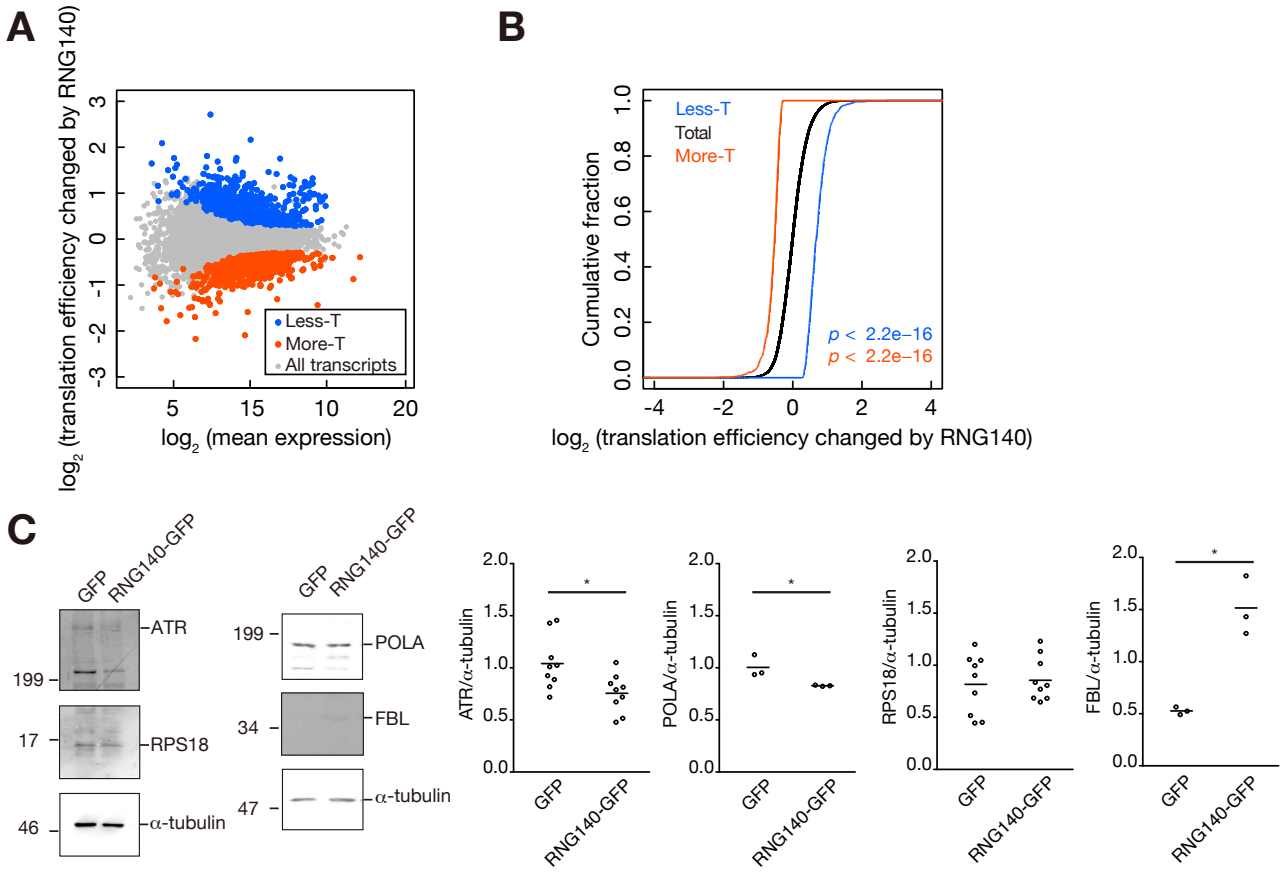
A
log2 (translation efficiency changed by RNG140)
log2 (mean expression)
Less-T
More-T
All transcripts
B
Cumulative fraction
log2 (translation efficiency changed by RNG140)
Less-T
Total
More-T
p < 2.2e−16
p < 2.2e−16
C
GFP
RNG140-GFP
ATR
RPS18
α-tubulin
POLA
FBL
ATR/α-tubulin
POLA/α-tubulin
RPS18/α-tubulin
FBL/α-tubulin

Fig. 5. RNG140 reduces translation of a set of mRNAs in CHO cells. *A*, an MA plot of mean transcript expression and the fold change in translation efficiency of the transcripts by RNG140 stable expression in CHO cells. Transcripts with decreased and increased translation efficiency by RNG140 expression (more-T and less-T, respectively) were identified statistically from two independent experiments with ribosome profiling and RNA-seq analysis. *B*, cumulative distribution fraction plots showing changes in translation efficiency of total transcripts and transcripts in the more-T and less-T groups by RNG140 expression. Significance is calculated by Mann–Whitney U-test. *C*, the stable clones (clones 1) were analyzed by Western blotting for proteins translated from more-T (Atr and Pola1) and less-T (Rps18 and Fbl). Their band intensities were normalized to those of α-tubulin. ATR, n=9, *p=0.0149; POLA, n=3, *p=0.0444; RPS18, n=9, p=0.676; FBL, n=3, *p=0.0252, *t* test.

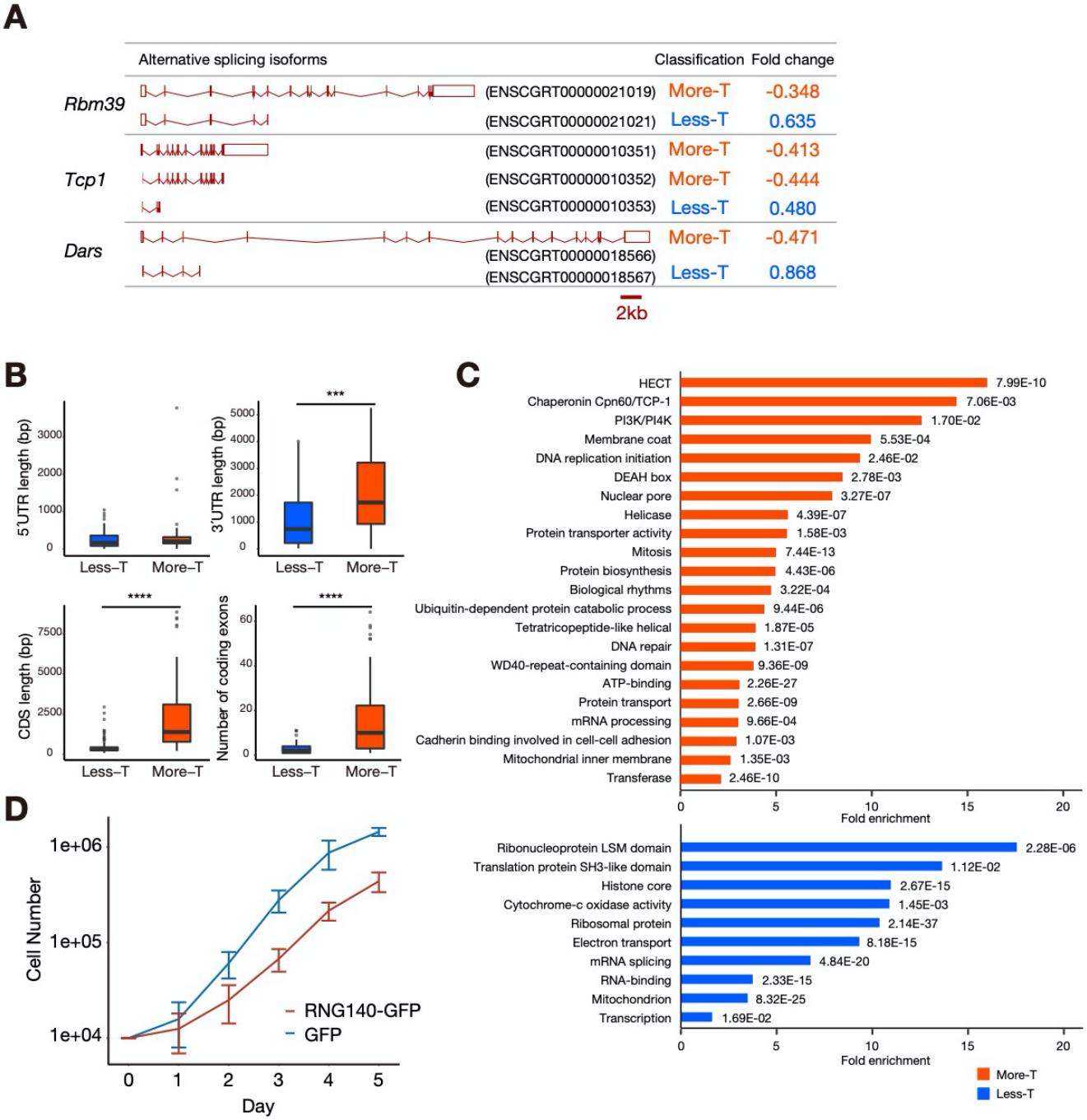
A
Alternative splicing isoforms
Classification
Fold change
Rbm39
(ENSCGRT00000021019)
More-T
-0.348
(ENSCGRT00000021021)
Less-T
0.635
Tcp1
(ENSCGRT00000010351)
More-T
-0.413
(ENSCGRT00000010352)
More-T
-0.444
(ENSCGRT00000010353)
Less-T
0.480
Dars
More-T
-0.471
(ENSCGRT00000018566)
(ENSCGRT00000018567)
Less-T
0.868
2kb
B
5'UTR length (bp)
3'UTR length (bp)
CDS length (bp)
Number of coding exons
Less–T
More–T
***
****
C
HECT 7.99E-10
Chaperonin Cpn60/TCP-1 7.06E-03
PI3K/PI4K 1.70E-02
Membrane coat 5.53E-04
DNA replication initiation 2.46E-02
DEAH box 2.78E-03
Nuclear pore 3.27E-07
Helicase 4.39E-07
Protein transporter activity 1.58E-03
Mitosis 7.44E-13
Protein biosynthesis 4.43E-06
Biological rhythms 3.22E-04
Ubiquitin-dependent protein catabolic process 9.44E-06
Tetratricopeptide-like helical 1.87E-05
DNA repair 1.31E-07
WD40-repeat-containing domain 9.36E-09
ATP-binding 2.26E-27
Protein transport 2.66E-09
mRNA processing 9.66E-04
Cadherin binding involved in cell-cell adhesion 1.07E-03
Mitochondrial inner membrane 1.35E-03
Transferase 2.46E-10
Fold enrichment
Ribonucleoprotein LSM domain 2.28E-06
Translation protein SH3-like domain 1.12E-02
Histone core 2.67E-15
Cytochrome-c oxidase activity 1.45E-03
Ribosomal protein 2.14E-37
Electron transport 8.18E-15
mRNA splicing 4.84E-20
RNA-binding 2.33E-15
Mitochondrion 8.32E-25
Transcription 1.69E-02
Fold enrichment
More-T
Less-T
D
Cell Number
Day
RNG140-GFP
GFP

Fig. 6. RNG140 reduces translation of mRNAs that are long and associated with proliferation in CHO cells. *A*, structure of alternative splicing isoforms of *Rbm39*, *Tcp1*, and *Dars*. Open box, UTR; closed box, CDS; line, intron. Ensembl transcript ID, classification into more-T and less-T, and the fold change (log_2) in translation efficiency by RNG140 expression are indicated to the right of each transcript. *B*, the top 100 transcripts in the more-T and less-T groups were analyzed for 5′UTR length, 3′UTR length, CDS length, and the number of coding exons. ***p=0.00237, ****p=1.02e-12 for CDS length, ****p=3.85e-12 for the number of coding exons, *t* test. *C*, gene ontology enrichment analysis of the more-T (red) and less-T (blue) groups. *D*, cell proliferation measurement of CHO cells stably expressing GFP and RNG140-GFP. *D*, the top 100 transcripts in the more-T and less-T groups were analyzed for 5′UTR length, 3′UTR length, CDS length, and the number of coding exons. ***p=0.00237, ****p=1.02e-12 for CDS length, ****p=3.85e-12 for the number of coding exons, *t* test. *E*, gene ontology enrichment analysis of the more-T (red) and less-T (blue) groups. *F*, cell proliferation measurement of CHO cells stably expressing GFP and RNG140-GFP.

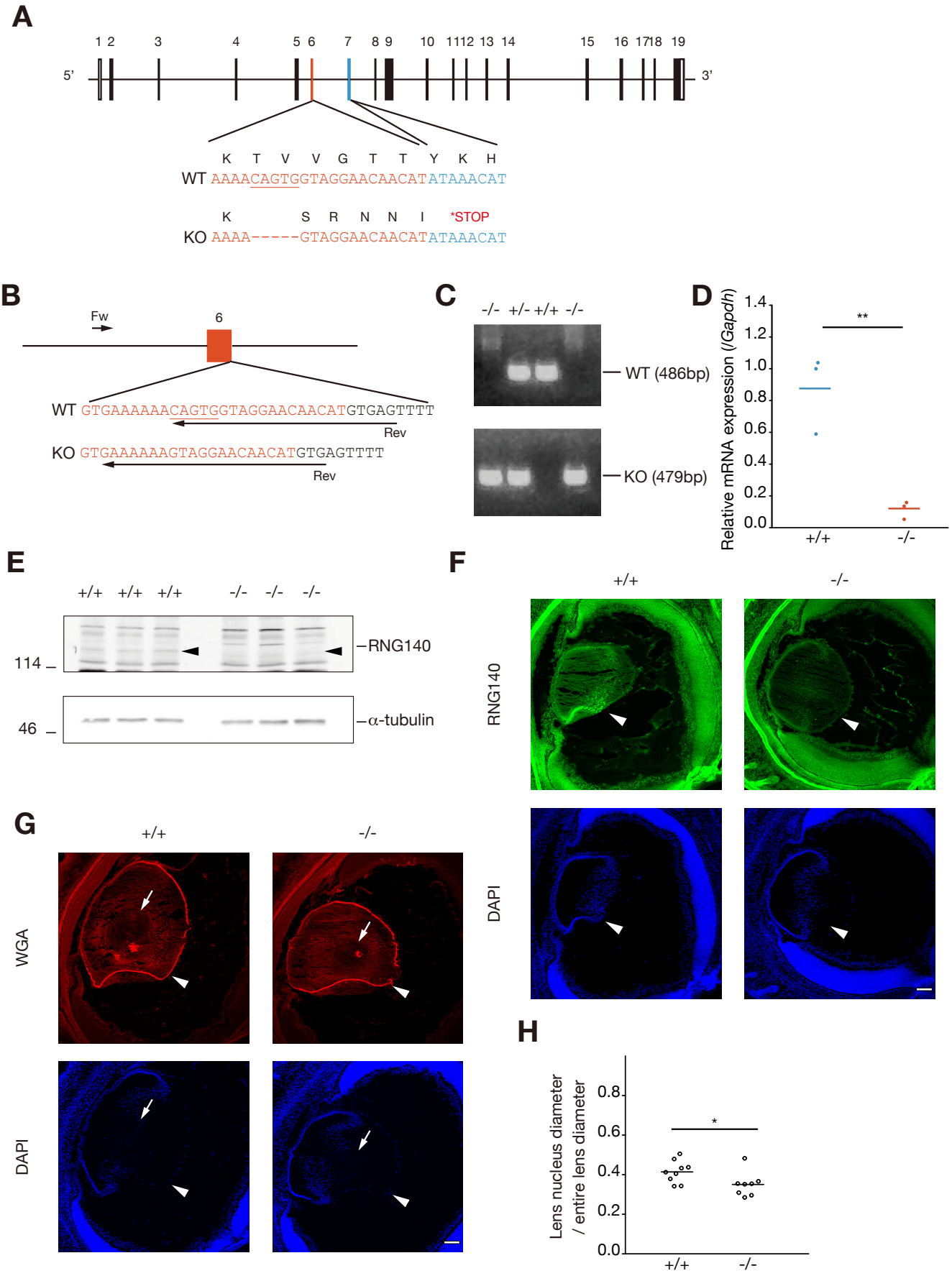
A
1 2 3 4 5 6 7 8 9 10 1112 13 14 15 16 1718 19
5'
3'
K T V V G T T Y K H
WT AAAACAGTGGTAGGAACAACATATAAACAT
K S R N N I *STOP
KO AAAA-----GTAGGAACAACATATAAACAT
B
Fw
6
WT GTGAAAAAACAGTGGTAGGAACAACATGTGAGTTTT
Rev
KO GTGAAAAAAGTAGGAACAACATGTGAGTTTT
Rev
C
-/- +/- +/+ -/-
WT (486bp)
KO (479bp)
D
Relative mRNA expression (/Gapdh)
1.4
1.2
1.0
0.8
0.6
0.4
0.2
0.0
**
+/+
-/-
E
+/+ +/+ +/+ -/- -/- -/-
114
RNG140
46
α-tubulin
F
+/+
-/-
RNG140
DAPI
G
+/+
-/-
WGA
DAPI
H
Lens nucleus diameter / entire lens diameter
0.8
0.6
0.4
0.2
0.0
*
+/+
-/-

Fig. 7. Generation of RNG140 knockout mice. *A*, gene structure of the *Rng140* genome. Nucleotide and amino acid sequences of wild-type (upper) and *Rng140* knockout (lower) alleles are shown. The first lysine (K) corresponds to the 210th amino acid of total 1,031 amino acids of RNG140. 5-bp deletion in the exon 6 sequence (red) caused a frame-shift and generated a downstream premature stop codon in the exon7 sequence (blue). *B*, the genomic region around exon 6 and nucleotide sequences of wild-type and *Rng140* knockout alleles. Arrows indicate the primer sets for PCR genotyping in *C*. *C*, PCR genotyping of the indicated genotypes. *D*, qRT-PCR analysis of *Rng140* mRNA in P0.5 $Rng140^{+/+}$ and $Rng140^{-/-}$ mouse eyes using exon 2-4 primers. *Rng140* mRNA expression was normalized by that of *Gapdh* mRNA. n=3, **p=0.00667, *t* test. *E*, Western blotting of eyes from P0.5 $Rng140^{+/+}$ and $Rng140^{-/-}$ mice for RNG140 and α-tubulin as a control. Arrowheads indicate the position of RNG140. *F*, staining of P0.5 eye slices with anti-RNG140 antibody and DAPI. Arrowheads indicate lens. *Scale bar*, 100 μm. *G*, staining of P0.5 eye slices with WGA and DAPI. Arrowheads and arrows indicate the lens and lens nucleus, respectively. *Scale bar*, 100 μm. *H*, quantification of lens nucleus diameter normalized to lens diameter. $Rng140^{+/+}$ mice, n=9; $Rng140^{-/-}$ mice, n=8; *p=0.0377. *t* test.

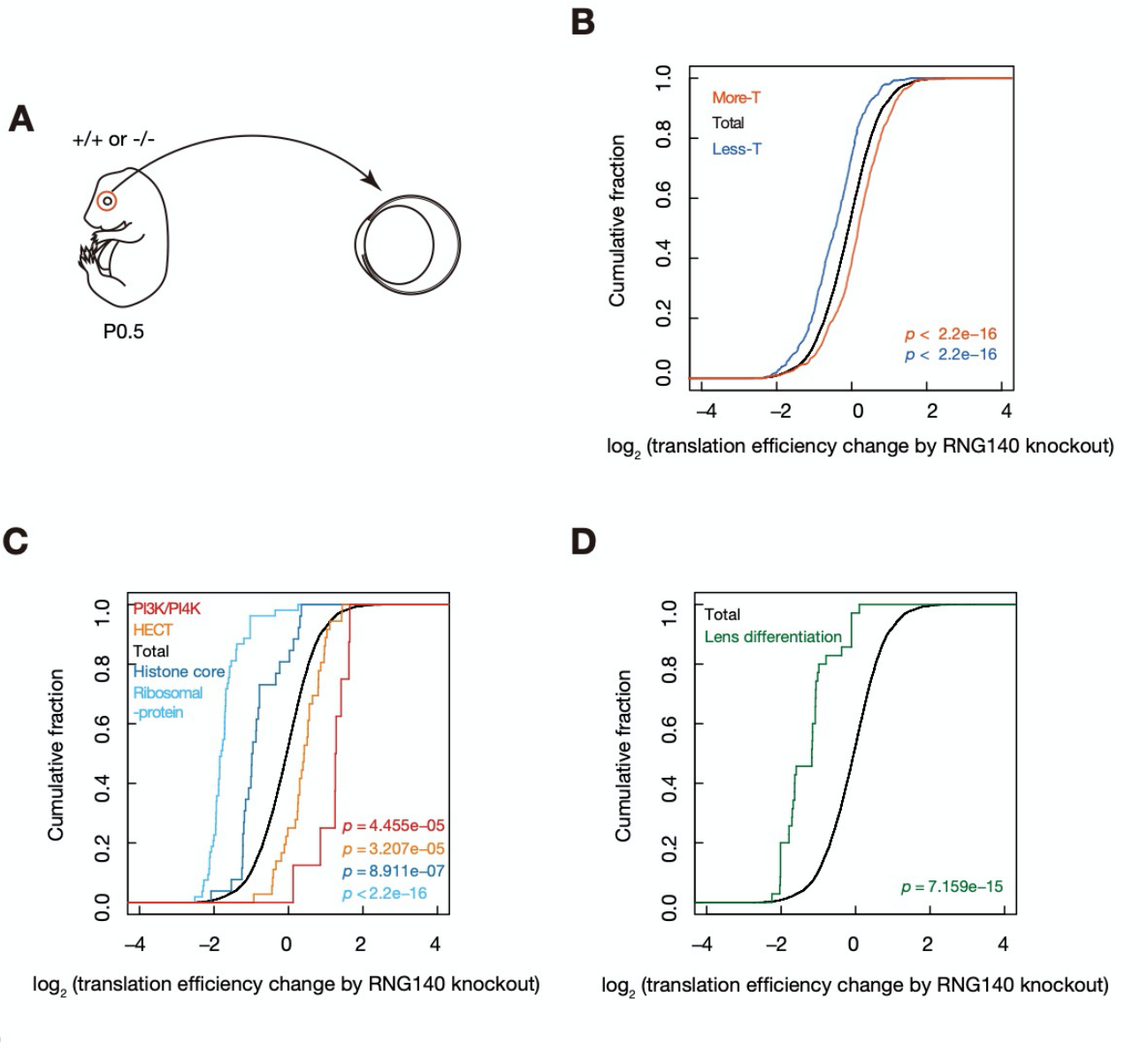
A
+/+ or -/-
P0.5
B
More-T
Total
Less-T
Cumulative fraction
p < 2.2e–16
p < 2.2e–16
log2 (translation efficiency change by RNG140 knockout)
C
PI3K/PI4K
HECT
Total
Histone core
Ribosomal
-protein
p = 4.455e–05
p = 3.207e–05
p = 8.911e–07
p < 2.2e–16
log2 (translation efficiency change by RNG140 knockout)
D
Total
Lens differentiation
p = 7.159e–15
log2 (translation efficiency change by RNG140 knockout)
E
5'UTR length (bp)
3'UTR length (bp)
CDS length (bp)
Number of coding exons
Transcripts whose translation efficiency is decreased by RNG140 knockout
Transcripts whose translation efficiency is increased by RNG140 knockout

Fig. 8. RNG140 deficiency in mouse eyes has an effect on translation efficiency that is opposite to the effect of RNG140 overexpression in CHO cells. *A*, mouse eyes were isolated from P0.5 *Rng140*$^{+/+}$ and *Rng140*$^{-/-}$ mice, and subjected to ribosome profiling. *B-D*, cumulative distribution fraction plots showing changes in translation efficiency of transcripts in the indicated groups by RNG140 knockout. Significance is calculated by Mann–Whitney U-test. *B*, total transcripts and transcripts corresponding to those in the more-T and less-T groups in the CHO ribosome profiling are plotted. *C*, transcripts corresponding to more-T enriched in "HECT" and "PI3K/PI4K", and less-T enriched in "Histone core" and "Ribosomal protein" in the CHO ribosome profiling are plotted. See Table S8 for the transcripts included in each group. *D*, transcripts encoding lens differentiation-related proteins, α-, β-, and γ-crystallins (*Crya*, *Cryb*, and *Cryg*), lens major intrinsic protein (*Mip*), CP115 (*Bfsp1*), and CP49 (*Bfsp2*) are plotted. See Table S8 for the transcripts included. *E*, top 100 transcripts of which translation efficiency was decreased and increased by RNG140 knockout were analyzed for 5′UTR length, 3′UTR length, CDS length, and the number of coding exons. ***p=0.00373 for 5′UTR length, ****p=6.79e-6 for 3′UTR length, ****p=0.000211 for CDS length, and ****p=1.61e-8 for the number of coding exons.

A

RNG140 dependent

B

General mode of eIF3

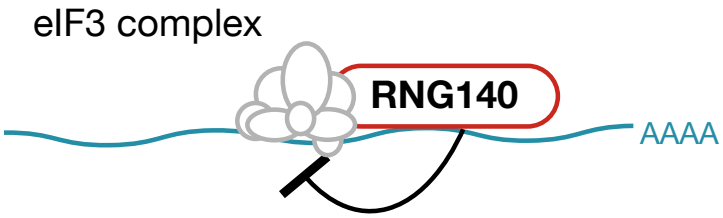

Selective mode of eIF3

Fig. 9. Models of translation repression by RNG140. *A*, RNG140 binds preferentially to long mRNAs and inhibits their translation through binding with eIF3. Short mRNAs are less bound by RNG140 and escape translation inhibition by RNG140. *B*, an alternative model in which the mRNA length selectivity depends on the properties of eIF3. eIF3 not only acts as a general translation initiation factor, but also targets selective and possibly short mRNAs in some cases. If RNG140 inhibits only the general mode but not the selective mode, short mRNAs would escape translation inhibition by RNG140.

Supplementary Table 1. RNG140-associated proteins identified by mass spectrometry

Accession	Gene symbol	Description	Score Mascot	Score ratio (RNG140-GFP/GFP)	Coverage [%]	Num. of peptide matches	Mass [Da]	emPAI
ALL27017.1	CAPRIN2	RNG140 (cytoplasmic activation/proliferation-associated protein 2)	11197	287.10	47	574	114208	6.56
pir|S31716|	HSPA8	heat shock cognate 71 kDa protein	4123	5.50	57	167	70884	10.1
NP_037215.1	HSPA5	endoplasmic reticulum chaperone BiP precursor	2451	10.47	45	100	72302	8.44
NP_001027985.1	TUBB	tubulin beta chain	1470	2.84	36	54	49639	5.06
ACJ13448.1	RPSA	40S ribosomal protein SA	1317	5.58	34	45	32699	3.15
WP_087674316.1	RPS3	30S ribosomal protein S3	1177	–	68	57	26657	51.69
NP_035862.2	YBX1	Y-box-binding protein 1	1058	–	50	33	35709	3.16
NP_001029835.1	TUBB4B	tubulin beta-4B chain	1056	2.93	36	42	49799	3.65
NP_075768.1	TUBB3	tubulin beta-3 chain	960	–	25	34	50386	2
P13383.3	NCL	nucleolin	881	–	22	36	77101	1.42
NP_001011995.1	TUBA1C	tubulin alpha-1C chain	869	–	39	37	49905	2.3
NP_071796.2	PLEC	plectin isoform 1	803	–	12	68	533370	0.61
AAD56625.1	NRP	nucleolin-related protein NRP	787	12.30	14	30	77393	0.84
NP_659554.1	SERBP1	plasminogen activator inhibitor 1 RNA-binding protein	691	–	33	33	42958	3.41
NP_058849.1	RPS3A	40S ribosomal protein S3a	626	–	47	30	29926	11.7
NP_598249.1	G3BP1	ras GTPase-activating protein-binding protein 1	566	–	43	31	51755	3.78
BAA05907.1	YBX3	Y-box-binding protein 3	543	17.52	24	19	31182	1.26
EDM01231.1	FXR1	fragile X mental retardation syndrome-related protein 1	508	–	22	32	76163	1.19
EDM15826.1	EIF3L	eukaryotic translation initiation factor 3 subunit L	499	–	30	20	66668	1.61
NP_001011990.1	EIF3E	eukaryotic translation initiation factor 3 subunit E	452	–	32	20	52187	4.12
EDL91929.1	HDLBP	vigilin	445	–	14	23	143044	0.61
NP_001020846.1	TUBB6	tubulin beta chain	418	–	22	17	50027	1.15
NP_599180.1	PABPC1	polyadenylate-binding protein 1	411	–	27	24	70656	1.79
NP_001094132.1	EIF3C	eukaryotic translation initiation factor 3 subunit C	384	–	8	18	105369	0.33
NP_000998.1	RPS4X	40S ribosomal protein S4, X isoform	375	–	37	15	29579	5.44
P48721.3	HSPA9	Stress-70 protein, mitochondrial	347	–	25	12	73812	1
NP_001004378.1	RACK1	receptor of activated protein C kinase 1	321	–	23	14	35055	1.33
NP_001264231.1	EIF3F	eukaryotic translation initiation factor 3 subunit F	309	–	26	11	37973	1.45
NP_001012197.2	HSP90B1	endoplasmin	305	–	15	13	92713	0.66
NP_742005.1	CANX	calnexin	300	–	10	8	67213	0.37
XP_006256714.1	DDX3X	DEAD-box helicase 3, X-linked	293	–	20	15	73100	1.14
XP_008763467.1	CKAP4	cytoskeleton-associated protein 4	270	3.14	12	9	77017	0.65
NP_001094117.1	FXR2	fragile X mental retardation syndrome-related protein 2	250	–	6	10	74329	0.26
BAA03136.1	HNRNPU	heterogeneous nuclear ribonucleoprotein U	248	–	11	12	87694	0.48
ACI04543.1	DDX5	DEAD (Asp-Glu-Ala-Asp) box polypeptide 5	247	–	21	14	69069	0.86
NP_062770.1	SYNCRIP	heterogeneous nuclear ribonucleoprotein Q	247	–	14	13	62633	0.85
AAB02288.1	ATP5F1B	ATP synthase subunit beta, mitochondrial	243	4.42	18	11	51171	0.79
NP_001101959.2	IQGAP1	IQ motif containing GTPase activating protein 1	240	–	6	10	188714	0.23
NP_032857.1	PHB	prohibitin	228	–	33	7	29802	1.71
NP_001032362.1	HNRNPF	heterogeneous nuclear ribonucleoprotein F	227	2.91	19	8	45701	0.59
P85125.1	CAVIN1	Caveolae-associated protein 1	225	–	16	6	43882	0.62
NP_062804.1	PRMT1	protein arginine N-methyltransferase 1	219	–	12	9	42408	0.49
NP_001099367.2	CCT8	T-complex protein 1 subunit theta	214	3.96	17	9	59550	0.91
EDL80377.1	PABPC4	polyadenylate-binding protein	213	–	10	9	69323	0.54
NP_001028855.1	VAT1	Synaptic vesicle membrane protein VAT-1 homolog	209	–	13	5	43091	0.64
AAC52531.1	PDAP1	28 kDa heat- and acid-stable phosphoprotein	207	–	38	7	20523	3.19
EDM06373.1	PSMC5	26S proteasome regulatory subunit 8	196	–	26	8	46535	1.08
NP_001108507.1	EIF3I	eukaryotic translation initiation factor 3 subunit I	195	–	31	12	36438	1.85
NP_001012104.1	DDOST	dolichyl-diphosphooligosaccharide--protein glycosyltransferase 48 kDa subunit	192	–	10	4	48865	0.42
NP_062229.1	EIF2S1	eukaryotic translation initiation factor 2 subunit 1	183	–	24	6	36085	1.03
ABD77309.1	SDHA	succinate dehydrogenase [ubiquinone] flavoprotein subunit, mitochondrial	181	–	7	3	61029	0.23
NP_942046.1	EIF3H	eukaryotic translation initiation factor 3 subunit H	178	–	29	8	39880	1.35
NP_001013113.1	EIF3G	eukaryotic translation initiation factor 3 subunit G	177	–	9	7	35629	0.43
NP_001003.1	RPS8	40S ribosomal protein S8	173	5.41	23	4	24190	1.01
EDM06287.1	NSF	vesicle-fusing ATPase	172	2.77	13	8	80040	0.53
EDM03871.1	RPS2	40S ribosomal protein S2	170	–	14	8	28571	0.81
NP_005007.2	PCBP2	poly(rC)-binding protein 2	163	–	12	6	38627	0.39
NP_001004283.1	EIF3D	eukaryotic translation initiation factor 3 subunit D	160	–	19	9	63948	0.6
AAA40784.1	ATP5F1A	ATP synthase subunit alpha, mitochondrial	160	–	14	7	58790	0.66
NP_001014011.1	G3BP2	ras GTPase-activating protein-binding protein 2	159	–	17	6	50739	0.65
P07153.1	RPN1	Dolichyl-diphosphooligosaccharide--protein glycosyltransferase subunit 1	153	–	20	9	68262	0.65
NP_035869.1	YWHAQ	14-3-3 protein theta	151	2.85	13	4	27761	0.84
AAD19638.1	PRM10	nucleic acid binding factor pRM10	151	–	15	5	33794	0.46
NP_955412.1	EIF2S2	eukaryotic translation initiation factor 2 subunit 2	150	–	12	4	38219	0.56
BAF79675.1	HNRNPA2B1	heterogeneous nuclear ribonucleoproteins A2/B1	148	–	19	5	36032	0.8
EDM10176.1	MAP1B	microtubule-associated protein 1b	148	–	5	9	255587	0.16
AAA41008.1	CYB5R3	NADH-cytochrome b5 reductase 3	148	3.61	17	4	34119	0.64
NP_001001.2	RPS6	40S ribosomal protein S6	146	4.56	15	8	28663	1.09
EDM15798.1	DDX17	DEAD-box helicase 17	145	–	8	8	58317	0.44
NP_573505.2	RBM39	RNA-binding protein 39	143	–	9	4	59370	0.33
O35824.1	DNAJA2	DnaJ homolog subfamily A member 2	141	3.13	13	6	45737	0.75
NP_001292806.1	MYH9	myosin-9	137	–	4	8	226273	0.16
NP_001011969.1	STRAP	serine-threonine kinase receptor-associated protein	137	3.81	14	3	38432	0.39
NP_112297.1	GNAI2	guanine nucleotide-binding protein G(i) subunit alpha-2	135	–	15	5	40473	0.69
NP_001161995.1	EIF3M	eukaryotic translation initiation factor 3 subunit M	134	–	15	3	42490	0.35
EDM04884.1	EIF4A1	eukaryotic translation initiation factor 4A1	123	3.32	15	5	44579	0.61
NP_001126766.1	HNRNPK	heterogeneous nuclear ribonucleoprotein K	122	–	10	3	50996	0.28
AAB07073.1	FMR1	synaptic functional regulator FMR1	118	–	3	4	61916	0.15
AAI68749.1	PSMD11	26S proteasome non-ATPase regulatory subunit 11	117	–	10	4	47938	0.43
AAH61542.1	PSMC2	26S proteasome regulatory subunit 7	117	–	10	5	48587	0.42
CAA55891.1	PDIA6	protein disulfide-isomerase A6	115	–	6	2	47191	0.2
EDL83733.1	SNX9	sorting nexin-9	114	–	6	2	43804	0.21
AAH62235.1	HNRNPA1	heterogeneous nuclear ribonucleoprotein A1	111	–	13	5	33599	0.66
AAH63811.1	RPL4	60S ribosomal protein L4	109	–	5	3	47271	0.31
NP_001008281.1	LRRC59	leucine-rich repeat-containing protein 59	109	–	12	3	34848	0.44
NP_001102318.1	ELAVL1	ELAV-like protein 1	108	–	10	3	36146	0.42
NP_942048.1	RPL3	60S ribosomal protein L3	108	–	5	5	46107	0.2
EDL93727.1	LTV1	LTV1 homolog	103	–	13	7	46966	0.44

NP_001102395.1	PSMD13	26S proteasome non-ATPase regulatory subunit 13	101	–	7	3	42790	0.35
NP_062250.1	YWHAB	14-3-3 protein beta/alpha	100	–	17	5	28037	1.12
NP_113808.1	PHGDH	D-3-phosphoglycerate dehydrogenase	99	–	4	2	56457	0.16
NP_001008694.1	RCN3	reticulocalbin-3	99	–	8	3	37918	0.4
EDL94579.1	EIF3A	eukaryotic translation initiation factor 3 subunit A	97	–	4	8	163069	0.14
NP_001026810.1	EIF3B	eukaryotic translation initiation factor 3 subunit B	97	–	5	6	90854	0.21
NP_445866.1	DDX1	ATP-dependent RNA helicase DDX1	95	–	9	6	82445	0.36
NP_001158143.1	DNAJA1	dnaJ homolog subfamily A member 1	95	–	10	3	44839	0.33
NP_001011901.1	HSPH1	heat shock protein 105 kDa	93	–	2	2	96357	0.09
EDL88713.1	TPD52L2	tumor protein D54	92	–	13	2	19933	0.52
NP_640354.1	HSPBP1	hsp70-binding protein 1	89	–	12	6	39151	0.54
CAA06295.1	RT1-CE5	MHC class Ib antigen	89	–	2	2	37565	0.12
NP_001127322.1	YWHAG	14-3-3 protein gamma	88	–	11	4	28285	0.82
NP_001004223.1	EEF1G	elongation factor 1-gamma	86	–	6	3	50029	0.29
AAP92615.1	-	Ab2-417	84	–	3	2	107343	0.08
P35435.2	ATP5F1C	ATP synthase subunit gamma, mitochondrial	83	–	12	3	30172	0.52
NP_058967.1	NUDC	nuclear migration protein nudC	83	–	6	2	38388	0.25
Q80WL2.3	BYSL	bystin	80	–	7	4	49980	0.41
NP_604444.1	CAVIN3	caveolae-associated protein 3	79	–	13	4	27894	0.83
EDM06698.1	JMJD6	bifunctional arginine demethylase and lysyl-hydroxylase JMJD6	75	–	2	7	31956	0.14
Q63617.1	HYOU1	Hypoxia up-regulated protein 1	75	–	6	5	111220	0.21
NP_001008282.1	PSMD3	26S proteasome non-ATPase regulatory subunit 3	75	–	10	5	60650	0.42
EDL95706.1	PKM	pyruvate kinase PKM	74	–	7	5	45215	0.33
NP_001005875.1	PSMD12	26S proteasome non-ATPase regulatory subunit 12	74	–	4	2	52903	0.17
EDM10361.1	DHX29	ATP-dependent RNA helicase DHX29	74	–	1	3	136474	0.06
NP_036915.1	BSG	basigin	74	–	6	2	29567	0.33
AAH99240.1	STUB1	STIP1 homology and U box-containing protein 1	73	–	14	3	25382	0.65
EDL92601.1	KARS1	lysine--tRNA ligase	70	–	4	2	57334	0.16
NP_037080.1	EMD	emerin	69	–	8	2	29657	0.33
NP_112361.1	RPL5	60S ribosomal protein L5	67	–	11	5	34437	0.45
NP_000964.1	RPL8	60S ribosomal protein L8	67	–	10	2	28007	0.35
NP_001102077.1	CSE1L	exportin-2	67	–	5	4	110144	0.17
NP_446195.1	CDC37	hsp90 co-chaperone Cdc37	66	–	8	2	44348	0.21
AAI66407.1	YTHDF2	Ythdf2 protein	64	–	6	5	62302	0.32
NP_663397.1	RTCB	tRNA-splicing ligase RtcB homolog	62	–	3	3	55214	0.17
NP_062115.1	IFRD1	interferon-related developmental regulator 1	62	–	5	2	49751	0.19
EDM07249.1	LDHA	l-lactate dehydrogenase A chain	61	–	6	2	32133	0.3
BAB03465.1	HNRNPD	heterogeneous nuclear ribonucleoprotein D0	60	–	6	2	38168	0.25
Q9Z2G8.1	NAP1L1	nucleosome assembly protein 1-like 1	58	–	9	4	45286	0.33
NP_001071138.1	EIF3J	eukaryotic translation initiation factor 3 subunit J	55	–	18	4	29169	0.54
P86252.1	PURA	RTranscriptional activator protein Pur-alpha	54	–	23	2	15313	0.72
EDM03561.1	PSMA3	proteasome subunit alpha type-3	52	–	10	2	22064	0.46
NP_598302.1	HADHB	trifunctional enzyme subunit beta, mitochondrial	51	–	5	2	51382	0.18
NP_659558.1	ARFGAP1	ADP-ribosylation factor GTPase-activating protein 1	50	–	5	2	45415	0.21
EDM18410.1	SERPINH1	serpin H1	50	–	2	2	44983	0.1
AAH91286.1	EIF2S3	eukaryotic translation initiation factor 2 subunit 3, X-linked	50	–	2	2	44392	0.1
NP_001108496.1	LMAN2	vesicular integral-membrane protein VIP36	48	–	10	2	40367	0.23
NP_032974.2	PSMC3	26S proteasome regulatory subunit 6A	47	–	6	2	49518	0.19
AAD44358.1	PUF60	poly(U)-binding-splicing factor PUF60	47	–	3	2	60250	0.15
NP_036004.2	PSMC4	26S proteasome regulatory subunit 6B	46	–	4	3	47379	0.31
EDL88050.1	FKBP9	peptidyl-prolyl cis-trans isomerase FKBP9	45	–	2	2	65678	0.14
Q00438.1	PTBP1	polypyrimidine tract-binding protein 1	45	–	1	2	59317	0.07
NP_446316.1	VCP	transitional endoplasmic reticulum ATPase	44	–	2	2	89293	0.1
EDM15030.1	SLC25A13	calcium-binding mitochondrial carrier protein Aralar2	44	–	3	2	62464	0.15
BAA76607.1	BAG6	large proline-rich protein BAG6	44	–	2	2	114859	0.08
NP_001100831.1	LARP4B	la-related protein 4B	42	–	2	2	81136	0.11
EDM05622.1	SRSF1	serine/arginine-rich splicing factor 1	41	–	13	3	24565	0.68
NP_001100896.1	PSMD7	26S proteasome non-ATPase regulatory subunit 7	41	–	6	2	36469	0.26
EDL88527.1	GRSF1	G-rich RNA sequence binding factor 1	41	–	9	2	32181	0.3
NP_446199.2	UBQLN1	ubiquilin-1	31	–	5	2	61975	0.15

"–" in Score ratio indicates that the peptides were detected only in RNG140-GFP immunoprecipitates but not in GFP immunoprecipitates.

Supplementary Table 2. Changes in translation efficiency of transcripts by RNG140 overexpression in CHO cells

Ensembl transcript ID	Gene symbol	Mean transcript expression (log2)	Translation fold change to mean (log2)	deviance	q value	Gene description
ENSCGRT00000007568	Tpt1	6.435869922	-2.172999169	3.771378581	0	tumor protein, translationally-controlled 1
ENSCGRT00000000027	ND4L	9.658736225	-2.093522393	1.827153634	4.61264E-05	NADH dehydrogenase subunit 4L [Source:NCBI gene;Acc:3979178]
ENSCGRT00000001699	Caprin2	5.180898514	-1.911303095	36.76107042	0	caprin family member 2 [Source:NCBI gene;Acc:100762439]
ENSCGRT00000001700	Caprin2	5.171951178	-1.820273727	35.98101483	0	caprin family member 2 [Source:NCBI gene;Acc:100762439]
ENSCGRT00000025124	Kif14	4.547685645	-1.787930969	2.797543175	0.022735514	kinesin family member 14 [Source:NCBI gene;Acc:100759691]
ENSCGRT00000013803	Eif1	6.392074241	-1.697765997	1.138777213	0	eukaryotic translation initiation factor 1
ENSCGRT00000003564	Gtdc1	5.438903158	-1.656267745	2.890865901	0.011969813	glycosyltransferase like domain containing 1 [Source:NCBI gene;Acc:100752161]
ENSCGRT00000010206	Coq3	7.744152875	-1.611903733	1.840910321	8.22833E-12	coenzyme Q3, methyltransferase [Source:NCBI gene;Acc:100763494]
ENSCGRT00000027432	Rps24	9.840426855	-1.587919629	1.170119499	0.001276723	ribosomal protein S24
ENSCGRT00000018701		2.942349176	-1.509301898	0.588567167	0.146627553	
ENSCGRT00000009929	Eif1	4.182642163	-1.505925766	0.587523925	6.52092E-06	eukaryotic translation initiation factor 1
ENSCGRT00000024150	Eif1	6.022236289	-1.492327584	1.956959276	4.44069E-12	eukaryotic translation initiation factor 1
ENSCGRT00000005796	Oma1	6.207356139	-1.482660322	0.848796972	0.000289014	OMA1 zinc metallopeptidase [Source:NCBI gene;Acc:100767334]
ENSCGRT00000000028	ND4	14.40935904	-1.436527591	3.968821556	1.25687E-05	NADH dehydrogenase subunit 4 [Source:NCBI gene;Acc:3979179]
ENSCGRT00000005158	Eml5	7.367247214	-1.433849569	1.498976365	0.016912465	echinoderm microtubule associated protein like 5 [Source:NCBI gene;Acc:100771482]
ENSCGRT00000005159	Eml5	7.377050257	-1.414520789	1.530434842	0.018813598	echinoderm microtubule associated protein like 5 [Source:NCBI gene;Acc:100771482]
ENSCGRT00000008185	Ankrd10	7.158631164	-1.357823865	2.098632523	0.011079043	ankyrin repeat domain 10
ENSCGRT00000025361	Rpl9	8.026136023	-1.35653921	1.608052497	1.3563E-09	ribosomal protein L9
ENSCGRT00000016663	Tpt1	6.893793749	-1.353848741	0.621642048	0.021317178	tumor protein, translationally-controlled 1
ENSCGRT00000000192	Ccnb1	6.901584678	-1.328516506	1.033321171	0.001672198	cyclin B1
ENSCGRT00000004044	Tpt1	11.77110131	-1.309242944	0.92745562	1.10491E-08	tumor protein, translationally-controlled 1 [Source:NCBI gene;Acc:100770904]
ENSCGRT00000006517	eIF1	6.622060134	-1.30308477	0.644572471	5.19684E-12	eukaryotic translation initiation factor 1 [Source:NCBI gene;Acc:100764637]
ENSCGRT00000003532	Atad2b	7.912069871	-1.300205593	0.671212146	1.36392E-06	ATPase family, AAA domain containing 2B [Source:NCBI gene;Acc:100763563]
ENSCGRT00000014371	Micu3	7.256954941	-1.298544451	1.629613053	0.000474188	mitochondrial calcium uptake family member 3 [Source:NCBI gene;Acc:100752287]
ENSCGRT00000000145	Atm	6.373237959	-1.286370056	6.651348538	0.032159929	ataxia telangiectasia mutated
ENSCGRT00000008273		2.184962707	-1.272442627	1.147225359	0.251244729	
ENSCGRT00000000568		4.259237819	-1.260032422	1.208034762	0.151614968	guanylate-binding protein 1-like [Source:NCBI gene;Acc:100762688]
ENSCGRT00000007732	0610010F05Ri	6.339382284	-1.227253754	0.546463693	0.064732852	KIAA1841 ortholog [Source:NCBI gene;Acc:100755497]
ENSCGRT00000016282	Wdr45	4.940846746	-1.226941237	2.232597419	0.172592269	WD repeat domain 45 [Source:NCBI gene;Acc:100759722]
ENSCGRT00000004909	Ppp2r3c	5.291063144	-1.198036311	1.469368159	0.010460423	protein phosphatase 2 regulatory subunit B"gamma
ENSCGRT00000012408	Atp9b	7.973812719	-1.18744989	2.177409591	1.87327E-05	ATPase phospholipid transporting 9B (putative) [Source:NCBI gene;Acc:100765138]
ENSCGRT00000013342	Fbxo15	5.558155672	-1.187315041	2.90126989	0.188447644	F-box protein 15 [Source:NCBI gene;Acc:100750915]
ENSCGRT00000012407	Atp9b	7.994585376	-1.182811972	1.911114003	1.85659E-05	ATPase phospholipid transporting 9B (putative) [Source:NCBI gene;Acc:100765138]
ENSCGRT00000004569	Dhrs9	3.308004759	-1.178791602	3.984034071	0.208627416	dehydrogenase/reductase 9 [Source:NCBI gene;Acc:100771741]
ENSCGRT00000014001	Dzank1	4.826626862	-1.160104152	2.595772654	0.126717363	double zinc ribbon and ankyrin repeat domains 1 [Source:NCBI gene;Acc:100767139]
ENSCGRT00000007937	Rpl4	4.804876314	-1.14978954	2.750096328	3.41711E-05	ribosomal protein L4
ENSCGRT00000007378	Ranbp17	6.826660893	-1.149499721	2.259106298	0.029864527	RAN binding protein 17 [Source:NCBI gene;Acc:100766027]
ENSCGRT00000000220	Aasdhppt	5.121400861	-1.149156679	2.642533691	0.026283913	aminoadipate-semialdehyde dehydrogenase-phosphopantetheinyl transferase
ENSCGRT00000002846	Odf2l	6.956798513	-1.115651849	2.607854635	0.011542829	outer dense fiber of sperm tails 2 like [Source:NCBI gene;Acc:100773183]
ENSCGRT00000010278		4.757917713	-1.113879094	3.413971109	0.101227935	
ENSCGRT00000002845	Odf2l	7.091303942	-1.109500442	3.216860981	0.00853016	outer dense fiber of sperm tails 2 like [Source:NCBI gene;Acc:100773183]
ENSCGRT00000000580		6.569400303	-1.105172618	3.314394621	0.071432533	
ENSCGRT00000003075	Dld	7.050917496	-1.090670046	1.053806498	0.033359451	dihydrolipoyl dehydrogenase, mitochondrial-like [Source:NCBI gene;Acc:100774281]
ENSCGRT00000015070	Set	8.8439907	-1.089600208	6.9816034	2.41773E-09	SET nuclear oncogene
ENSCGRT00000002844	Odf2l	7.114383661	-1.081348582	3.51233941	0.010471846	outer dense fiber of sperm tails 2 like [Source:NCBI gene;Acc:100773183]
ENSCGRT00000027281	Dbi	3.717134619	-1.075540561	4.067294457	0.016796104	diazepam binding inhibitor, acyl-CoA binding protein
ENSCGRT00000000117		3.712779935	-1.071385666	3.481782403	0.483749387	
ENSCGRT00000000116		3.712779935	-1.071385666	3.481782403	0.483749387	
ENSCGRT00000001286	Arhgap5	11.28691677	-1.059080347	2.530889334	1.98107E-11	Rho GTPase activating protein 5 [Source:NCBI gene;Acc:100765474]
ENSCGRT00000000105		5.248708361	-1.058657865	0.87465121	0.085775324	
ENSCGRT00000004195	Abhd18	6.45751924	-1.051647044	3.267608637	0.006099327	abhydrolase domain containing 18 [Source:NCBI gene;Acc:100772269]
ENSCGRT00000020997		6.309076862	-1.049726511	3.388386142	0.063489821	casein kinase 1 gamma 1 [Source:NCBI gene;Acc:100774663]
ENSCGRT00000019417	Ttc3	8.376152602	-1.046117928	0.508947983	0.000107948	tetratricopeptide repeat domain 3 [Source:NCBI gene;Acc:100750887]
ENSCGRT00000020063	Fam72a	5.220550026	-1.043202498	1.758292398	0.163881448	family with sequence similarity 72 member A [Source:NCBI gene;Acc:100757979]
ENSCGRT00000012396	Slf1	9.61337666	-1.041959942	4.080238762	4.43323E-11	SMC5-SMC6 complex localization factor 1 [Source:NCBI gene;Acc:100753941]
ENSCGRT00000017633	Ccdc138	6.169150523	-1.038680374	0.180472801	0.039708792	coiled-coil domain containing 138 [Source:NCBI gene;Acc:100761168]
ENSCGRT00000015353	Mbd4	6.112462239	-1.036705461	1.116419151	0.087179073	methyl-CpG binding domain 4, DNA glycosylase [Source:NCBI gene;Acc:100772468]
ENSCGRT00000019172	Phka2	7.310268253	-1.034678575	1.407686597	0.00514423	phosphorylase kinase regulatory subunit alpha 2

ENSCGRT00000024386		4.856617948	-1.032281633	2.858054702	0.092191223	
ENSCGRT00000014222	Cyp39a1	5.39341805	-1.031986131	1.654282903	0.085255742	24-hydroxycholesterol 7-alpha-hydroxylase [Source:NCBI gene;Acc:100759356]
ENSCGRT00000024037	Wdpcp	6.507658304	-1.026563303	1.917419312	0.073032149	WD repeat containing planar cell polarity effector [Source:NCBI gene;Acc:100769859]
ENSCGRT00000004332	Pola1	10.67741977	-1.023015794	3.397728898	1.16911E-10	DNA polymerase alpha 1, catalytic subunit [Source:NCBI gene;Acc:100758493]
ENSCGRT00000011496	Snrk	6.564625221	-1.022701674	1.34567343	0.088890325	SNF related kinase [Source:NCBI gene;Acc:100770428]
ENSCGRT00000001607		6.364833443	-1.018849098	3.745226126	0.146723695	centlein [Source:NCBI gene;Acc:100755760]
ENSCGRT00000008099	Vps13a	11.36338375	-1.016498263	3.596941623	2.01066E-06	vacuolar protein sorting 13 homolog A [Source:NCBI gene;Acc:100762383]
ENSCGRT00000009246	Wsb1	7.980736779	-1.015679782	3.001168351	8.66566E-05	WD repeat and SOCS box containing 1 [Source:NCBI gene;Acc:100760356]
ENSCGRT00000008810	Tmem68	6.412362005	-1.014618112	0.207295001	0.034204247	transmembrane protein 68 [Source:NCBI gene;Acc:100754539]
ENSCGRT00000001762	Ino80	9.454459163	-1.013873047	0.302756905	6.5474E-06	INO80 complex subunit [Source:NCBI gene;Acc:100762469]
ENSCGRT00000016843	Orc4	9.172485332	-1.010040143	6.194720788	8.4237E-10	origin recognition complex subunit 4 [Source:NCBI gene;Acc:100689043]
ENSCGRT00000020354	Sucla2	9.46206646	-1.001686032	3.507383887	1.39025E-07	succinate-CoA ligase ADP-forming beta subunit [Source:NCBI gene;Acc:100761589]
ENSCGRT00000017927	Chd9	7.772847258	-1.000533608	1.789219103	0.005547907	chromodomain helicase DNA binding protein 9 [Source:NCBI gene;Acc:100769940]
ENSCGRT00000010148	Nf1	10.67211178	-0.999683057	1.433166958	1.37185E-10	neurofibromin [Source:NCBI gene;Acc:100770202]
ENSCGRT00000004194	Abhd18	6.505521596	-0.999323709	2.900662323	0.00875013	abhydrolase domain containing 18 [Source:NCBI gene;Acc:100772269]
ENSCGRT00000011868	Gen1	7.962426496	-0.998572725	2.252738734	0.102835443	GEN1, Holliday junction 5' flap endonuclease [Source:NCBI gene;Acc:100754800]
ENSCGRT00000018792	Ankrd10	8.632701078	-0.995704604	2.00375364	0.002429101	ankyrin repeat domain 10 [Source:NCBI gene;Acc:100766146]
ENSCGRT00000010149	Nf1	10.66047893	-0.995568735	1.360494674	1.72055E-10	neurofibromin [Source:NCBI gene;Acc:100770202]
ENSCGRT00000024244		2.908996534	-0.994370859	3.08541486	0.195953016	
ENSCGRT00000014313	Cox11	6.471276913	-0.994107554	1.156229633	0.003865355	cytochrome c oxidase assembly protein COX11, mitochondrial [Source:NCBI gene;Acc:100763079]
ENSCGRT00000008685		3.846585287	-0.991382209	1.070930322	0.394976807	
ENSCGRT00000001197	Jak2	10.15175117	-0.991107296	0.810297426	7.64129E-05	Janus kinase 2 [Source:NCBI gene;Acc:100769337]
ENSCGRT00000019685	Etnk1	7.470138561	-0.989973256	0.745929217	2.51324E-06	ethanolamine kinase 1 [Source:NCBI gene;Acc:100765795]
ENSCGRT00000015881	MKLN1	6.797107953	-0.988334824	3.47791947	0.011575321	muskelin 1 [Source:NCBI gene;Acc:100754523]
ENSCGRT00000006698	Nova1	6.513354626	-0.986661918	1.976784863	0.170283219	NOVA alternative splicing regulator 1 [Source:NCBI gene;Acc:100764229]
ENSCGRT00000007731	Kiaa1841	8.403871894	-0.985887573	0.734634828	0.000850438	KIAA1841 ortholog [Source:NCBI gene;Acc:100755497]
ENSCGRT00000023046	Kpna4	9.83642787	-0.984910409	2.503033292	5.14194E-05	karyopherin subunit alpha 4 [Source:NCBI gene;Acc:100757318]
ENSCGRT00000001348	Rpl22l1	9.317111854	-0.983094469	4.636977397	8.34215E-10	ribosomal protein L22 like 1 [Source:NCBI gene;Acc:100750612]
ENSCGRT00000005800	Klf3	4.992237277	-0.979052235	2.649346935	0.201911456	Kruppel like factor 3 [Source:NCBI gene;Acc:100762113]
ENSCGRT00000006252	Arl9	4.962771057	-0.978670144	1.494525731	0.34160565	ADP ribosylation factor like GTPase 9 [Source:NCBI gene;Acc:100759276]
ENSCGRT00000020122	Med4	8.971801404	-0.978266937	1.197503646	0.000129195	mediator complex subunit 4 [Source:NCBI gene;Acc:100761008]
ENSCGRT00000025776	4930402H24R	7.735464656	-0.975273698	0.813825589	0.000121996	chromosome unknown open reading frame, human C20orf194 [Source:NCBI gene;Acc:100774555]
ENSCGRT00000003563	Gtdc1	6.520225038	-0.975097242	2.815742799	0.046527876	glycosyltransferase like domain containing 1 [Source:NCBI gene;Acc:100752161]
ENSCGRT00000015808	Pde7a	8.306996029	-0.971647885	1.831491128	0.00284492	phosphodiesterase 7A [Source:NCBI gene;Acc:100760222]
ENSCGRT00000023911	Smim14	4.109711651	-0.968022519	0.958999423	0.034212762	small integral membrane protein 14
ENSCGRT00000025777	4930402H24R	7.775801281	-0.963794142	0.658187489	0.000133324	chromosome unknown open reading frame, human C20orf194 [Source:NCBI gene;Acc:100774555]
ENSCGRT00000025985	Seh1l	6.296063425	-0.963725083	2.845264582	0.006223759	nucleoporin SEH1-like [Source:NCBI gene;Acc:100764449]
ENSCGRT00000024963	Mid2	7.402916977	-0.962358529	0.579678079	0.002093484	midline 2 [Source:NCBI gene;Acc:100759244]
ENSCGRT00000015810	Pde7a	8.306993466	-0.959231238	1.767760456	0.003456333	phosphodiesterase 7A [Source:NCBI gene;Acc:100760222]
ENSCGRT00000024036	Wdpcp	6.609454706	-0.958629949	2.812827593	0.094699297	WD repeat containing planar cell polarity effector [Source:NCBI gene;Acc:100769859]
ENSCGRT00000015953	Rps3a	9.934974151	-0.950060918	2.772037458	1.47511E-12	ribosomal protein S3A
ENSCGRT00000023614	Dusp16	6.691640927	-0.948749947	2.959976286	0.060143725	dual specificity phosphatase 16 [Source:NCBI gene;Acc:100774758]
ENSCGRT00000024964	Mid2	7.413901962	-0.948526477	0.854499201	0.002333353	midline 2 [Source:NCBI gene;Acc:100759244]
ENSCGRT00000002580	Adamts6	8.528588824	-0.947761498	2.95644273	0.010969859	ADAM metallopeptidase with thrombospondin type 1 motif 6 [Source:NCBI gene;Acc:100760416]
ENSCGRT00000004697		5.999368097	-0.9458102	1.014724367	0.211327856	THO complex subunit 1 [Source:NCBI gene;Acc:100758451]
ENSCGRT00000007645		4.777246794	-0.945604187	1.738293432	0.143422215	
ENSCGRT00000009891		6.938370248	-0.943733326	1.064138586	0.143621699	
ENSCGRT00000002632	Papola	8.848325827	-0.941248288	2.858458504	0.000382804	poly(A) polymerase alpha
ENSCGRT00000001354	Cep135	9.680383571	-0.939670413	2.194653485	0.000699724	centrosomal protein 135 [Source:NCBI gene;Acc:100689465]
ENSCGRT00000021004	Shpk	4.587628814	-0.93621062	4.034257791	0.336027749	sedoheptulokinase [Source:NCBI gene;Acc:100771420]
ENSCGRT00000013993	Dock3	7.596239692	-0.934826951	1.68158136	0.024019217	dedicator of cytokinesis 3 [Source:NCBI gene;Acc:100768911]
ENSCGRT00000023497	Ireb2	9.735449206	-0.934213367	1.388986596	1.59698E-09	iron responsive element binding protein 2 [Source:NCBI gene;Acc:100756122]
ENSCGRT00000023496	Ireb2	9.735810978	-0.933801381	1.351763747	1.59698E-09	iron responsive element binding protein 2 [Source:NCBI gene;Acc:100756122]
ENSCGRT00000015329	Prdx1	5.210100352	-0.929765233	3.613877398	4.79956E-05	peroxiredoxin 1
ENSCGRT00000002025	Mindy3	8.10667254	-0.925422434	1.619579951	0.000486805	MINDY lysine 48 deubiquitinase 3 [Source:NCBI gene;Acc:100769292]
ENSCGRT00000019686	Etnk1	6.972494801	-0.918684958	0.580166029	0.000110205	ethanolamine kinase 1 [Source:NCBI gene;Acc:100765795]
ENSCGRT00000013994	Dock3	7.616287268	-0.91465066	1.59861695	0.027372556	dedicator of cytokinesis 3 [Source:NCBI gene;Acc:100768911]
ENSCGRT00000022179	Rapgef4	5.262783789	-0.911732491	0.980253547	0.354187344	Rap guanine nucleotide exchange factor 4 [Source:NCBI gene;Acc:100774346]
ENSCGRT00000018680	Glmn	8.411037691	-0.911274542	3.41887156	0.009097229	glomulin, FKBP associated protein [Source:NCBI gene;Acc:100762721]
ENSCGRT00000003433	Nr1d2	9.433948394	-0.907752068	0.549508622	0.022692239	nuclear receptor subfamily 1 group D member 2 [Source:NCBI gene;Acc:100768895]

Supplementary Table 3. Transcripts of which translation efficiency was decreased by RNG140 expression (more-T)

Ensembl transcript ID	Gene symbol	Mean transcript expression (log2)	Translation fold change to mean (log2)	deviance	q value	5'UTR length	3'UTR length	CDS length	Number of coding exons	Gene description
ENSCGRT00000007568	Tpt1	6.435869922	-2.172999169	3.771378581	0			471	3	tumor protein, translationally-controlled 1
ENSCGRT00000000027	Nd4l	9.658736225	-2.093522393	1.827153634	4.61264E-05			297	1	NADH dehydrogenase subunit 4L [Source:NCBI gene;Acc:3979178]
ENSCGRT00000001699	Caprin2	5.180898514	-1.911303095	36.76107042	0					caprin family member 2 [Source:NCBI gene;Acc:100762439]
ENSCGRT00000001700	Caprin2	5.171951178	-1.820273727	35.98101483	0					caprin family member 2 [Source:NCBI gene;Acc:100762439]
ENSCGRT00000025124	Kif14	4.547685645	-1.787930969	2.797543175	0.022735514			207	2	kinesin family member 14 [Source:NCBI gene;Acc:100759691]
ENSCGRT00000013803	Eif1	6.392074241	-1.697765997	1.138777213	0			330	2	eukaryotic translation initiation factor 1
ENSCGRT00000003564	Gtdc1	5.438903158	-1.656267745	2.890865901	0.011969813			711	5	glycosyltransferase like domain containing 1 [Source:NCBI gene;Acc:100752161]
ENSCGRT00000010206	Coq3	7.744152875	-1.611903733	1.840910321	8.22833E-12	62	116	1104	7	coenzyme Q3, methyltransferase [Source:NCBI gene;Acc:100763494]
ENSCGRT00000027432	Rps24	9.840426855	-1.587919629	1.170119499	0.001276723			393	1	ribosomal protein S24
ENSCGRT00000009929	Eif1	4.182642163	-1.505925766	0.587523925	6.52092E-06			303	2	eukaryotic translation initiation factor 1
ENSCGRT00000024150	Eif1	6.022236289	-1.492327584	1.956959276	4.44069E-12			336	2	eukaryotic translation initiation factor 1
ENSCGRT00000005796	Oma1	6.207356139	-1.482660322	0.848796972	0.000289014			717	5	OMA1 zinc metallopeptidase [Source:NCBI gene;Acc:100767334]
ENSCGRT00000000028	Nd4	14.40935904	-1.436527591	3.968821556	1.25687E-05			1378	1	NADH dehydrogenase subunit 4 [Source:NCBI gene;Acc:3979179]
ENSCGRT00000005158	Eml5	7.367247214	-1.433849569	1.498976365	0.016912465			5802	44	echinoderm microtubule associated protein like 5 [Source:NCBI gene;Acc:100771482]
ENSCGRT00000005159	Eml5	7.377050257	-1.414520789	1.530434842	0.018813598			5757	41	echinoderm microtubule associated protein like 5 [Source:NCBI gene;Acc:100771482]
ENSCGRT00000008185	Ankrd10	7.158631164	-1.357823865	2.098632523	0.011079043			1122	2	ankyrin repeat domain 10
ENSCGRT00000025361	Rpl9	8.026136023	-1.35653921	1.608052497	1.3563E-09			447	2	ribosomal protein L9
ENSCGRT00000016663	Tpt1	6.893793749	-1.353848741	0.621642048	0.021317178			360	3	tumor protein, translationally-controlled 1
ENSCGRT00000000192	Ccnb1	6.901584678	-1.328516506	1.033321171	0.001672198			1065	5	cyclin B1
ENSCGRT00000004044	Tpt1	11.77110131	-1.309242944	0.92745562	1.10491E-08			417	4	tumor protein, translationally-controlled 1 [Source:NCBI gene;Acc:100770904]
ENSCGRT00000006517	eIF1	6.622060134	-1.30308477	0.644572471	5.19684E-12			354	2	eukaryotic translation initiation factor 1 [Source:NCBI gene;Acc:100764637]
ENSCGRT00000003532	Atad2b	7.912069871	-1.300205593	0.671212146	1.36392E-06			3993	26	ATPase family, AAA domain containing 2B [Source:NCBI gene;Acc:100763563]
ENSCGRT00000014371	Micu3	7.256954941	-1.298544451	1.629613053	0.000474188			1236	14	mitochondrial calcium uptake family member 3 [Source:NCBI gene;Acc:100752287]
ENSCGRT00000000145	Atm	6.373237959	-1.286370056	6.651348538	0.032159929	1581		396	3	ataxia telangiectasia mutated
ENSCGRT00000004909	Ppp2r3c	5.291063144	-1.198036311	1.469368159	0.010460423			1344	2	protein phosphatase 2 regulatory subunit B"gamma
ENSCGRT00000012408	Atp9b	7.973812719	-1.18744989	2.177409591	1.87327E-05			3411	30	ATPase phospholipid transporting 9B (putative) [Source:NCBI gene;Acc:100765138]
ENSCGRT00000012407	Atp9b	7.994585376	-1.182811972	1.911114003	1.85659E-05	99	1035	3342	29	ATPase phospholipid transporting 9B (putative) [Source:NCBI gene;Acc:100765138]
ENSCGRT00000007937	Rpl4	4.804876314	-1.14978954	2.750096328	3.41711E-05			837	3	ribosomal protein L4
ENSCGRT00000007378	Ranbp17	6.826660893	-1.149499721	2.259106298	0.029864527			1440	11	RAN binding protein 17 [Source:NCBI gene;Acc:100766027]
ENSCGRT00000000220	Aasdhppt	5.121400861	-1.149156679	2.642533691	0.026283913			762	3	aminoadipate-semialdehyde dehydrogenase-phosphopantetheinyl transferase
ENSCGRT00000002846	Odf2l	6.956798513	-1.115651849	2.607854635	0.011542829			1641	14	outer dense fiber of sperm tails 2 like [Source:NCBI gene;Acc:100773183]
ENSCGRT00000002845	Odf2l	7.091303942	-1.109500442	3.216860981	0.00853016	148	3215	1770	15	outer dense fiber of sperm tails 2 like [Source:NCBI gene;Acc:100773183]
ENSCGRT00000003075	Dld	7.050917496	-1.090670046	1.053806498	0.033359451			1389	4	dihydrolipoyl dehydrogenase, mitochondrial-like [Source:NCBI gene;Acc:100774281]
ENSCGRT00000015070	Set	8.8439907	-1.089600208	6.9816034	2.41773E-09			447	2	SET nuclear oncogene
ENSCGRT00000002844	Odf2l	7.114383661	-1.081348582	3.51233941	0.010471846	203	3215	1899	16	outer dense fiber of sperm tails 2 like [Source:NCBI gene;Acc:100773183]
ENSCGRT00000027281	Dbi	3.717134619	-1.075540561	4.067294457	0.016796104			261	1	diazepam binding inhibitor, acyl-CoA binding protein
ENSCGRT00000001286	Arhgap5	11.28691677	-1.059080347	2.530889334	1.98107E-11	168	2338	4512	6	Rho GTPase activating protein 5 [Source:NCBI gene;Acc:100765474]
ENSCGRT00000004195	Abhd18	6.45751924	-1.051647044	3.267608637	0.006099327			1374	11	abhydrolase domain containing 18 [Source:NCBI gene;Acc:100772269]
ENSCGRT00000019417	Ttc3	8.376152602	-1.046117928	0.508947983	0.000107948			903	10	tetratricopeptide repeat domain 3 [Source:NCBI gene;Acc:100750887]
ENSCGRT00000012396	Slf1	9.61337666	-1.041959942	4.080238762	4.43323E-11		485	3183	20	SMC5-SMC6 complex localization factor 1 [Source:NCBI gene;Acc:100753941]
ENSCGRT00000017633	Ccdc138	6.169150523	-1.038680374	0.180472801	0.039708792			1851	15	coiled-coil domain containing 138 [Source:NCBI gene;Acc:100761168]
ENSCGRT00000019172	Phka2	7.310268253	-1.034678575	1.407686597	0.00514423	345		1614	15	phosphorylase kinase regulatory subunit alpha 2
ENSCGRT00000004332	Pola1	10.67741977	-1.023015794	3.397728898	1.16911E-10	132	903	4407	37	DNA polymerase alpha 1, catalytic subunit [Source:NCBI gene;Acc:100758493]
ENSCGRT00000008099	Vps13a	11.36338375	-1.016498263	3.596941623	2.01066E-06			8844	64	vacuolar protein sorting 13 homolog A [Source:NCBI gene;Acc:100762383]
ENSCGRT00000009246	Wsb1	7.980736779	-1.015679782	3.001168351	8.66566E-05	5	923	1224	8	WD repeat and SOCS box containing 1 [Source:NCBI gene;Acc:100760356]
ENSCGRT00000008810	Tmem68	6.412362005	-1.014618112	0.207295001	0.034204247	250	3296	990	6	transmembrane protein 68 [Source:NCBI gene;Acc:100754539]
ENSCGRT00000001762	Ino80	9.454459163	-1.013873047	0.302756905	6.5474E-06			3426	27	INO80 complex subunit [Source:NCBI gene;Acc:100762469]
ENSCGRT00000016843	Orc4	9.172485332	-1.010040143	6.194720788	8.4237E-10	174	951	1311	13	origin recognition complex subunit 4 [Source:NCBI gene;Acc:100689043]
ENSCGRT00000020354	Sucla2	9.46206646	-1.001686032	3.507383887	1.39025E-07	556	700	675	6	succinate-CoA ligase ADP-forming beta subunit [Source:NCBI gene;Acc:100761589]
ENSCGRT00000017927	Chd9	7.772847258	-1.000533608	1.789219103	0.005547907	331		2622	18	chromodomain helicase DNA binding protein 9 [Source:NCBI gene;Acc:100769940]
ENSCGRT00000010148	Nf1	10.67211178	-0.999683057	1.433166958	1.37185E-10			8481	58	neurofibromin [Source:NCBI gene;Acc:100770202]
ENSCGRT00000004194	Abhd18	6.505521596	-0.999323709	2.900662323	0.00875013	215	4211	1392	12	abhydrolase domain containing 18 [Source:NCBI gene;Acc:100772269]
ENSCGRT00000018792	Ankrd10	8.632701078	-0.995704604	2.00375364	0.002429101	157	945	1248	6	ankyrin repeat domain 10 [Source:NCBI gene;Acc:100766146]
ENSCGRT00000010149	Nf1	10.66047893	-0.995568735	1.360494674	1.72055E-10			8418	57	neurofibromin [Source:NCBI gene;Acc:100770202]
ENSCGRT00000014313	Cox11	6.471276913	-0.994107554	1.156229633	0.003865355	104	4617	408	3	cytochrome c oxidase assembly protein COX11, mitochondrial [Source:NCBI gene;Acc:100763079]
ENSCGRT00000001197	Jak2	10.15175117	-0.991107296	0.810297426	7.64129E-05	180	1231	3399	23	Janus kinase 2 [Source:NCBI gene;Acc:100769337]
ENSCGRT00000019685	Etnk1	7.470138561	-0.989973256	0.745929217	2.51324E-06	253	39	936	7	ethanolamine kinase 1 [Source:NCBI gene;Acc:100765795]
ENSCGRT00000015881	MKLN1	6.797107953	-0.988334824	3.47791947	0.011575321			504	5	muskelin 1 [Source:NCBI gene;Acc:100754523]
ENSCGRT00000007731	Kiaa1841	8.403871894	-0.985887573	0.734634828	0.000850438	256	2006	2157	20	KIAA1841 ortholog [Source:NCBI gene;Acc:100755497]
ENSCGRT00000023046	Kpna4	9.83642787	-0.984910409	2.503033292	5.14194E-05	167	1853	1494	16	karyopherin subunit alpha 4 [Source:NCBI gene;Acc:100757318]
ENSCGRT00000001348	Rpl22l1	9.317111854	-0.983094469	4.636977397	8.34215E-10	72	1197	369	4	ribosomal protein L22 like 1 [Source:NCBI gene;Acc:100750612]
ENSCGRT00000020122	Med4	8.971801404	-0.978266937	1.197503646	0.000129195	356	512	813	7	mediator complex subunit 4 [Source:NCBI gene;Acc:100761008]
ENSCGRT00000025776	4930402H24Rik	7.735464656	-0.975273698	0.813825589	0.000121996			3453	36	chromosome unknown open reading frame, human C20orf194 [Source:NCBI gene;Acc:100774555]
ENSCGRT00000003563	Gtdc1	6.520225038	-0.975097242	2.815742799	0.046527876			1335	10	glycosyltransferase like domain containing 1 [Source:NCBI gene;Acc:100752161]
ENSCGRT00000015808	Pde7a	8.306996029	-0.971647885	1.831491128	0.00284492			1371	13	phosphodiesterase 7A [Source:NCBI gene;Acc:100760222]
ENSCGRT00000023911	Smim14	4.109711651	-0.968022519	0.958999423	0.034212762			249	3	small integral membrane protein 14
ENSCGRT00000025777	4930402H24Rik	7.775801281	-0.963794142	0.658187489	0.000133324			3459	37	chromosome unknown open reading frame, human C20orf194 [Source:NCBI gene;Acc:100774555]
ENSCGRT00000025985	Seh1l	6.296063425	-0.963725083	2.845264582	0.006223759			924	1	nucleoporin SEH1-like [Source:NCBI gene;Acc:100764449]

ENSCGRT00000024963	Mid2	7.402916977	-0.962358529	0.579678079	0.002093484	149	3902	2058	9	midline 2 [Source:NCBI gene;Acc:100759244]
ENSCGRT00000015810	Pde7a	8.306993466	-0.959231238	1.767760456	0.003456333	297	4098	1326	12	phosphodiesterase 7A [Source:NCBI gene;Acc:100760222]
ENSCGRT00000015953	Rps3a	9.934974151	-0.950060918	2.772037458	1.47511E-12			780	2	ribosomal protein S3A
ENSCGRT00000024964	Mid2	7.413901962	-0.948526477	0.854499201	0.002333353			2199	10	midline 2 [Source:NCBI gene;Acc:100759244]
ENSCGRT00000002580	Adamts6	8.528588824	-0.947761498	2.95644273	0.010969859	568	3159	3354	24	ADAM metallopeptidase with thrombospondin type 1 motif 6 [Source:NCBI gene;Acc:100760416]
ENSCGRT00000002632	Papola	8.848325827	-0.941248288	2.858458504	0.000382804			2118	7	poly(A) polymerase alpha
ENSCGRT00000001354	Cep135	9.680383571	-0.939670413	2.194653485	0.000699724		2	3321	23	centrosomal protein 135 [Source:NCBI gene;Acc:100689465]
ENSCGRT00000013993	Dock3	7.596239692	-0.934826951	1.68158136	0.024019217			6063	52	dedicator of cytokinesis 3 [Source:NCBI gene;Acc:100768911]
ENSCGRT00000023497	Ireb2	9.735449206	-0.934213367	1.388986596	1.59698E-09			2904	22	iron responsive element binding protein 2 [Source:NCBI gene;Acc:100756122]
ENSCGRT00000023496	Ireb2	9.735810978	-0.933801381	1.351763747	1.59698E-09	205	4949	2892	22	iron responsive element binding protein 2 [Source:NCBI gene;Acc:100756122]
ENSCGRT00000015329	Prdx1	5.210100352	-0.929765233	3.613877398	4.79956E-05			582	2	peroxiredoxin 1
ENSCGRT00000002025	Mindy3	8.10667254	-0.925422434	1.619579951	0.000486805	216	1150	1335	15	MINDY lysine 48 deubiquitinase 3 [Source:NCBI gene;Acc:100769292]
ENSCGRT00000019686	Etnk1	6.972494801	-0.918684958	0.580166029	0.00011020 5			891	6	ethanolamine kinase 1 [Source:NCBI gene;Acc:100765795]
ENSCGRT00000013994	Dock3	7.616287268	-0.91465066	1.59861695	0.027372556			6054	52	dedicator of cytokinesis 3 [Source:NCBI gene;Acc:100768911]
ENSCGRT00000018680	Glmn	8.411037691	-0.911274542	3.41887156	0.009097229	87		1791	18	glomulin, FKBP associated protein [Source:NCBI gene;Acc:100762721]
ENSCGRT00000003433	Nr1d2	9.433948394	-0.907752068	0.549508622	0.022692239			1716	8	nuclear receptor subfamily 1 group D member 2 [Source:NCBI gene;Acc:100768895]
ENSCGRT00000011170	Senp6	7.995303753	-0.902942602	1.75449003	0.024324567			612	5	SUMO specific peptidase 6 [Source:NCBI gene;Acc:100765457]
ENSCGRT00000000032	Nd5	11.93492927	-0.898213499	3.474812967	0.000107794			1821	1	NADH dehydrogenase subunit 5 [Source:NCBI gene;Acc:3979180]
ENSCGRT00000004384	Ints6l	7.525080317	-0.892854442	2.43139295	0.007775681		458	1251	9	sarcoma antigen 1 [Source:NCBI gene;Acc:100768803]
ENSCGRT00000001761	Ino80	10.08301657	-0.888993706	0.138964961	1.38159E-05		1310	4680	35	INO80 complex subunit [Source:NCBI gene;Acc:100762469]
ENSCGRT00000018537	Dst	9.475444451	-0.886978601	2.165754034	0.006794759			7938	24	dystonin [Source:NCBI gene;Acc:100773919]
ENSCGRT00000007014	Nbeal1	8.32712357	-0.880682877	0.543273929	0.001393159	660	1602	8040	54	neurobeachin like 1 [Source:NCBI gene;Acc:100768393]
ENSCGRT00000004677	ZNF345	7.643701651	-0.877525237	1.54019462	0.017459898			1695	2	zinc finger protein 345
ENSCGRT00000019614	Smarcad1	9.289380938	-0.875568829	2.324033917	3.12457E-05	197	2145	3072	23	SWI/SNF-related, matrix-associated actin-dependent regulator of chromatin, subfamily a, containing DEAD/H box 1 [Source:NCBI gene;Acc:100767543]
ENSCGRT00000020255	Trdmt1	8.064826661	-0.875018987	5.421277957	0.000477392	60	2065	1176	11	tRNA aspartic acid methyltransferase 1 [Source:NCBI gene;Acc:100773025]
ENSCGRT00000022383	Ccdc88a	10.24032634	-0.874209541	0.459133958	3.61795E-07	306	2937	5538	31	coiled-coil domain containing 88A [Source:NCBI gene;Acc:100765924]
ENSCGRT00000019415	Ttc3	7.575299152	-0.873255316	5.021683798	0.019012774	3777	5257	384	4	tetratricopeptide repeat domain 3 [Source:NCBI gene;Acc:100750887]
ENSCGRT00000000016	Cox1	16.74699803	-0.872158891	7.933255593	1.48586E-05			1545	1	cytochrome c oxidase subunit I [Source:NCBI gene;Acc:3979185]
ENSCGRT00000005682	Sbf2	8.463951699	-0.863377136	5.280466068	0.007595738			1503	14	SET binding factor 2 [Source:NCBI gene;Acc:100764737]
ENSCGRT00000008723	Nop58	10.69054153	-0.863240464	2.136718489	2.39916E-09			1335	13	NOP58 ribonucleoprotein [Source:NCBI gene;Acc:100764223]
ENSCGRT00000022531	Ralgapa1	10.25235092	-0.86261685	2.228973936	0.000912462			6000	39	Ral GTPase activating protein catalytic alpha subunit 1 [Source:NCBI gene;Acc:100753551]
ENSCGRT00000009108	Zfp260	6.983311646	-0.862492694	2.718992557	0.037879335	290		1629	3	zinc finger protein 260 [Source:NCBI gene;Acc:100771943]
ENSCGRT00000019416	Ttc3	10.96139672	-0.860953935	3.443764177	1.30142E-08	1885	3565	3543	32	tetratricopeptide repeat domain 3 [Source:NCBI gene;Acc:100750887]
ENSCGRT00000010563	Pnpt1	10.68777213	-0.860467719	3.132171816	0.000236677			2355	29	polyribonucleotide nucleotidyltransferase 1 [Source:NCBI gene;Acc:100766803]
ENSCGRT00000021364	Atp13a3	12.67204726	-0.856544669	1.266549077	9.44561E-11					ATPase 13A3 [Source:NCBI gene;Acc:100769908]
ENSCGRT00000022382	Ccdc88a	10.26099296	-0.855411878	0.617224986	6.16372E-07					coiled-coil domain containing 88A [Source:NCBI gene;Acc:100765924]
ENSCGRT00000004678	ZNF345	7.630671802	-0.855131282	1.87915382	0.021772281					zinc finger protein 345
ENSCGRT00000003094	Strn3	10.12779023	-0.851102825	2.70531366	1.68821E-05					striatin 3 [Source:NCBI gene;Acc:100765220]
ENSCGRT00000003095	Strn3	10.10805659	-0.85012077	2.710233624	1.86131E-05					striatin 3 [Source:NCBI gene;Acc:100765220]
ENSCGRT00000021363	Atp13a3	12.73261319	-0.848486799	1.526191609	1.16911E-10					ATPase 13A3 [Source:NCBI gene;Acc:100769908]
ENSCGRT00000009272	Ptpn12	8.852699088	-0.847557171	3.53154058	3.50835E-05					protein tyrosine phosphatase, non-receptor type 12 [Source:NCBI gene;Acc:100758766]
ENSCGRT00000016255	Msantd2	7.124791494	-0.842606157	1.976961686	0.049295653					Myb/SANT DNA binding domain containing 2 [Source:NCBI gene;Acc:100769065]
ENSCGRT00000011346	Cul4b	10.44574874	-0.841602091	3.688264573	1.13309E-08					cullin 4B [Source:NCBI gene;Acc:100763989]
ENSCGRT00000019058	Aste1	6.971920506	-0.841225705	1.060284402	0.049589667					asteroid homolog 1 [Source:NCBI gene;Acc:100765786]
ENSCGRT00000000187	Hace1	10.09850225	-0.839956428	1.270996795	9.80415E-05					HECT domain and ankyrin repeat containing E3 ubiquitin protein ligase 1 [Source:NCBI gene;Acc:100769328]
ENSCGRT00000018053	Ascc3	11.25149386	-0.839455615	3.031580357	3.2474E-05					activating signal cointegrator 1 complex subunit 3 [Source:NCBI gene;Acc:100762460]
ENSCGRT00000023753	Sos2	9.411287713	-0.836327743	2.238821102	0.00039067					SOS Ras/Rho guanine nucleotide exchange factor 2 [Source:NCBI gene;Acc:100769325]
ENSCGRT00000023662	Pank3	8.295671924	-0.834862888	0.331979324	0.000861857					pantothenate kinase 3 [Source:NCBI gene;Acc:100767141]
ENSCGRT00000004917	Trim59	8.10559808	-0.833183046	2.441244346	0.000787186					tripartite motif containing 59 [Source:NCBI gene;Acc:100767039]
ENSCGRT00000001019	Prelid1	3.792484687	-0.832999726	1.192907239	0.047956539					PRELI domain containing 1
ENSCGRT00000001794	Haus3	9.060143134	-0.83207116	1.099539498	8.7534E-05					HAUS augmin like complex subunit 3 [Source:NCBI gene;Acc:100770464]
ENSCGRT00000023754	Sos2	9.405700074	-0.830473769	2.198920732	0.000477392					SOS Ras/Rho guanine nucleotide exchange factor 2 [Source:NCBI gene;Acc:100769325]
ENSCGRT00000012602	Zfp644	10.03250307	-0.83039516	3.516721655	0.00029974					zinc finger protein 644 [Source:NCBI gene;Acc:100762160]
ENSCGRT00000016644	Eif3m	11.34306558	-0.829259675	2.385702216	0.043263888					eukaryotic translation initiation factor 3 subunit M [Source:NCBI gene;Acc:100768213]
ENSCGRT00000003486	Rpp30	9.331633169	-0.829057851	5.076249742	4.4074E-06					ribonuclease P/MRP subunit p30 [Source:NCBI gene;Acc:100764835]
ENSCGRT00000025365	Ccng1	9.07617874	-0.82868952	5.158538183	0.005547907					cyclin G1 [Source:NCBI gene;Acc:100771963]
ENSCGRT00000017391	Xrn1	8.835587252	-0.827549799	1.756294145	3.05688E-05					5'-3' exoribonuclease 1 [Source:NCBI gene;Acc:100760243]
ENSCGRT00000023663	Pank3	8.295672432	-0.827530013	0.336484742	0.000981398					pantothenate kinase 3 [Source:NCBI gene;Acc:100767141]
ENSCGRT00000005117	Kyat3	6.985348557	-0.82619489	1.966912058	0.01677694					kynurenine aminotransferase 3
ENSCGRT00000023752	Sos2	9.438446916	-0.826165093	2.126668242	0.00045597					SOS Ras/Rho guanine nucleotide exchange factor 2 [Source:NCBI gene;Acc:100769325]
ENSCGRT00000012604	Zfp644	9.975136681	-0.8236621	3.769170277	0.000400219					zinc finger protein 644 [Source:NCBI gene;Acc:100762160]
ENSCGRT00000022119	Btbd9	7.782727337	-0.823397857	2.911861274	0.029846249					BTB domain containing 9 [Source:NCBI gene;Acc:100756253]
ENSCGRT00000003830	Mmd	8.088521561	-0.822953193	5.325431169	0.024271211					monocyte to macrophage differentiation associated [Source:NCBI gene;Acc:100759398]
ENSCGRT00000014261	Ankib1	10.39455145	-0.821507748	2.277229156	0.00019017					ankyrin repeat and IBR domain containing 1 [Source:NCBI gene;Acc:100759287]
ENSCGRT00000015596	Chm	8.042823406	-0.819284237	1.85658992	0.0035231					CHM, Rab escort protein 1 [Source:NCBI gene;Acc:100763141]
ENSCGRT00000011439	Vwa5a	6.277996479	-0.814374438	0.50035503	0.004623918					von Willebrand factor A domain-containing protein 5A-like [Source:NCBI gene;Acc:107976981]
ENSCGRT00000008695	Ccne2	7.740722424	-0.813486059	1.834074508	0.002049261					cyclin E2 [Source:MGI Symbol;Acc:MGI:1329034]
ENSCGRT00000007453	Dhx29	9.904420589	-0.811818803	1.65724961	4.915E-07					DExH-box helicase 29 [Source:NCBI gene;Acc:100768526]
ENSCGRT00000019234	Rpl5	6.774493394	-0.810125408	3.220943433	3.84509E-06					ribosomal protein L5
ENSCGRT00000015957	Tarsl2	8.23897738	-0.809587648	0.290304394	0.005047956					threonyl-tRNA synthetase like 2 [Source:NCBI gene;Acc:100772235]

Supplementary Table 4. Transcripts of which translation efficiency was increased by RNG140 expression (less-T)

Ensembl transcript ID	Gene symbol	Mean transcript expression (log2)	Translation fold change to mean (log2)	deviance	q value	5'UTR length	3'UTR length	CDS length	Number of coding exons	description
ENSCGRT00000015234	Serf2	7.408417878	2.710755355	6.207667681	0			129	3	small EDRK-rich factor 2 [Source:NCBI gene;Acc:100754083]
ENSCGRT00000023275	Rpl41	10.03348639	2.163544969	1.487283354	6.22197E-07			78	3	ribosomal protein L41 [Source:MGI Symbol;Acc:MGI:1915195]
ENSCGRT00000026294	Tma7	4.244923669	2.087727925	1.937738245	0.000825044			294	1	translation machinery associated 7 homolog
ENSCGRT00000017721	Fbl	7.180922129	1.809194934	4.690053338	0.00016871			243	3	fibrillarin [Source:NCBI gene;Acc:100765730]
ENSCGRT00000015738	Pnrc2	9.107872918	1.768655895	0.825159307	2.17642E-06	437	1107	420	1	proline rich nuclear receptor coactivator 2 [Source:NCBI gene;Acc:100753045]
ENSCGRT00000027120	Tma7	5.030440741	1.76310717	9.416013507	0.000151413			192	1	translation machinery associated 7 homolog
ENSCGRT00000013861	Hinfp	11.96292997	1.751667216	6.244320773	0.000109352	353		312	1	histone H4 [Source:NCBI gene;Acc:100752605]
ENSCGRT00000002016	Tmem263	9.064156819	1.70875345	2.889398365	3.60018E-05	541	2779	348	2	transmembrane protein 263 [Source:NCBI gene;Acc:100761080]
ENSCGRT00000003127	Rilpl2	7.879128763	1.688063053	0.871761035	3.15241E-05	275	410	597	4	Rab interacting lysosomal protein like 2 [Source:NCBI gene;Acc:100774122]
ENSCGRT00000027320	Cox6b1	3.566942215	1.645705338	5.09382205	0.00339414			267	1	cytochrome c oxidase subunit 6B1 [Source:NCBI gene;Acc:100768457]
ENSCGRT00000025820	Rps29	5.221654317	1.62183281	1.869837927	0.004647214			171	1	40S ribosomal protein S29 [Source:NCBI gene;Acc:100771687]
ENSCGRT00000019970	Maml3	7.132807948	1.560236047	4.125955777	0.020760567			2940	5	mastermind like transcriptional coactivator 3 [Source:NCBI gene;Acc:100767462]
ENSCGRT00000001099	Tma7	5.111266646	1.548134665	2.119710802	0.049518592			180	2	translation machinery associated 7 homolog
ENSCGRT00000022071	Coa5	8.038771361	1.529091835	2.348267979	0.00029271	113	1495	225	3	cytochrome c oxidase assembly factor 5 [Source:NCBI gene;Acc:100766959]
ENSCGRT00000027044	Rps29	4.636970069	1.500427254	3.505594611	0.010117472			171	1	40S ribosomal protein S29 [Source:NCBI gene;Acc:100757259]
ENSCGRT00000018179	Hmgn1	11.20395168	1.459187623	3.788137503	0	61		219	3	high mobility group nucleosome binding domain 1 [Source:NCBI gene;Acc:100754560]
ENSCGRT00000007437	Tma7	9.515365202	1.445400467	3.556239264	1.20648E-05			195	4	translational machinery associated 7 [Source:MGI Symbol;Acc:MGI:1913417]
ENSCGRT00000015422	Snrpg	6.969566836	1.419252609	1.467230265	2.01793E-06			210	2	small nuclear ribonucleoprotein polypeptide G
ENSCGRT00000001547	Mgst1	6.953985562	1.418120265	1.500498276	6.12451E-06			141	2	microsomal glutathione S-transferase 1 [Source:NCBI gene;Acc:100774867]
ENSCGRT00000003966	Atf4	11.72879936	1.417374773	1.237821218	0	459	80	1047	2	activating transcription factor 4 [Source:NCBI gene;Acc:100689386]
ENSCGRT00000003937	Arl6ip4	9.508062491	1.370355884	4.134297117	1.71286E-06	801	3270	675	5	ADP ribosylation factor like GTPase 6 interacting protein 4 [Source:NCBI gene;Acc:100772007]
ENSCGRT00000017575	Higd2a	7.295771972	1.369885224	0.787077176	1.86603E-05	82	258	321	2	HIG1 hypoxia inducible domain family member 2A [Source:NCBI gene;Acc:100750940]
ENSCGRT00000010474	H2afz	7.694751786	1.36135508	4.046378306	0.035043807			273	2	Histone H2A.Z
ENSCGRT00000000692	Ndufs6	9.033759848	1.361255305	5.508933901	7.43519E-08	52	124	351	4	NADH:ubiquinone oxidoreductase subunit S6 [Source:NCBI gene;Acc:100751523]
ENSCGRT00000011478	Mmp10	4.959250215	1.35844619	3.947967872	0.011574188			1353	11	stromelysin-1-like [Source:NCBI gene;Acc:100754565]
ENSCGRT00000001504	Timm8b	7.559720246	1.347865084	2.727459928	2.13761E-05	81	217	252	2	translocase of inner mitochondrial membrane 8 homolog B [Source:NCBI gene;Acc:100774369]
ENSCGRT00000026236	Gng5	7.908355271	1.347244577	3.840064167	0.011616967			207	1	G protein subunit gamma 5 [Source:NCBI gene;Acc:100757206]
ENSCGRT00000027074	H2afx	12.64861977	1.344695598	3.686394432	0.000193846			432	1	histone H2AX [Source:NCBI gene;Acc:100757539]
ENSCGRT00000015938	Gng5	7.751332583	1.335421203	4.574143849	0.016401827			186	2	guanine nucleotide binding protein (G protein), gamma 5
ENSCGRT00000026664	Rps29	8.131912862	1.323408973	6.939078073	1.28623E-05			171	1	ribosomal protein S29
ENSCGRT00000027067	Hinfp	14.08567317	1.323099353	7.300298432	2.71234E-06			312	1	histone H4 [Source:NCBI gene;Acc:100754396]
ENSCGRT00000009191	Dda1	8.503461567	1.322284251	2.567094432	2.36436E-07	4	17	306	4	DET1 and DDB1 associated 1
ENSCGRT00000003892	Cks1brt	5.776890209	1.313149506	2.384967381	0.033059402			282	2	CDC28 protein kinase 1b, retrogene [Source:MGI Symbol;Acc:MGI:3643620]
ENSCGRT00000027109	Hinfp	12.88810649	1.293441102	7.20278731	0.001767662			312	1	histone H4 [Source:NCBI gene;Acc:100750560]
ENSCGRT00000003745	Cdk2ap1	9.260012972	1.286965762	0.798246035	3.74084E-06	551	663	303	4	cyclin dependent kinase 2 associated protein 1 [Source:NCBI gene;Acc:100773827]
ENSCGRT00000008061	Romo1	8.662716963	1.280710936	5.814628678	6.85884E-08		81	240	2	reactive oxygen species modulator 1 [Source:NCBI gene;Acc:100757211]
ENSCGRT00000026924	Hist4h4	8.887424133	1.277792113	3.682419656	0.011431215			312	1	histone H4 [Source:NCBI gene;Acc:100755357]
ENSCGRT00000004791	Wipf1	9.083719424	1.268084255	3.843113777	6.30799E-08	311	804	1485	7	WAS/WASL interacting protein family member 1 [Source:NCBI gene;Acc:100756222]
ENSCGRT00000017029	Hist1h4c	13.57447348	1.245418281	6.289824717	1.36123E-05	359		312	1	histone H3.1 [Source:NCBI gene;Acc:100761179]
ENSCGRT00000002536	Hist4h4	13.57447363	1.244660495	6.346084395	1.05843E-05	356		312	1	histone H4 [Source:NCBI gene;Acc:100755357]
ENSCGRT00000020896	Rpl24	5.446854435	1.226914618	10.65007018	8.4887E-06			666	2	60S ribosomal protein L24
ENSCGRT00000025387	Ptms	8.828515236	1.222589888	4.997344704	8.27154E-05		2008	264	4	parathymosin [Source:MGI Symbol;Acc:MGI:1916452]
ENSCGRT00000025263	Rnf5	7.927463748	1.222018613	1.82683406	0.000145396	85		543	6	ring finger protein 5 [Source:NCBI gene;Acc:100757912]
ENSCGRT00000013609	Hinfp	13.97720467	1.219537541	6.670856461	1.83841E-05			309	2	histone H4
ENSCGRT00000011857	Eif4ebp1	10.26469528	1.218976193	2.938783605	1.56018E-11	72	815	354	3	eukaryotic translation initiation factor 4E binding protein 1 [Source:NCBI gene;Acc:100769654]
ENSCGRT00000012418	Serp1	7.94692756	1.215185254	4.447346468	0.00234705	274	1822	201	3	stress associated endoplasmic reticulum protein 1 [Source:NCBI gene;Acc:100772255]
ENSCGRT00000025720	Bola1	6.91189346	1.214921827	1.094549512	0.012285229	114	65	414	1	bolA family member 1 [Source:NCBI gene;Acc:100758926]
ENSCGRT00000026413	Hist1h4c	14.07989529	1.206401394	6.538147889	1.29532E-05			312	1	histone H4 [Source:NCBI gene;Acc:107977157]
ENSCGRT00000027198	Hist1h4c	14.07989529	1.206401394	6.538147889	1.29532E-05			312	1	histone H4 [Source:NCBI gene;Acc:100767612]
ENSCGRT00000022185	Cox6b1	9.926057356	1.20086036	4.291111935	4.17947E-13	689	270	297	3	cytochrome c oxidase subunit 6B1 [Source:NCBI gene;Acc:100766809]
ENSCGRT00000010465	Prr13	6.68092761	1.195498126	4.462164046	1.84425E-05	135	562	414	3	proline rich 13 [Source:NCBI gene;Acc:100766907]
ENSCGRT00000026681	Ubald2	7.335129159	1.181138311	2.51898136	0.009057904			489	1	UBA-like domain-containing protein 2
ENSCGRT00000026954	Hist1h4c	12.57468027	1.178400351	3.653303552	0.000304738			312	1	histone H4 [Source:NCBI gene;Acc:100757199]
ENSCGRT00000027045	Timm13	8.772072858	1.176694519	3.891977991	1.13459E-05			366	1	translocase of inner mitochondrial membrane 13 [Source:NCBI gene;Acc:100772547]
ENSCGRT00000004078	Carhsp1	7.553522607	1.176308282	3.197756568	0.001018405	162	2508	447	3	calcium regulated heat stable protein 1 [Source:NCBI gene;Acc:100764910]
ENSCGRT00000000295	Txn2	7.856788951	1.172070483	3.494131878	0.001508566			360	3	thioredoxin 2
ENSCGRT00000026243	Timm13	9.776380168	1.166343731	2.574257927	1.45505E-07			240	1	mitochondrial import inner membrane translocase subunit Tim13-like [Source:NCBI gene;Acc:107976998]
ENSCGRT00000021308	Mapk6	12.81809713	1.165678308	1.308063733	0	882	2443	2169	5	mitogen-activated protein kinase 6 [Source:NCBI gene;Acc:100764603]
ENSCGRT00000027333	Hist1h4c	13.87873992	1.164009671	6.299940066	0.000168645			312	1	histone H4 [Source:NCBI gene;Acc:100768756]
ENSCGRT00000007794	Srsf11	10.05303463	1.162764216	1.880749764	9.25196E-10			1269	11	serine and arginine rich splicing factor 11 [Source:NCBI gene;Acc:100750677]
ENSCGRT00000027417	Rps15	3.978465428	1.160414806	4.609753779	0.043594006			438	1	40S ribosomal protein S15 [Source:NCBI gene;Acc:100759804]
ENSCGRT00000016435	4833439L19Rik	9.939753309	1.159385869	1.824918914	0.000387613	187	1224	912	7	KIAA1191 ortholog [Source:NCBI gene;Acc:100751525]
ENSCGRT00000026458	Hist2h2bb	13.63935428	1.154210983	6.436640774	0			381	1	histone H2B type 2-F [Source:NCBI gene;Acc:100774845]
ENSCGRT00000006617	Cks1b	9.163762161	1.15103116	3.178072235	4.38924E-08			240	3	cyclin-dependent kinases regulatory subunit 1 [Source:NCBI gene;Acc:103160037]
ENSCGRT00000014179	Uqcrq	7.949097488	1.141299083	3.322839486	0.033536595			114	2	cytochrome b-c1 complex subunit 8
ENSCGRT00000026261	Cox7a2	9.667209086	1.139050118	2.123630066	4.55058E-11			252	1	cytochrome c oxidase subunit 7A2, mitochondrial [Source:NCBI gene;Acc:100767351]
ENSCGRT00000002506	Actg1	12.15187496	1.132100932	5.28950554	0			399	3	actin, gamma, cytoplasmic 1
ENSCGRT00000022097	Cenpx	5.603071628	1.131489451	2.72674842	0.015365261	56	312	237	5	centromere protein X [Source:NCBI gene;Acc:100769252]

ENSCGRT00000019551	Bola3	7.20697547	1.129261032	0.777241388	0.003240529	72	183	332	4	bolA family member 3 [Source:NCBI gene;Acc:100769793]
ENSCGRT00000008920	Hist2h3c2	13.46557984	1.124073506	2.918196812	0.012580856	1047	409	411	1	uncharacterized LOC100757491 [Source:NCBI gene;Acc:100757491]
ENSCGRT00000014724	Cox17	8.400723973	1.121521176	4.019486803	0.000432848	146	737	192	2	cytochrome c oxidase copper chaperone [Source:NCBI gene;Acc:100758878]
ENSCGRT00000004285	Calm3	9.074453783	1.112333521	2.546428136	1.41059E-06	19	199	447	5	calmodulin 3 [Source:NCBI gene;Acc:100762749]
ENSCGRT00000026661	Hist1h3e	13.37441185	1.105643829	2.913783444	0.041944593			342	1	histone H3.3 [Source:NCBI gene;Acc:107979446]
ENSCGRT00000004524	Sp4	8.506536497	1.101962713	1.297322489	0.006070495	109		2559	5	Sp4 transcription factor [Source:NCBI gene;Acc:100770723]
ENSCGRT00000015735	Gata2	7.217549876	1.099518691	4.723270793	0.018089141	691	2002	1443	5	GATA binding protein 2 [Source:NCBI gene;Acc:100762331]
ENSCGRT00000019406	Gata4	6.344843905	1.09856747	0.973547444	0.038727046	103	1443	717	5	GATA binding protein 4 [Source:NCBI gene;Acc:100756123]
ENSCGRT00000015180	Hypk	10.11542988	1.098124938	4.073855205	1.69179E-10	33	63	390	4	huntingtin interacting protein K [Source:NCBI gene;Acc:100753787]
ENSCGRT00000022609	Lsm3	8.95976291	1.095858426	2.538605726	0.002093484	166	1728	309	4	LSM3 homolog, U6 small nuclear RNA and mRNA degradation associated [Source:NCBI gene;Acc:100765189]
ENSCGRT00000025579	C3H11orf98	8.500945623	1.091004216	1.323962267	3.22432E-05			372	4	chromosome 3 C11orf98 homolog
ENSCGRT00000009853	Mrpl34	7.917432063	1.088556519	3.787195662	0.007595738	72	221	279	2	mitochondrial ribosomal protein L34 [Source:NCBI gene;Acc:100755355]
ENSCGRT00000014587	Yaf2	8.725243295	1.086301831	2.17667654	0.001874369	223	1099	390	2	YY1-associated factor 2 [Source:NCBI gene;Acc:100760251]
ENSCGRT00000003148	Snrpg	9.6883737	1.084536558	2.602772904	3.68517E-10	106	128	231	4	small nuclear ribonucleoprotein polypeptide G [Source:NCBI gene;Acc:100774499]
ENSCGRT00000009049	Mrps5	8.570790985	1.083211908	2.016877266	0.000202298			393	5	mitochondrial ribosomal protein S5 [Source:NCBI gene;Acc:100773581]
ENSCGRT00000016987	Akip1	8.725650526	1.081944159	1.013032438	0.001499079	955	1018	639	5	A-kinase interacting protein 1 [Source:NCBI gene;Acc:100751192]
ENSCGRT00000022828	Myl6b	8.580703747	1.080602159	5.134533083	0.00714532	297	198	624	6	myosin light chain 6B [Source:NCBI gene;Acc:100766814]
ENSCGRT00000012516	Atf4	6.467502358	1.079546624	0.666746991	0.002169962			972	4	activating transcription factor 4
ENSCGRT00000009970	Poln	8.530849138	1.074940446	5.121778684	0.048780225			894	7	DNA polymerase nu
ENSCGRT00000019992	Lsm7	7.450209148	1.074861002	3.869330043	0.045382792			267	2	LSM7 homolog, U6 small nuclear RNA and mRNA degradation associated [Source:NCBI gene;Acc:100772252]
ENSCGRT00000020872	Zfp593	8.034642431	1.07347742	1.069227447	0.00021744	124	3972	405	3	zinc finger protein 593 [Source:NCBI gene;Acc:100769424]
ENSCGRT00000023017	Elof1	8.58666176	1.071810081	1.879047826	5.27147E-05	190	546	252	3	elongation factor 1 homolog [Source:NCBI gene;Acc:100753010]
ENSCGRT00000005776	Atp5e	10.44565364	1.070795241	6.809534635	2.27043E-07	301	3183	123	1	ATP synthase, H+ transporting, mitochondrial F1 complex, epsilon subunit [Source:MGI Symbol;Acc:MGI:1855697]
ENSCGRT00000027124	Cox7c	5.9095515	1.067539119	4.134192955	0.000116737			192	1	cytochrome c oxidase subunit 7C, mitochondrial [Source:NCBI gene;Acc:100774785]
ENSCGRT00000022829	Fam32a	8.507399715	1.067330957	3.87672833	0.029935373	74	4013	339	4	family with sequence similarity 32 member A [Source:NCBI gene;Acc:100759796]
ENSCGRT00000013423	2310022A10Rik	7.596323847	1.062250307	3.008277005	0.042184568			1122	9	chromosome unknown open reading frame, human C19orf47 [Source:NCBI gene;Acc:100768636]
ENSCGRT00000001511	Myc	6.978695202	1.060445056	4.72498833	0.007188427	584	875	96	1	myc proto-oncogene protein [Source:NCBI gene;Acc:100773301]
ENSCGRT00000014864	Hmga2	7.176835602	1.054909509	1.066693491	0.024381211			216	4	high mobility group AT-hook 2 [Source:NCBI gene;Acc:103158819]
ENSCGRT00000008174	Zfp346	7.18993742	1.054745461	0.579302253	0.023444171			753	6	zinc finger protein 346 [Source:NCBI gene;Acc:100765614]
ENSCGRT00000026953	Psmb3	7.704923584	1.052900923	4.495216953	2.18325E-06			159	1	proteasome subunit beta type-3
ENSCGRT00000022610	Lsm3	8.953038463	1.052056343	2.795119922	0.00569687			300	4	LSM3 homolog, U6 small nuclear RNA and mRNA degradation associated [Source:NCBI gene;Acc:100765189]
ENSCGRT00000027292	Ccdc85b	9.578257294	1.04715125	3.931200752	0.000131706			609	1	coiled-coil domain containing 85B [Source:NCBI gene;Acc:100766533]
ENSCGRT00000008025	Vgll4	7.863833261	1.044301385	1.672097722	0.00154842					vestigial like family member 4 [Source:NCBI gene;Acc:100753837]
ENSCGRT00000001623	Tmem167a	6.269769662	1.043246129	5.976284909	0.003708301					transmembrane protein 167A [Source:NCBI gene;Acc:100772159]
ENSCGRT00000006465	Mrpl17	7.453501162	1.042774289	1.955359939	0.007277484					mitochondrial ribosomal protein L17 [Source:NCBI gene;Acc:100758899]
ENSCGRT00000004102	Rps19bp1	8.147382944	1.042766912	4.706144995	0.010971174					ribosomal protein S19 binding protein 1 [Source:NCBI gene;Acc:100770022]
ENSCGRT00000007479	Timm17b	7.870767224	1.039248522	0.865374919	0.000116737					translocase of inner mitochondrial membrane 17B [Source:NCBI gene;Acc:100762818]
ENSCGRT00000013114	Lsm4	8.945703719	1.038667434	3.429808294	5.83254E-06					LSM4 homolog, U6 small nuclear RNA and mRNA degradation associated [Source:NCBI gene;Acc:100769464]
ENSCGRT00000013115	Lsm4	8.945703719	1.038667434	3.429808294	5.83254E-06					LSM4 homolog, U6 small nuclear RNA and mRNA degradation associated [Source:NCBI gene;Acc:100769464]
ENSCGRT00000014438	Rpl38	6.480850058	1.036912587	3.851632506	0.012777651					60S ribosomal protein L38-like [Source:NCBI gene;Acc:100765839]
ENSCGRT00000012287	H2afz	9.485670999	1.030896647	5.59648906	0.000358607					Histone H2A.Z
ENSCGRT00000018910	Mettl26	6.077980811	1.020265336	0.709365621	0.032309532					methyltransferase like 26 [Source:NCBI gene;Acc:100770910]
ENSCGRT00000001922	Nckap5l	7.666435139	1.020093226	1.998420479	0.034526355					NCK associated protein 5 like [Source:NCBI gene;Acc:100757554]
ENSCGRT00000001827	Gng10	6.939329039	1.016157399	1.227441268	0.034632355					G protein subunit gamma 10 [Source:NCBI gene;Acc:100755995]
ENSCGRT00000023042	Fam168a	5.233985381	1.015915458	0.088430676	0.037681547					family with sequence similarity 168 member A [Source:NCBI gene;Acc:100752186]
ENSCGRT00000015287	Mrpl54	8.761694346	1.015557422	2.222154973	0.001113429					mitochondrial ribosomal protein L54 [Source:NCBI gene;Acc:100763792]
ENSCGRT00000022543	Avpi1	7.764339103	1.014676638	0.53681544	0.012412604					arginine vasopressin induced 1 [Source:NCBI gene;Acc:100759679]
ENSCGRT00000020769	Abcc5	7.066145972	1.013901869	0.147785389	0.04349276					ATP binding cassette subfamily C member 5 [Source:NCBI gene;Acc:100774121]
ENSCGRT00000026606	Hist2h2aa1	13.90092037	1.012039984	6.407810004	2.26911E-07					histone H2A type 2-A [Source:NCBI gene;Acc:100758350]
ENSCGRT00000023043	Fam168a	5.23398438	1.010451445	0.076429753	0.039266681					family with sequence similarity 168 member A [Source:NCBI gene;Acc:100752186]
ENSCGRT00000013750	Cox8a	8.674751885	1.009361796	4.786154112	0.001471051					cytochrome c oxidase subunit 8A, mitochondrial [Source:NCBI gene;Acc:100755207]
ENSCGRT00000013116	Lsm4	8.470865999	1.007297153	2.348497775	0.000304738					LSM4 homolog, U6 small nuclear RNA and mRNA degradation associated [Source:NCBI gene;Acc:100769464]
ENSCGRT00000014312	Prrx1	6.952100452	1.007040827	3.589400461	0.012285229					paired related homeobox 1 [Source:NCBI gene;Acc:100753942]
ENSCGRT00000027235	Hist1h2br	13.26883428	1.006944812	4.277511256	0					histone H2B type 1 [Source:NCBI gene;Acc:100757322]
ENSCGRT00000008087	D8Ertd738e	8.322886995	1.005910608	2.045854403	0.000174468					chromosome unknown open reading frame, human C19orf53 [Source:NCBI gene;Acc:100766214]
ENSCGRT00000022942	Thap7	8.83433623	1.003209845	2.249087229	0.00531405					THAP domain containing 7 [Source:NCBI gene;Acc:100753121]
ENSCGRT00000007766	Tnfrsf12a	10.75932652	0.996640873	5.122883913	1.04543E-06					TNF receptor superfamily member 12A [Source:NCBI gene;Acc:100768739]
ENSCGRT00000013795	Trmt112	8.289663057	0.993392141	2.698844903	0.000905116					tRNA methyltransferase subunit 11-2 [Source:NCBI gene;Acc:100758109]
ENSCGRT00000005793	Arpc1b	9.441710111	0.99209613	4.569078076	0.000940429					actin related protein 2/3 complex subunit 1B [Source:NCBI gene;Acc:100774796]
ENSCGRT00000019247	Edf1	9.622552525	0.991703313	4.160640674	2.15763E-09					endothelial differentiation related factor 1 [Source:NCBI gene;Acc:100763269]
ENSCGRT00000003817	Snrnp27	10.07087722	0.990100658	2.323533101	6.16372E-07					small nuclear ribonucleoprotein U4/U6.U5 subunit 27 [Source:NCBI gene;Acc:100773920]
ENSCGRT00000013424	2310022A10Rik	7.675789398	0.989985704	3.502407169	0.017747528					chromosome unknown open reading frame, human C19orf47 [Source:NCBI gene;Acc:100768636]
ENSCGRT00000026578	Hist1h2be	12.82645419	0.988222504	3.689269273	0					histone H2B type 1 [Source:NCBI gene;Acc:100758641]
ENSCGRT00000013113	Lsm4	8.620704244	0.985902231	1.944027484	9.67044E-05					LSM4 homolog, U6 small nuclear RNA and mRNA degradation associated [Source:NCBI gene;Acc:100769464]
ENSCGRT00000026506	Hist2h2aa2	14.18919148	0.985480748	6.109219728	5.33578E-07					histone H2A type 2-A [Source:NCBI gene;Acc:100758065]
ENSCGRT00000001770	Desi1	7.072012925	0.983399928	1.624608616	0.008208554					desumoylating isopeptidase 1 [Source:NCBI gene;Acc:100770500]
ENSCGRT00000003365	1810037I17Rik	6.909631257	0.983134295	3.601074233	0.014720013					chromosome unknown open reading frame, human C4orf3 [Source:NCBI gene;Acc:100755608]
ENSCGRT00000009960	Smim7	6.121073267	0.981404302	3.67229196	0.005446231					small integral membrane protein 7 [Source:MGI Symbol;Acc:MGI:1914068]
ENSCGRT00000008003	Ndufb7	9.694105725	0.975044374	1.754474497	1.86131E-05					NADH:ubiquinone oxidoreductase subunit B7 [Source:NCBI gene;Acc:100754222]
ENSCGRT00000008515	Srsf7	9.548950038	0.974220782	2.73255398	3.0455E-07					serine and arginine rich splicing factor 7 [Source:NCBI gene;Acc:100758380]

Supplementary Table 5. Gene ontology enrichment analysis of transcripts of which translation efficiency was decreased by RNG140 expression (more-T)

Term	Count	Genes	Fold Enrichment	FDR
HECT	14	UBE3A, HERC4, HACE1, HERC2, UBE3C, HERC1, G2E3, HUWE1, NEDD4, UBR5, SMURF2, ITCH, TRIP12, HECTD1	16.03358914	7.99.E-10
Chaperonin Cpn60/TCP-1	7	TCP1, CCT4, CCT8, PIKFYVE, CCT2, CCT6A, HSPD1	14.43023023	7.06.E-03
PI3K/PI4K	7	PIK3CB, PIK3C2A, PRKDC, SMG1, ATR, TRRAP, ATM	12.6084	1.70.E-02
Membrane coat	10	COPB2, COPA, AP2B1, COPG2, COPG1, AP4E1, AP1G1, SYNJ1, CLTC, AP3B1	9.960486322	5.53.E-04
DNA replication initiation	8	CCNE2, SLF1, POLA1, ORC4, ORC5, MCM4, ORC3, MCM6	9.388369678	2.46.E-02
DEAH box	10	DHX9, CHD9, DHX29, SMARCA5, DHX15, CHD1, BRIP1, DHX36, DHX40, ERCC6L	8.476235294	2.78.E-03
Nuclear pore	17	RANBP17, NUP133, NUP98, NUP160, PCID2, XPO4, AHCTF1, NUP155, SEH1L, NUP205, KPNA6, NUP37, TNKS, KPNA4, RANBP2, KPNA3, KPNA2	7.937262538	3.27.E-07
Helicase	22	SMARCAD1, DHX9, BRIP1, INO80, SKIV2L2, DDX5, HLTF, MCM4, SETX, MCM6, CHD9, MCM8, DHX29, ASCC3, EIF4A2, DHX15, SMARCA5, DDX50, CHD1, DHX36, DHX40, ERCC6L	5.619551751	4.39.E-07
Protein transporter activity	14	VPS29, XPO1, AP2B1, AP1G1, IPO7, ZFYVE16, IPO5, USO1, KPNA6, VPS35, KPNA4, KPNA3, KPNA2, VPS26A	5.575455977	1.58.E-03
Mitosis	39	KIF23, HAUS3, SEPT2, KNTC1, AHCTF1, INO80, CDC16, CCNG1, CLTC, RPS3, WAPL, NCAPH, SEH1L, TNKS, NUP37, CLASP2, ZWILCH, ASPM, KIF2A, ERCC6L, CSNK1A1, PDS5B, BRCC3, PDS5A, CKAP5, SMC5, BIRC6, CENPE, SMC2, SMC3, NCAPD3, SMC4, CCNB1, KNL1, KIF20B, BUB1B, NEK9, CIT, SEPT7	5.000197855	7.44.E-13
Protein biosynthesis	22	EFL1, EEF1A1, EIF2S3X, DARS, EEF2, EIF2A, ETF1, KARS, IARS, DHX29, EIF2S1, EIF3E, RARS, EIF4A2, EIF3F, FARSB, EEF1G, EIF1, GUF1, TARSL2, EIF3M, EIF2B5	4.969671617	4.43.E-06
Biological rhythms	18	NAMPT, DHX9, UBE3A, ROCK2, PRKDC, DDX5, SIRT1, PPP1CB, HNRNPU, SETX, RACK1, HDAC2, NR1D2, OGT, KDM5A, KDM5B, TOP2A, KDM5C	4.743777452	3.22.E-04
Ubiquitin-dependent protein catabolic process	24	USP40, UBE3A, USP1, UBA6, UBR3, UBR2, RNF213, TTC3, CUL2, CUL5, PSMA5, PSMD11, PSMA4, USP47, SMURF2, CUL4B, USP48, ITCH, USP34, USP25, USP24, USP15, USP14, HDAC6	4.389367642	9.44.E-06
Tetratricopeptide-like helical	26	COPS2, NAA15, TRRAP, CDC16, CLTC, TTC3, ZFC3H1, INTS8, P4HA1, RANBP2, OGT, ERCC6L, GTF3C3, CSTF3, ZC3H7A, TTC21B, CNOT10, PRPF39, ATR, CDC27, PSMD11, TOMM70A, TRAPPC8, PPID, TMTC3, SRP72	3.941029265	1.87.E-05
DNA repair	33	SMARCAD1, SLF1, INO80, PRKDC, SETX, RPS3, MCM8, SUPT16, TRIP12, MMS22L, BRCC3, DDB1, USP1, POLE, PRIMPOL, SMC5, BRCA2, BRIP1, SMG1, SMC6, ATR, HERC2, SMC3, PSMD14, HUWE1, ASCC3, FANCD2, UBR5, PARPBP, USP47, PSME4, CUL4B, REV3L	3.927643697	1.31.E-07
WD40-repeat-containing domain	38	COPA, HPS5, UTP18, STRAP, KNTC1, LRBA, EIF2A, NBEA, SF3B3, PLAA, RACK1, COPB2, WDR75, DMXL1, SEH1L, NUP37, WDHD1, NSMAF, NBEAL1, PPWD1, TBL1XR1, ELP2, RBBP4, IFT80, DDB1, STRN3, UBR4, BIRC6, NUP155, RBBP7, HERC1, EML5, VPS8, BRWD3, WSB1, NOL10, LRRK2, WDR43	3.827469163	9.36.E-09
ATP-binding	127	PRPF4B, CTPS, IDE, INO80, CCT2, MTHFD1L, SETX, ATP2B1, ORC4, ORC5, DHX36, DARS, ROCK1, KIF5B, ROCK2, PIK3CB, MTPAP, OLA1, HNRNPU, MAPK1, DHX29, RFC1, ASCC3, ATP9B, ATP2C1, RARS, SMARCA5, RIPK2, NEK9, YME1L1, LRRK2, PRPS2, GLUD1, UBA6, MYO9A, RIOK2, KARS, ERCC6L, RHOBTB3, DHX9, MYO1B, ACACA, AK2, BRIP1, SMG1, ATP11C, ATR, DDX5, ATP13A3, ABCB7, ATM, TRNT1, CCT4, CCT8, DDX50, DHX40, HSPD1, MYH10, KIF23, UBE2D2A, SKIV2L2, PKM, ACTR2, MCM8, PDPK1, SLK, VWA8, MCCC1, SUCLA2, TOP2B, TOP2A, TARSL2, CHUK, CDK14, CDK13, KIF2A, KIF14, SRPK2, ABCE1, SGK3, PIK3C2A, TRPM7, KIF15, PRKCI, CCT6A, HLTF, MCM4, GMPS, MCM6, GAK, ACVR2A, PANK3, EIF4A2, ADK, RRM1, FARSB, BUB1B, MELK, MYO5A, SMARCAD1, PRKDC, ASNS, IARS, CHD9, PIKFYVE, DHX15, ABCD3, ETNK1, CHD1, YES1, ACSL4, SPATA5, ACSL3, CSNK1A1, TCP1, SMC5, SMC6, CENPE, SMC2, SMC3, SMC4, RPS6KA3, PAPOLA, KIF20B, JAK1, JAK2, CIT	3.094070547	2.26.E-27
Protein transport	53	COPA, XPO1, SEC24A, AP4E1, AP1G1, XPO4, VPS37A, COPB2, AP2B1, SEH1L, CEP290, VPS13A, NUP37, RANBP2, VPS13B, AP3B1, SEC23A, NUP133, ECT2, COPG2, COPG1, ATG4C, IPO7, IPO5, ARCN1, USO1, RAB5A, KPNA6, KPNA4, KPNA3, VPS26A, KPNA2, SNX13, SEC23B, MYO5A, VPS29, NUP98, AFTPH, NUP160, SNX6, BBS9, AHCTF1, ARFGEF1, TMED5, SEC22A, TNKS, VPS35, EXOC5, RANBP17, NUP155, COG5, PPID, DENND4C	3.050158466	2.66.E-09
mRNA processing	28	NCBP1, PRPF4B, STRAP, PNPT1, CMTR2, SKIV2L2, SF3B3, RNGTT, SF3B1, CNOT6L, NUDT21, DHX15, MAGOHB, PABPC1, PPWD1, CDK13, SRPK2, CSTF3, GRSF1, MTPAP, PRPF39, DDX5, HNRNPU, PAPOLA, AQR, RBM39, THOC2, THOC1	3.028600589	9.66.E-04
Cadherin binding involved in cell-cell adhesion	29	LDHA, SEPT2, RPL14, EIF2A, RDX, PRDX1, PKM, RACK1, BZW1, PICALM, SLK, EIF3E, EIF2S3X, KIF5B, CKAP5, MYO1B, OLA1, EEF2, ARFIP1, RSL1D1, GAPVD1, DHX29, RARS, CCT8, USO1, EEF1G, SPTBN1, GIGYF2, SEPT7	2.939033246	1.07.E-03
Mitochondrial inner membrane	34	UQCRC2, COX11, SAMM50, GLUD1, CYTB, HADHA, HADHB, RPS3, GHITM, MCCC1, CSDE1, SLC25A3, ABCD3, GUF1, NDUFS2, OMA1, SCO1, OPA1, IMMT, ND5, MICU2, AK2, HERC2, ABCB7, VDAC2, VDAC3, COQ3, SLC25A13, COX1, YME1L1, HSPD1, LRRK2, GPAM, PMPCB	2.625244457	1.35.E-03
Transferase	106	PRPF4B, CMTR2, G2E3, FNTA, NT5C3, OGT, ITCH, TGS1, ROCK1, PIK3CB, ROCK2, UGCG, POLE, MTPAP, TNKS2, MAPK1, HUWE1, TRMT11, UBR5, PARP14, RIPK2, NEK9, LRRK2, PRPS2, SRM, STRAP, PHKA1, PNPT1, RIOK2, PPAT, HADHB, CEPT1, NAA50, ANKIB1, TNKS, HECTD1, UAP1, PRIMPOL, AK2, HACE1, SMG1, TKT, ATR, ATM, TRNT1, GBE1, NEDD4, MTR, SMURF2, GTDC1, NAMPT, UBE2D2A, ALG6, RNGTT, PKM, PDPK1, AASDHPPT, SLK, CHUK, CDK14, CDK13, SRPK2, ZCCHC11, SGK3, PIK3C2A, TRPM7, PRKCI, HERC4, HERC2, HERC1, GAK, ACVR2A, COQ3, PANK3, ADK, ZDHHC13, BUB1B, GPAM, UGP2, MELK, REV3L, GALNT1, UBE3A, TIPARP, POLA1, PRKDC, UBE3C, POLR2A, CDYL, TRDMT1, OXCT1, PIKFYVE, ETNK1, PCMT1, KYAT3, YES1, TRIP12, CSNK1A1, BIRC6, PAPOLA, RPS6KA3, DPM1, JAK1, JAK2, CIT, SETD3	2.128103307	2.46.E-10

Supplementary Table 6. Gene ontology enrichment analysis of transcripts of which translation efficiency was increased by RNG140 expression (less-T)

Term	Count	Genes	Fold Enrichment	FDR
Ribonucleoprotein LSM domain	10	LSM8, LSM6, SNRPD3, LSM7, SNRPD2, LSM4, LSM3, SNRPF, SNRPE, SNRPG	17.54173765	2.28.E-06
Translation protein SH3-like domain	7	MRPL24, RPL21, RPL8, RPL27, EIF5A, SUPT5, PTMS	13.64357373	1.12.E-02
Histone core	25	HIST1H2AB, HIST2H2AA2, HIST1H2AA, HIST1H2AF, HIST2H3C2, HIST2H2AA1, H2AFV, HIST1H2BK, CENPA, H2AFZ, H2AFX, HIST1H2BR, HIST1H2BB, HIST1H2BE, HIST1H2BH, H2AFJ, HIST2H2BB, HIST1H3A, HIST1H2AI, H3F3A, HIST1H2AH, H3F3B, HIST1H3D, HIST1H3E, HIST1H3F	10.96358603	2.67.E-15
cytochrome-c oxidase activity	9	COX7A2, COX7B, COX8A, COX6B1, COX7C, COX4I1, COX6A1, COX7A2L, COX5B	10.88862691	1.45.E-03
Ribosomal protein	57	RPL18, MRPS36, RPL17, RPL36A, MRPL42, MRPS33, MRPL41, RPL13, RPS27L, RPLP0, MRPL36, MRPL33, MRPL34, RPL36AL, MRPL53, MRPL51, MRPS5, RPS18, RPL41, RPS16, MRPS18A, RPS15, RPS12, RPS11, MRPL43, UBA52, MRPS11, RPL27A, RPL35, RPL36, RPL38, RPL39, RPL30, RPS28, MRPL12, RPS29, RPL31, MRPL14, MRPL17, RPL8, MRPL54, RPL7A, MRPS26, MRPS25, MRPS24, RPL27, RPL24, MRPS21, RPL28, RPL29, MRPL24, MRPL23, RPL18A, RPL22, MRPL27, RPL21, RPL37A	10.37178479	2.14.E-37
Electron transport	27	NDUFB3, NDUFB4, NDUFB7, TXN2, NDUFB8, UQCRQ, NDUFB2, NDUFS7, NDUFS6, UQCR10, UQCR11, HIGD1A, NDUFA2, NDUFA3, NDUFB10, NDUFA8, NDUFA6, CYCS, NDUFA7, CYB5A, NDUFA1, NDUFA11, NDUFV3, UQCRH, NDUFV1, HIGD2A, UQCRB	9.320831684	8.18.E-15
mRNA splicing	44	SRSF1, RALY, LSM8, LSM6, SNRPD3, TRA2B, PPIL1, CWC15, LSM7, SNRPD2, ZCRB1, SF3B6, SF3B5, HNRNPA3, SFSWAP, HNRNPM, HNRNPK, RBM8A, PQBP1, ISY1, LSM4, LSM3, ACIN1, ARL6IP4, DDX41, ALYREF, SAP18, RNPS1, MBNL1, SMN1, SRSF3, SNRNP48, SRSF7, ZRANB2, SYF2, SNRPA, RBM39, SNRNP27, SNRPF, SNRPE, PRPF38B, PUF60, SNRPG, RBM17	6.771986971	4.84.E-20
RNA-binding	61	RALY, SRSF1, GTF3A, SRP14, LSM8, LSM6, SNRPD3, RBM3, LSM7, YBX3, EIF5A, SFSWAP, IMP3, RBM8A, LSM4, LSM3, CHTOP, RBM42, EXOSC1, MBNL1, SMN1, EIF4G1, RPS18, TRNAU1AP, SNRPA, RBM39, RPS11, SNRPF, SNRPE, NOL12, SNRPG, CARHSP1, TRA2B, ZCRB1, SF3B6, HNRNPA3, HNRNPM, HNRNPK, EIF3G, SAFB, RPL8, SNRNP70, DDX41, EWSR1, HNRNPAB, ZFP346, EIF1AD, ALYREF, RNPS1, PARK7, FBL, SAFB2, SRSF3, EIF4E, SRSF7, RPL22, ZRANB2, CIRBP, DDX54, PUF60, RBM17	3.749126049	2.33.E-15
Mitochondrion	100	MRPS36, MRPL42, GRPEL1, MRPS33, MRPL41, AURKAIP1, PNKD, MPV17, ROMO1, COX5B, UQCR10, UQCR11, MRPL36, MRPL33, MRPL34, HIGD1A, MRPL53, MRPL51, TIMM8B, ISCU, MRPS18A, MRPL43, HIGD2A, HAX1, STK11, TXN2, COX7B, MRPS11, COX7C, CHCHD2, CHCHD4, CHCHD6, ATF2, GADD45GIP1, MRPL54, COX6B1, HSPE1, MRPL58, SLC35F6, MRPS26, ATP5J2, MRPS25, COX8A, MRPS24, AK2, MRPS21, MMAB, NDUFV3, RNF5, NDUFV1, COX6A1, ATP5E, COA3, TIMM17B, UQCRQ, NDUFS7, NDUFS6, DYNLL1, GPX4, COX17, NDUFB10, SSBP1, CYCS, MRPS5, COX4I1, NDUFA11, PFDN2, UQCRH, CARD19, TOMM22, UQCRB, NDUFB3, NDUFB4, FKBP8, GLRX5, NDUFB7, NDUFB8, ATP5G1, COX7A2L, TIMM13, NDUFB2, MRPL12, MRPL14, MRPL17, NDUFA2, NDUFA3, COX7A2, NDUFA8, NDUFA6, NDUFA7, NDUFA1, PARK7, SOD2, MRPL24, UQCC2, MRPL23, SMDT1, MRPL27, BNIP3L, MGST1	3.491314816	8.32.E-25
Transcription	82	RALY, GTF3A, PPARD, E2F4, CCDC85B, PRR13, HINT1, COPRS, FOXK2, YBX3, SFSWAP, MAX, GATA2, DPY30, DYNLL1, HSF1, ELOF1, MED29, GATA4, PQBP1, SUPT5, MYC, GABPB2, EGR1, CHTOP, POLR1D, ZHX1, IRF2BP2, MBD2, HMGA2, HMGA1, JUNB, ZFP593, MED19, SS18, CHMP1A, TGIF1, EDF1, RUVBL2, VGLL4, RBM39, COMMD5, EID1, THAP7, POLR2F, HMGB2, CNBP, POLR2E, LITAF, POLR2K, TFE3, FHL2, CHCHD2, ZNRD1, ELK3, ZFP112, ATF2, SRRT, HNRNPK, DRAP1, SAFB, HINFP, LEO1, EWSR1, HNRNPAB, BRD3, RYBP, SAP18, WWTR1, USF1, SAFB2, ATF4, MED30, NUPR1, YAF2, PNRC2, MLX, SP4, POLR2M, ID3, DDX54, PUF60	1.629330329	1.69.E-02

Supplementary Table 7. Changes in translation efficiency of transcripts by RNG140 knockout in mouse eyes

UCSC transcript ID	Gene symbol	Mean transcript expression (log2)	Translation fold change to mean (log2)	deviance	q value	Gene description
uc008zeo.3	Gm13841	4.715639027	-2.753081648	8.708092176	0.340420048	#N/A
uc007avm.2	Gm8210	4.7161704	-2.714993412	8.407498327	0.415862958	#N/A
uc009mhc.2	Hmox1	4.378546908	-2.695325291	2.474455674	0.737633154	heme oxygenase 1 [Source:MGI Symbol;Acc:MGI:96163]
uc007kzt.1	Samd14	4.500404469	-2.693167524	4.42649742	0.744734678	sterile alpha motif domain containing 14 [Source:MGI Symbol;Acc:MGI:2384945]
uc007vcs.2	Rpl37	6.996980091	-2.576631532	8.73098538	0.452235542	ribosomal protein L37 [Source:MGI Symbol;Acc:MGI:1914531]
uc008dju.2	Mtcl1	5.455706557	-2.55691421	5.932314598	0.582026548	microtubule crosslinking factor 1 [Source:MGI Symbol;Acc:MGI:1915867]
uc008dcn.2	Rpl36	6.346954631	-2.514941435	8.253876421	0.326643454	ribosomal protein L36 [Source:MGI Symbol;Acc:MGI:1860603]
uc009fgq.1	Gltscr2	3.699859386	-2.474332778	5.802497944	0.233997912	#N/A
uc008ojx.2	Dido1	5.429113079	-2.457387162	6.154533965	0.722353639	#N/A
uc007rtr.1	Rnf180	4.799865722	-2.44848008	9.508574308	0.115154401	ring finger protein 180 [Source:MGI Symbol;Acc:MGI:1919066]
uc008eko.1	Fam13b	5.281672646	-2.44783594	8.380064896	0.365438032	family with sequence similarity 13, member B [Source:MGI Symbol;Acc:MGI:2447834]
uc007rtt.1	Rnf180	4.564105854	-2.438064588	8.503715079	0.115154401	ring finger protein 180 [Source:MGI Symbol;Acc:MGI:1919066]
uc008ojw.2	Dido1	5.547757134	-2.423688194	5.662473719	0.691852454	death inducer-obliterator 1 [Source:MGI Symbol;Acc:MGI:1344352]
uc009djc.1	Rpl32	8.716815628	-2.42197282	6.754355565	0.638206285	ribosomal protein L32 [Source:MGI Symbol;Acc:MGI:98038]
uc007lrs.3	Rundc3a	3.684017699	-2.403147013	5.502024647	0.731494074	#N/A
uc007cat.2	Hes6	3.090408447	-2.402213692	4.0514634	0.115154401	#N/A
uc007rts.1	Rnf180	4.849429983	-2.398873654	9.516044076	0.115154401	ring finger protein 180 [Source:MGI Symbol;Acc:MGI:1919066]
uc007joh.1	Rpl26	8.262374094	-2.36592444	7.894475003	0.605953388	ribosomal protein L26 [Source:MGI Symbol;Acc:MGI:106022]
uc007joi.1	Rpl26	8.262374094	-2.36592444	7.894475003	0.605953388	ribosomal protein L26 [Source:MGI Symbol;Acc:MGI:106022]
uc007lrr.3	Rundc3a	4.57825991	-2.33582081	7.289849217	0.665289328	RUN domain containing 3A [Source:MGI Symbol;Acc:MGI:1858752]
uc007nrp.2	Rps29	7.481806023	-2.317148587	4.940035239	0.665289328	ribosomal protein S29 [Source:MGI Symbol;Acc:MGI:107681]
uc029vci.1	#N/A	5.79827763	-2.311311458	5.324198209	0.770131557	#N/A
uc007sra.1	Rps24	7.103277139	-2.296792262	6.132005167	0.676755153	#N/A
uc007bkv.2	Rpl37a	7.457118193	-2.290659839	6.946456316	0.464968196	ribosomal protein L37a [Source:MGI Symbol;Acc:MGI:98068]
uc008djw.2	Mtcl1	5.915783371	-2.283203644	6.532283322	0.452829838	microtubule crosslinking factor 1 [Source:MGI Symbol;Acc:MGI:1915867]
uc009nue.2	Rpl13	8.4836878	-2.271422726	6.572541672	0.639042177	#N/A
uc007lrq.3	Rundc3a	4.261390466	-2.259623822	6.874905081	0.744734678	RUN domain containing 3A [Source:MGI Symbol;Acc:MGI:1858752]
uc009gqb.2	Nr1h2	3.999758058	-2.253786691	5.810305373	0.685746322	nuclear receptor subfamily 1, group H, member 2 [Source:MGI Symbol;Acc:MGI:1352463]
uc009gqc.2	Nr1h2	3.999758058	-2.253786691	5.810305373	0.685746322	nuclear receptor subfamily 1, group H, member 2 [Source:MGI Symbol;Acc:MGI:1352463]
uc007bhv.1	Crygf	10.06349922	-2.247026576	4.071605892	0.811905822	crystallin, gamma F [Source:MGI Symbol;Acc:MGI:88526]
uc009juc.1	Maz	5.483754819	-2.244419011	3.914011526	0.340420048	MYC-associated zinc finger protein (purine-binding transcription factor) [Source:MGI Symbol;Acc:MGI:1338823]
uc009kug.1	Arglu1	5.066745297	-2.242216863	3.271277041	0.685008824	arginine and glutamate rich 1 [Source:MGI Symbol;Acc:MGI:2442985]
uc008djv.2	Mtcl1	5.833538577	-2.241641524	6.418044628	0.46393982	microtubule crosslinking factor 1 [Source:MGI Symbol;Acc:MGI:1915867]
uc007qro.2	Ddx41	4.249567105	-2.239656857	4.347773759	0.588617347	DEAD (Asp-Glu-Ala-Asp) box polypeptide 41 [Source:MGI Symbol;Acc:MGI:1920185]
uc008rjd.2	Rpl34	7.151479732	-2.227512358	10.571651	0.587922453	ribosomal protein L34 [Source:MGI Symbol;Acc:MGI:1915686]
uc008rje.3	Rpl34	7.151479732	-2.227512358	10.571651	0.587922453	ribosomal protein L34 [Source:MGI Symbol;Acc:MGI:1915686]
uc033hzx.1	Rpl34	7.151479732	-2.227512358	10.571651	0.587922453	ribosomal protein L34 [Source:MGI Symbol;Acc:MGI:1915686]
uc007srb.1	Rps24	8.311615393	-2.224148047	6.768456824	0.665289328	#N/A
uc007src.1	Rps24	8.365009076	-2.212835383	6.752426714	0.670401107	ribosomal protein S24 [Source:MGI Symbol;Acc:MGI:98147]
uc009gpz.2	Nr1h2	4.03398964	-2.21084448	6.01312993	0.699985605	nuclear receptor subfamily 1, group H, member 2 [Source:MGI Symbol;Acc:MGI:1352463]
uc009gqa.2	Nr1h2	4.03398964	-2.21084448	6.01312993	0.699985605	nuclear receptor subfamily 1, group H, member 2 [Source:MGI Symbol;Acc:MGI:1352463]
uc007sre.1	Rps24	8.351299535	-2.204167168	6.749352528	0.675886096	ribosomal protein S24 [Source:MGI Symbol;Acc:MGI:98147]
uc008xnp.2	Rpl9	7.613966138	-2.172105414	9.681172938	0.680657018	ribosomal protein L9 [Source:MGI Symbol;Acc:MGI:1298373]
uc008oju.2	Dido1	5.682483051	-2.170921562	5.371249059	0.737633154	death inducer-obliterator 1 [Source:MGI Symbol;Acc:MGI:1344352]
uc008ojv.2	Dido1	5.682483051	-2.170921562	5.371249059	0.737633154	death inducer-obliterator 1 [Source:MGI Symbol;Acc:MGI:1344352]
uc007nfs.2	Rps7	8.443373446	-2.170051547	7.637678462	0.676755153	ribosomal protein S7 [Source:MGI Symbol;Acc:MGI:1333818]
uc008kiw.2	Selenoh	3.340177472	-2.169157389	10.39190542	0.308629495	selenoprotein H [Source:MGI Symbol;Acc:MGI:1919907]
uc007srd.1	Rps24	8.743156719	-2.16509655	6.395335457	0.685746322	ribosomal protein S24 [Source:MGI Symbol;Acc:MGI:98147]
uc008jnz.1	Rpl35	8.262761544	-2.160763149	6.578906361	0.678602112	ribosomal protein L35 [Source:MGI Symbol;Acc:MGI:1913739]
uc009jdc.2	Eif3f	6.590993709	-2.146055724	7.925170301	0.464968196	eukaryotic translation initiation factor 3, subunit F [Source:MGI Symbol;Acc:MGI:1913335]
uc008wfd.2	Dvl1	3.715121117	-2.143930788	11.34606548	0.452829838	#N/A
uc008aia.1	Tagap1	5.431630442	-2.143822555	8.551921679	0.452235542	T cell activation GTPase activating protein 1 [Source:MGI Symbol;Acc:MGI:1919786]
uc009eto.2	Caprin2	5.375461379	-2.139241007	5.469779858	0.340420048	caprin family member 2 [Source:MGI Symbol;Acc:MGI:2448541]
uc033ihb.1	Rpl22	4.288115975	-2.130711868	8.949162416	0.340420048	#N/A
uc007mfk.1	Rpl38	7.142756958	-2.117806339	5.949709358	0.665289328	ribosomal protein L38 [Source:MGI Symbol;Acc:MGI:1914921]
uc007mfl.1	Rpl38	7.142756958	-2.117806339	5.949709358	0.665289328	ribosomal protein L38 [Source:MGI Symbol;Acc:MGI:1914921]
uc029tlb.1	Six3os1	3.329908139	-2.115982184	3.890726785	0.784826993	#N/A
uc009kqe.2	Shank2	3.203316117	-2.11393719	5.346989378	0.722353639	SH3 and multiple ankyrin repeat domains 2 [Source:MGI Symbol;Acc:MGI:2671987]
uc008bzt.2	Rps28	6.572815654	-2.104120646	7.766610647	0.678602112	#N/A
uc008oir.1	Rps21	6.629704024	-2.099818711	9.473661131	0.525971465	ribosomal protein S21 [Source:MGI Symbol;Acc:MGI:1913731]
uc008ois.1	Rps21	6.629704024	-2.099818711	9.473661131	0.525971465	#N/A
uc007mbr.1	Cep112	4.090649601	-2.093212904	8.326739092	0.452829838	centrosomal protein 112 [Source:MGI Symbol;Acc:MGI:1923673]
uc008bpi.1	Rps10	7.193369069	-2.091926187	10.15055146	0.650581019	ribosomal protein S10 [Source:MGI Symbol;Acc:MGI:1914347]
uc008bph.1	Rps10	7.650981366	-2.085562706	10.52500687	0.637961627	ribosomal protein S10 [Source:MGI Symbol;Acc:MGI:1914347]
uc008wvt.2	Cenpa	2.982297462	-2.080398055	5.01698732	0.452829838	centromere protein A [Source:MGI Symbol;Acc:MGI:88375]
uc009pdn.1	Rps25	7.515723122	-2.072522076	7.599848604	0.678493924	ribosomal protein S25 [Source:MGI Symbol;Acc:MGI:1922867]
uc008cak.1	Rps18	6.241461634	-2.067699419	7.493911493	0.665289328	#N/A
uc009kuh.1	Arglu1	4.572407931	-2.067250844	4.16560114	0.770074746	arginine and glutamate rich 1 [Source:MGI Symbol;Acc:MGI:2442985]

uc009nuu.3	Vps9d1	3.560518244	-2.060120333	6.296164932	0.698842742	VPS9 domain containing 1 [Source:MGI Symbol;Acc:MGI:1914143]
uc029qyg.1	#N/A	13.21660619	-2.058496608	2.431356963	0.827560446	#N/A
uc029wdl.1	#N/A	13.17002554	-2.051799808	2.407495015	0.827560446	#N/A
uc007meu.1	Fam104a	3.419088927	-2.04933181	7.382640474	0.305869677	family with sequence similarity 104, member A [Source:MGI Symbol;Acc:MGI:106351]
uc008ciu.2	Ppp1r18	3.973103299	-2.049034448	6.537231628	0.464968196	protein phosphatase 1, regulatory subunit 18 [Source:MGI Symbol;Acc:MGI:1923698]
uc008civ.2	Ppp1r18	3.973103299	-2.049034448	6.537231628	0.464968196	protein phosphatase 1, regulatory subunit 18 [Source:MGI Symbol;Acc:MGI:1923698]
uc012ars.1	Ppp1r18	3.973103299	-2.049034448	6.537231628	0.464968196	protein phosphatase 1, regulatory subunit 18 [Source:MGI Symbol;Acc:MGI:1923698]
uc007ufc.2	Spata13	4.463909237	-2.042803529	7.751119856	0.340420048	spermatogenesis associated 13 [Source:MGI Symbol;Acc:MGI:104838]
uc011zna.2	Spata13	4.463909237	-2.042803529	7.751119856	0.340420048	spermatogenesis associated 13 [Source:MGI Symbol;Acc:MGI:104838]
uc008fzb.1	Rps6kb2	3.071748638	-2.040759114	6.340666128	0.731494074	ribosomal protein S6 kinase, polypeptide 2 [Source:MGI Symbol;Acc:MGI:1927343]
uc009rgv.1	Bfsp2	7.563377824	-2.036687846	10.75613547	0.676755153	beaded filament structural protein 2, phakinin [Source:MGI Symbol;Acc:MGI:1333828]
uc008jtu.1	Baz2b	6.317756597	-2.033871905	6.683607983	0.588617347	#N/A
uc008jtv.1	Baz2b	5.987638715	-2.032778542	7.259752997	0.637961627	#N/A
uc009pdm.1	Rps25	7.352791959	-2.030074795	8.070547017	0.665289328	ribosomal protein S25 [Source:MGI Symbol;Acc:MGI:1922867]
uc007elo.1	Gje1	3.564466527	-2.028444456	10.24919318	0.313884135	gap junction protein, epsilon 1 [Source:MGI Symbol;Acc:MGI:1923993]
uc008rwn.2	Rps20	7.301350187	-2.025142444	5.379171129	0.716478694	ribosomal protein S20 [Source:MGI Symbol;Acc:MGI:1914677]
uc007bhj.2	Crygb	10.88658527	-2.022461416	4.343484746	0.830895446	crystallin, gamma B [Source:MGI Symbol;Acc:MGI:88522]
uc009nuv.3	Vps9d1	3.744125681	-2.019197623	6.645860925	0.685008824	VPS9 domain containing 1 [Source:MGI Symbol;Acc:MGI:1914143]
uc057awz.1	Rps15	7.367136328	-2.017845218	10.41000755	0.637961627	ribosomal protein S15 [Source:MGI Symbol;Acc:MGI:98117]
uc008ysv.2	Crybb1	10.47320603	-2.016993006	5.968660383	0.823637791	crystallin, beta B1 [Source:MGI Symbol;Acc:MGI:104992]
uc057buy.1	Crybb1	10.47320603	-2.016993006	5.968660383	0.823637791	crystallin, beta B1 [Source:MGI Symbol;Acc:MGI:104992]
uc057buz.1	Crybb1	10.47320603	-2.016993006	5.968660383	0.823637791	crystallin, beta B1 [Source:MGI Symbol;Acc:MGI:104992]
uc057bva.1	Crybb1	10.47320603	-2.016993006	5.968660383	0.823637791	#N/A
uc009nux.3	Vps9d1	3.477678273	-2.015392993	5.93849496	0.726767184	#N/A
uc009gvf.1	Ftl1	7.697509185	-2.006861688	3.592745504	0.722353639	ferritin light polypeptide 1 [Source:MGI Symbol;Acc:MGI:95589]
uc008bzs.2	Rps28	7.259522867	-2.002405772	9.025234024	0.665289328	#N/A
uc009tvy.2	Igbp1	2.837670168	-1.991031927	2.979887648	0.305869677	#N/A
uc007gea.2	Csnk1g2	5.262233403	-1.989506867	13.25229201	0.305869677	casein kinase 1, gamma 2 [Source:MGI Symbol;Acc:MGI:1920014]
uc008upe.2	Pabpc4	4.681856672	-1.984019137	9.421069415	0.340420048	#N/A
uc007rht.1	Adgrv1	5.68313209	-1.981689414	7.881457208	0.305869677	adhesion G protein-coupled receptor V1 [Source:MGI Symbol;Acc:MGI:1274784]
uc007kil.3	Rpl23a	8.483667094	-1.98038215	5.758867655	0.722353639	#N/A
uc009ihl.2	Crebzf	5.129469788	-1.971167362	5.759965513	0.74977518	CREB/ATF bZIP transcription factor [Source:MGI Symbol;Acc:MGI:2675296]
uc008uic.1	Rps8	8.169302489	-1.970934705	7.031257365	0.685008824	ribosomal protein S8 [Source:MGI Symbol;Acc:MGI:98166]
uc008oiq.1	Rps21	5.199044592	-1.97047244	8.110142021	0.685746322	#N/A
uc008air.2	Tagap	4.569574799	-1.960673106	10.49531907	0.512008755	T cell activation Rho GTPase activating protein [Source:MGI Symbol;Acc:MGI:3615484]
uc007geb.2	Csnk1g2	5.282416836	-1.956839995	13.69311464	0.305869677	casein kinase 1, gamma 2 [Source:MGI Symbol;Acc:MGI:1920014]
uc009gds.2	Tbcb	3.240277449	-1.956253182	7.442571952	0.624582908	tubulin folding cofactor B [Source:MGI Symbol;Acc:MGI:1913661]
uc033jgb.1	Unc13a	3.699577408	-1.955733426	9.428002925	0.637961627	#N/A
uc009gth.2	Rps11	7.643590885	-1.955071151	7.755040688	0.665289328	ribosomal protein S11 [Source:MGI Symbol;Acc:MGI:1351329]
uc007gcn.2	Rps15	7.685076261	-1.952985745	9.936030775	0.673769346	ribosomal protein S15 [Source:MGI Symbol;Acc:MGI:98117]
uc008wck.1	Hes5	3.502191354	-1.95141769	5.738502182	0.340420048	hes family bHLH transcription factor 5 [Source:MGI Symbol;Acc:MGI:104876]
uc007esu.1	Soga3	4.342499307	-1.947971004	2.317831244	0.305869677	#N/A
uc008jtt.1	Baz2b	6.167600746	-1.946363859	6.550250972	0.651693928	#N/A
uc007mpt.2	Cbx2	3.761090148	-1.946181532	6.87893587	0.654624632	chromobox 2 [Source:MGI Symbol;Acc:MGI:88289]
uc008ziq.3	Rpl6	8.344219118	-1.945797702	9.548957631	0.718005542	ribosomal protein L6 [Source:MGI Symbol;Acc:MGI:108057]
uc009fgp.1	Selenow	4.892160159	-1.944662129	6.862606961	0.415862958	selenoprotein W [Source:MGI Symbol;Acc:MGI:1100878]
uc009syc.2	Rpl39	6.485970268	-1.94400973	7.270151749	0.742930035	ribosomal protein L39 [Source:MGI Symbol;Acc:MGI:1914498]
uc008fpw.2	Rpl17	8.444159833	-1.943779066	7.570191992	0.716871538	ribosomal protein L17 [Source:MGI Symbol;Acc:MGI:2448270]
uc033jgc.1	Unc13a	3.801890491	-1.943447918	9.789116431	0.609728377	unc-13 homolog A [Source:MGI Symbol;Acc:MGI:3051532]
uc009rjn.1	Rpl29	7.724738732	-1.93701352	10.4580196	0.665289328	#N/A
uc009rjo.1	Rpl29	7.724738732	-1.93701352	10.4580196	0.665289328	#N/A
uc007fzr.3	Rnf126	4.302793164	-1.935618331	8.272799128	0.665289328	ring finger protein 126 [Source:MGI Symbol;Acc:MGI:1917544]
uc012fgr.1	Rps16	7.521264746	-1.925605829	7.577702141	0.670401107	ribosomal protein S16 [Source:MGI Symbol;Acc:MGI:98118]
uc009jub.1	Maz	6.307948327	-1.923241577	3.049618204	0.350648092	#N/A
uc009rru.2	Atrip	3.718318887	-1.922475803	5.400034856	0.605953388	ATR interacting protein [Source:MGI Symbol;Acc:MGI:1925349]
uc012bof.1	Cacul1	2.532550217	-1.919331382	4.134665883	0.340420048	CDK2 associated, cullin domain 1 [Source:MGI Symbol;Acc:MGI:1926082]
uc007asq.1	#N/A	5.100506219	-1.918302892	5.787814373	0.400624673	#N/A
uc007lky.2	Hap1	3.772985667	-1.91669679	4.839643966	0.305869677	huntingtin-associated protein 1 [Source:MGI Symbol;Acc:MGI:1261831]
uc012bqv.1	Ankrd16	4.176321942	-1.911180135	5.524389665	0.877312364	#N/A
uc007asp.1	Rev1	5.099283378	-1.903349846	5.933076755	0.382936331	#N/A
uc008axz.2	Rps2	8.093014932	-1.890058801	4.422972563	0.685008824	ribosomal protein S2 [Source:MGI Symbol;Acc:MGI:105110]
uc008axy.2	Rps2	8.529494744	-1.889580919	3.901789952	0.723491763	ribosomal protein S2 [Source:MGI Symbol;Acc:MGI:105110]
uc008ayb.2	Rps2	8.529494744	-1.889580919	3.901789952	0.723491763	ribosomal protein S2 [Source:MGI Symbol;Acc:MGI:105110]
uc007pog.2	Yae1d1	2.361841617	-1.886002798	4.057004022	0.340420048	Yae1 domain containing 1 [Source:MGI Symbol;Acc:MGI:1914258]
uc009fml.2	Clasrp	5.159846571	-1.884756037	5.078915247	0.552022463	CLK4-associating serine/arginine rich protein [Source:MGI Symbol;Acc:MGI:1855695]
uc009mam.1	Uba52	8.29770459	-1.876937625	7.118574445	0.726767184	ubiquitin A-52 residue ribosomal protein fusion product 1 [Source:MGI Symbol;Acc:MGI:98887]
uc008iwf.1	Rpl7a	8.418192661	-1.875504345	7.669471398	0.731494074	ribosomal protein L7A [Source:MGI Symbol;Acc:MGI:1353472]
uc007rhs.1	Adgrv1	6.397330996	-1.873040743	5.474420939	0.367665416	adhesion G protein-coupled receptor V1 [Source:MGI Symbol;Acc:MGI:1274784]
uc007hnk.2	Rpl41	5.031578379	-1.871557447	6.30572237	0.69991034	ribosomal protein L41 [Source:MGI Symbol;Acc:MGI:1915195]
uc008kxa.2	Dgkz	3.775890731	-1.868719284	8.654075166	0.69991034	#N/A

Supplementary Table 8. Transcripts included in “HECT”, “PI3K/PI4K”, “Histone core”, “Ribosomal protein” and “Lens differentiation” in Fig. 8C and D

Term	Genes
HECT	Ube3a, Herc4, Hace1, Herc2, Ube3c, Herc1, G2e3, Huwe1, Nedd4, Ubr5, Smurf2, Itch, Trip12, Hectd1
PI3K/PI4K	Pik3cb, Pik3c2a, Prkdc, Smg1, Atr, Trrap, Atm
Histone core	H2afv, H3f3a, Hist1h2ab, H3f3b, Hist1h2af, Hist1h2ai, Hist1h2bb, Hist1h3f, Hist1h2be, Hist1h2bh, Hist1h2bk, Hist1h2br, Hist1h3a, Hist2h2aa2, H2afx, H2afz, Hist1h3e, Hist2h2bb, Hist2h3c2, Cenpa, Hist1h2ah
Ribosomal protein	Rpl17, Rpl18, Rpl21, Rpl36al, Rpl39, Rps12, Rps18, Rps27l, Rpl30, Rpl35, Rps28, Rpl36, Rpl38, Rpl24, Rpl41, Rps15, Rps29, Mrpl24, Mrps18a, Rpl13, Rpl18a, Rpl22, Rpl27, Rpl27a, Rpl28, Rpl29, Rpl31, Rpl36a, Rpl7a, Rpl37a, Rpl8, Rplp0, Rps11, Rps16, Uba52
Lens differentiation	Cryaa, Cryab, Cryba1, Cryba2, Cryba4, Crybb1, Crybb2, Crybb3, Cryga, Crygb, Crygc, Crygd, Crygs, Crygn, Crygf, Cryge, Bfsp1, Bfsp2, Mip

Supplementary Table 9. Top 100 transcripts of which translation efficiency was increased by RNG140 knockout

UCSC transcript ID	Gene symbol	Mean transcript expression (log2)	Translation fold change to mean (log2)	deviance	q value	5'UTR length	3'UTR length	CDS length	Number of coding exons	Gene description
uc007jmm.1	Myh8	7.426236355	3.190929058	2.419288887	0.115154401				0	myosin, heavy polypeptide 8, skeletal muscle, perinatal [Source:MGI Symbol;Acc:MGI:1339712]
uc007jms.1	Myh8	5.244491562	3.073196848	2.823946925	0.284243044	989	2202	852	4	myosin, heavy polypeptide 8, skeletal muscle, perinatal [Source:MGI Symbol;Acc:MGI:1339712]
uc007jmr.1	Myh8	5.391484998	2.970411493	3.594237978	0.305869677				0	myosin, heavy polypeptide 8, skeletal muscle, perinatal [Source:MGI Symbol;Acc:MGI:1339712]
uc007jmn.1	Myh8	8.539177522	2.683027463	1.534961839	0.340205443	184	151	5814	38	myosin, heavy polypeptide 8, skeletal muscle, perinatal [Source:MGI Symbol;Acc:MGI:1339712]
uc007jml.1	Myh8	5.175640661	2.635948004	5.762259233	0.049702839	73	1645	588	4	myosin, heavy polypeptide 8, skeletal muscle, perinatal [Source:MGI Symbol;Acc:MGI:1339712]
uc009suq.3	Agtr2	4.868194778	2.521840854	1.941721655	0.340420048	247	1944	1092	1	angiotensin II receptor, type 2 [Source:MGI Symbol;Acc:MGI:87966]
uc033jov.1	#N/A	4.829972907	2.508304644	2.052333657	0.340420048					#N/A
uc007vei.1	Nup155	6.638538515	2.495871771	10.22233045	0.115154401	110	240	4041	34	nucleoporin 155 [Source:MGI Symbol;Acc:MGI:2181182]
uc007sek.1	Flnb	6.378406231	2.472201052	6.417541472	0.153900925	195	1095	7793	46	Filamin, beta [Source:MGI Symbol;Acc:MGI:2446089]
uc007sel.2	Flnb	6.381470133	2.461344029	6.406270454	0.153900925	195	1096	7809	46	Filamin, beta [Source:MGI Symbol;Acc:MGI:2446089]
uc008swu.1	Abca1	6.380137422	2.428813443	4.989007038	0.308629495	320	3156	6786	49	ATP-binding cassette, sub-family A (ABC1), member 1 [Source:MGI Symbol;Acc:MGI:99607]
uc007vej.2	Nup155	6.72056526	2.384896675	9.022923976	0.140452795	173	3483	4176	35	nucleoporin 155 [Source:MGI Symbol;Acc:MGI:2181182]
uc009auj.2	Pds5b	5.451748292	2.285416347	6.33077848	0.115154401					PDS5 cohesin associated factor B [Source:MGI Symbol;Acc:MGI:2140945]
uc007otq.2	Fbln5	3.476614243	2.28102848	2.09152807	0.452235542				0	Fibulin 5 [Source:MGI Symbol;Acc:MGI:1346091]
uc008wpj.1	Reln	5.081535675	2.244313917	8.216381646	0.340420048				0	Reelin [Source:MGI Symbol;Acc:MGI:103022]
uc007evm.2	Lama4	3.634453827	2.24281776	1.906599247	0.745894531				0	Laminin, alpha 4 [Source:MGI Symbol;Acc:MGI:109321]
uc007gru.3	Mybpc1	6.959522829	2.230701402	4.17319816	0.264096306	100	268	3384	28	myosin binding protein C, slow-type [Source:MGI Symbol;Acc:MGI:1336213]
uc008mkc.1	Atrn	5.611121783	2.211231881	4.783863972	0.120659164	66	4392	4287	29	Attractin [Source:MGI Symbol;Acc:MGI:1341628]
uc007grt.3	Mybpc1	6.938928521	2.194350627	4.401146303	0.285223642	227	320	3375	28	myosin binding protein C, slow-type [Source:MGI Symbol;Acc:MGI:1336213]
uc007esi.1	#N/A	4.116967629	2.171156109	3.653848685	0.59140271					#N/A
uc007evp.2	Lama4	4.481936558	2.166955087	1.503354215	0.745894531	440	154	5470	38	Laminin, alpha 4 [Source:MGI Symbol;Acc:MGI:109321]
uc007hgc.2	Srgap1	5.367402004	2.15526949	7.926106338	0.305869677	115	4407	3189	22	SLIT-ROBO Rho GTPase activating protein 1 [Source:MGI Symbol;Acc:MGI:2152936]
uc012bea.2	Piezo2	5.034974615	2.123033849	9.221264896	0.415862958	188	114	8262	52	piezo-type mechanosensitive ion channel component 2 [Source:MGI Symbol;Acc:MGI:1918781]
uc008jqv.1	Neb	7.726476265	2.114783418	5.720626437	0.335101611	130	596	20730	151	nebulin [Source:MGI Symbol;Acc:MGI:97292]
uc008mgq.2	Anapc1	7.02762279	2.114643456	2.649699556	0.320565803	263	2844	5835	47	anaphase promoting complex subunit 1 [Source:MGI Symbol;Acc:MGI:103097]
uc009ujx.2	Nrk	5.696888974	2.102972882	2.713258045	0.437751338	322	1914	4368	28	Nik related kinase [Source:MGI Symbol;Acc:MGI:1351326]
uc007esh.1	#N/A	4.604194577	2.102708335	3.089638618	0.619780755					#N/A
uc008tjw.3	Mpdz	6.979275338	2.099600559	4.651648584	0.305869677	54	1118	6069	45	multiple PDZ domain protein [Source:MGI Symbol;Acc:MGI:1343489]
uc008tjx.2	Mpdz	6.996907389	2.098253556	4.215052594	0.305869677	224	1123	6171	46	multiple PDZ domain protein [Source:MGI Symbol;Acc:MGI:1343489]
uc007hgb.2	Srgap1	5.359973061	2.09406296	8.171848651	0.326643454	122	4407	3258	22	SLIT-ROBO Rho GTPase activating protein 1 [Source:MGI Symbol;Acc:MGI:2152936]
uc012dgl.2	Mpdz	6.960303644	2.08562221	4.105025265	0.305869677	63	22	6210	47	multiple PDZ domain protein [Source:MGI Symbol;Acc:MGI:1343489]
uc007evo.2	Lama4	4.266320261	2.083199721	1.766077505	0.726767184				0	Laminin, alpha 4 [Source:MGI Symbol;Acc:MGI:109321]
uc008xkx.1	Anapc4	5.701237207	2.074544134	4.304861521	0.292881649	538	115	2088	26	Anaphase promoting complex subunit 4 [Source:MGI Symbol;Acc:MGI:1098673]
uc007jlx.1	Myh3	7.664253172	2.074342898	3.246972382	0.443988199	46	125	5823	39	myosin, heavy polypeptide 3, skeletal muscle, embryonic [Source:MGI Symbol;Acc:MGI:1339709]
uc009avl.2	Col1a2	5.797400898	2.068287912	2.055993057	0.722353639				0	Collagen, type I, alpha 2 [Source:MGI Symbol;Acc:MGI:88468]
uc007mdh.1	Abca9	3.348536774	2.063352789	2.970209148	0.809466216	296	1216	4872	38	ATP-binding cassette, sub-family A (ABC1), member 9 [Source:MGI Symbol;Acc:MGI:2386796]
uc009mzx.2	Cdh5	4.440526596	2.061036652	3.777684714	0.787797955	127	1513	2355	11	cadherin 5 [Source:MGI Symbol;Acc:MGI:105057]
uc008vjf.2	Hspg2	6.653347591	2.060907386	2.557591267	0.801462472	93	966	13128	97	#N/A
uc007dlu.2	Ddr2	4.418973127	2.055861655	3.598032616	0.665289328	312	51	2565	16	discoidin domain receptor family, member 2 [Source:MGI Symbol;Acc:MGI:1345277]
uc011wvr.1	Ddr2	4.418973127	2.055861655	3.598032616	0.665289328	177	5547	2565	16	discoidin domain receptor family, member 2 [Source:MGI Symbol;Acc:MGI:1345277]
uc007apo.2	Uggt1	4.050742769	2.051378079	3.358716684	0.305869677	178	4199	4656	41	#N/A
uc009fbw.1	Peg3	8.558329241	2.042659	3.05175519	0.654624632	364	3614	4716	7	paternally expressed 3 [Source:MGI Symbol;Acc:MGI:104748]
uc007aws.1	Col5a2	5.223530711	2.039583479	3.297316115	0.450987871	368	510	1092	16	#N/A
uc009fbx.1	Peg3	8.457018002	2.036022058	3.495697087	0.641071254	364	3614	4716	7	#N/A
uc007pkv.2	Dip2c	5.695992108	2.021592946	7.01172086	0.305869677	454	2898	4671	37	#N/A
uc007evn.2	Lama4	4.048250565	2.005094263	2.147121059	0.74977518				0	#N/A
uc008ksz.1	Nup160	5.486343473	1.984461988	2.480142287	0.289562359	651	824	4209	36	#N/A
uc008ixt.2	Col5a1	8.09828108	1.981614835	1.537129778	0.726767184	391	2498	5517	66	collagen, type V, alpha 1 [Source:MGI Symbol;Acc:MGI:88457]
uc008rbk.2	Col11a1	6.485742756	1.981080436	1.988772374	0.676755153	361	1891	5415	67	collagen, type XI, alpha 1 [Source:MGI Symbol;Acc:MGI:88446]
uc007dpp.2	Copa	5.605235075	1.975899397	2.059120913	0.305869677			2578	0	#N/A
uc008yfk.1	Fras1	5.346795127	1.975417025	3.553449327	0.678493924	858	2957	12033	74	Fraser extracellular matrix complex subunit 1 [Source:MGI Symbol;Acc:MGI:2385368]
uc009qus.2	Col12a1	8.848731443	1.974615732	1.577487386	0.801462472	135	2178	9198	65	collagen, type XII, alpha 1 [Source:MGI Symbol;Acc:MGI:88448]
uc033fsw.1	Mon2	6.066599484	1.961779551	6.853031217	0.305869677	543	3610	5148	36	MON2 homolog, regulator of endosome to Golgi trafficking [Source:MGI Symbol;Acc:MGI:1914324]
uc008ksw.1	Nup160	5.498162835	1.957211136	2.269551253	0.305869677	651	824	4209	36	nucleoporin 160 [Source:MGI Symbol;Acc:MGI:1926227]
uc011xpe.1	Mon2	6.081361096	1.957164665	7.442166503	0.308629495	63	109	5130	34	MON2 homolog, regulator of endosome to Golgi trafficking [Source:MGI Symbol;Acc:MGI:1914324]
uc007pfl.1	Jag2	5.299326569	1.956997228	9.321107584	0.340420048	292	1070	3744	26	jagged 2 [Source:MGI Symbol;Acc:MGI:1098270]
uc008ppo.1	#N/A	6.285751886	1.954491184	5.447485703	0.305869677					#N/A
uc007hgk.2	Mon2	6.081354252	1.946698671	7.32288314	0.308629495	63	321	5127	34	MON2 homolog, regulator of endosome to Golgi trafficking [Source:MGI Symbol;Acc:MGI:1914324]

uc007hgj.2	Mon2	6.091583221	1.942466905	6.896925478	0.308629495	543	3609	5148	35	#N/A
uc008wnl.1	Sema3c	4.936024281	1.938316725	1.822967169	0.678493924	723	2512	2256	17	#N/A
uc008xkw.1	Anapc4	5.833498297	1.932633487	3.383075484	0.305869677	252	1178	2424	28	anaphase promoting complex subunit 4 [Source:MGI Symbol;Acc:MGI:1098673]
uc009izk.2	Dchs1	5.855939803	1.927380056	5.963866972	0.305869677	306	69	3696	6	#N/A
uc009jrf.1	Atp2a1	5.93946339	1.923340762	3.684355194	0.305869677	186	306	2985	22	ATPase, Ca++ transporting, cardiac muscle, fast twitch 1 [Source:MGI Symbol;Acc:MGI:105058]
uc011yry.1	Dlk1	5.894702445	1.920593488	1.956399779	0.664352525	125	2976	1005	6	delta like non-canonical Notch ligand 1 [Source:MGI Symbol;Acc:MGI:94900]
uc011yrz.1	Dlk1	5.79503307	1.913265149	2.026590814	0.653339302	169	21	939	6	delta like non-canonical Notch ligand 1 [Source:MGI Symbol;Acc:MGI:94900]
uc008xej.1	Afap1	4.408736123	1.905239609	3.917578504	0.320565803	224	4198	2196	16	actin filament associated protein 1 [Source:MGI Symbol;Acc:MGI:1917542]
uc008vjc.2	Hspg2	7.845697962	1.891149302	2.052428907	0.800313869	59	965	13152	97	perlecan (heparan sulfate proteoglycan 2) [Source:MGI Symbol;Acc:MGI:96257]
uc009tnz.1	Flna	8.36606685	1.890460566	1.673474935	0.654624632	207	329	7920	46	#N/A
uc008kfo.1	Ttn	10.46321804	1.885820752	4.221306925	0.739665786	131	1051	80661	191	titin [Source:MGI Symbol;Acc:MGI:98864]
uc008ezn.1	Fbn2	8.150246272	1.865616062	1.406759755	0.809506217	682	1635	8724	65	fibrillin 2 [Source:MGI Symbol;Acc:MGI:95490]
uc007rjg.1	Vcan	7.56149158	1.861902225	1.647867453	0.676755153	443	1919	10065	14	versican [Source:MGI Symbol;Acc:MGI:102889]
uc008rwf.2	Wls	4.291244348	1.858639564	7.283605098	0.512827303	270	1663	1626	12	#N/A
uc007rku.2	Thbs4	5.391291937	1.856348634	2.955809446	0.731494074	145	161	2892	22	thrombospondin 4 [Source:MGI Symbol;Acc:MGI:1101779]
uc009nzs.1	Nrp1	4.126145869	1.855532629	2.504811501	0.665289328				0	#N/A
uc008dkh.1	Lama1	6.246677717	1.848215927	5.570387083	0.44417915	76	198	9252	63	laminin, alpha 1 [Source:MGI Symbol;Acc:MGI:99892]
uc009quu.2	Col12a1	6.934240663	1.844136765	2.76311671	0.78308465				0	#N/A
uc029upj.1	Wls	4.658438084	1.836384145	6.57496303	0.46393982	205	219	1626	12	wntless WNT ligand secretion mediator [Source:MGI Symbol;Acc:MGI:1915401]
uc007dyv.2	Rab3gap2	4.636945621	1.835839219	7.554570066	0.390620572	125	2763	4164	35	#N/A
uc008kfn.1	Ttn	10.78115043	1.834865804	3.530580234	0.770074746	223	1047	100404	312	titin [Source:MGI Symbol;Acc:MGI:98864]
uc012cff.1	Rrbp1	4.239656087	1.815325191	5.667298167	0.340420048	286	264	786	3	#N/A
uc008mgr.2	Anapc1	6.39839168	1.813806746	2.700159485	0.340420048	248	324	3642	27	anaphase promoting complex subunit 1 [Source:MGI Symbol;Acc:MGI:103097]
uc009izh.2	Dchs1	7.110896708	1.810654806	4.413405306	0.474068431	410	468	9876	20	dachsous cadherin related 1 [Source:MGI Symbol;Acc:MGI:2685011]
uc007rji.2	Vcan	6.84434202	1.792194507	1.868695912	0.665376444	256	891	7185	13	versican [Source:MGI Symbol;Acc:MGI:102889]
uc007wod.2	Myh9	4.517328819	1.790901173	5.951917272	0.452235542				0	#N/A
uc008rwe.2	Wls	4.636606588	1.781004681	6.667318808	0.512008755	270	1663	1626	12	wntless WNT ligand secretion mediator [Source:MGI Symbol;Acc:MGI:1915401]
uc007awr.1	Col5a2	7.574822856	1.780934868	1.449596245	0.737633154	368	1763	4494	54	collagen, type V, alpha 2 [Source:MGI Symbol;Acc:MGI:88458]
uc007iet.1	Xpo1	7.326321572	1.780465578	1.614540495	0.639042177	438	1490	3216	24	#N/A
uc007kdp.1	Serpinf1	5.291759585	1.77851968	3.635741468	0.787797955	213	365	1254	7	serine (or cysteine) peptidase inhibitor, clade F, member 1 [Source:MGI Symbol;Acc:MGI:108080]
uc009oye.2	AW551984	4.283146661	1.776715745	4.521594737	0.450987871	273	1536	2415	18	expressed sequence AW551984 [Source:MGI Symbol;Acc:MGI:2143322]
uc009oyf.1	AW551984	4.283146661	1.776715745	4.521594737	0.450987871	228	1650	2415	18	expressed sequence AW551984 [Source:MGI Symbol;Acc:MGI:2143322]
uc007pam.2	Dlk1	6.156012083	1.775861796	2.245166815	0.683825571	519	2976	1158	5	delta like non-canonical Notch ligand 1 [Source:MGI Symbol;Acc:MGI:94900]
uc007pao.2	Dlk1	6.156012083	1.775861796	2.245166815	0.683825571	205	340	1158	5	delta like non-canonical Notch ligand 1 [Source:MGI Symbol;Acc:MGI:94900]
uc008syr.1	Svep1	5.343206021	1.775135295	2.315985034	0.851911765	220	705	10704	48	sushi, von Willebrand factor type A, EGF and pentraxin domain containing 1 [Source:MGI Symbol;Acc:MGI:1928849]
uc008dfy.1	Man2a1	5.105706902	1.773884167	4.645989441	0.770074746	1000	2538	3453	22	mannosidase 2, alpha 1 [Source:MGI Symbol;Acc:MGI:104669]
uc008wmy.2	Cacna2d1	5.803715215	1.773857678	8.293171743	0.340420048	226	377	3276	39	calcium channel, voltage-dependent, alpha2/delta subunit 1 [Source:MGI Symbol;Acc:MGI:88295]
uc011zck.1	Vcan	6.577243399	1.766822978	2.436786694	0.552022463	268	586	4848	13	versican [Source:MGI Symbol;Acc:MGI:102889]
uc009umk.2	Capn6	5.423812419	1.764938692	2.021517126	0.665289328	222	1413	1926	12	#N/A
uc008rbj.1	Col11a1	4.108458583	1.761505641	1.788198988	0.69991034	361	2	822	6	Collagen, type XI, alpha 1 [Source:MGI Symbol;Acc:MGI:88446]
uc008pbf.1	Fat4	7.922049225	1.760855558	3.826066885	0.678602112	20	1143	14946	17	FAT atypical cadherin 4 [Source:MGI Symbol;Acc:MGI:3045256]
uc008wnm.1	Sema3c	4.063943349	1.760794721	1.799331561	0.770074746	468	2511	1098	7	sema domain, immunoglobulin domain (Ig), short basic domain, secreted, (semaphorin) 3C [Source:MGI Symbol;Acc:MGI:107557]
uc009ptm.1	Cspg4	4.105718323	1.754765546	3.472204814	0.731494074	157	980	6984	10	chondroitin sulfate proteoglycan 4 [Source:MGI Symbol;Acc:MGI:2153093]
uc008rzo.1	Virma	5.976836691	1.752673014	4.303667068	0.326643454	85	449	3420	13	vir like m6A methyltransferase associated [Source:MGI Symbol;Acc:MGI:1913435]
uc007evq.2	Lama4	5.64577178	1.748853323	1.711433516	0.861255497	440	155	5451	38	laminin, alpha 4 [Source:MGI Symbol;Acc:MGI:109321]
uc008wmx.2	Cacna2d1	5.793828676	1.747239308	8.620223642	0.340420048	226	3830	3255	38	calcium channel, voltage-dependent, alpha2/delta subunit 1 [Source:MGI Symbol;Acc:MGI:88295]
uc007dyu.2	Rab3gap2	5.118146612	1.745657205	7.57862844	0.403737103	125	2763	4164	35	RAB3 GTPase activating protein subunit 2 [Source:MGI Symbol;Acc:MGI:1916043]

Supplementary Table 10. Top 100 transcripts of which translation efficiency was decreased by RNG140 knockout

UCSC transcript ID	Gene symbol	Mean transcript expression (log2)	Translation fold change to mean (log2)	deviance	q value	5' UTR length	3' UTR length	CDS length	Number of coding exon	Gene description
uc008zeo.3	Gm13841	4.715639027	-2.753081648	8.708092176	0.340420048				0	#N/A
uc007avm.2	Gm8210	4.7161704	-2.714993412	8.407498327	0.415862958				0	#N/A
uc009mhc.2	Hmox1	4.378546908	-2.695325291	2.474455674	0.737633154	129	570	870	5	heme oxygenase 1 [Source:MGI Symbol;Acc:MGI:96163]
uc007kzt.1	Samd14	4.500404469	-2.693167524	4.42649742	0.744734678	710	1354	1254	9	sterile alpha motif domain containing 14 [Source:MGI Symbol;Acc:MGI:2384945]
uc007vcs.2	Rpl37	6.996980091	-2.576631532	8.73098538	0.452235542	37	504	294	4	ribosomal protein L37 [Source:MGI Symbol;Acc:MGI:1914531]
uc008dju.2	Mtcl1	5.455706557	-2.55691421	5.932314598	0.582026548		972	4491	12	microtubule crosslinking factor 1 [Source:MGI Symbol;Acc:MGI:1915867]
uc008dcn.2	Rpl36	6.346954631	-2.514941435	8.253876421	0.326643454	35	30	318	3	ribosomal protein L36 [Source:MGI Symbol;Acc:MGI:1860603]
uc009fgq.1	Gltscr2	3.699859386	-2.474332778	5.802497944	0.233997912	840	47	567	6	#N/A
uc008ojx.2	Dido1	5.429113079	-2.457387162	6.154533965	0.722353639				0	#N/A
uc007rtr.1	Rnf180	4.799865722	-2.44848008	9.508574308	0.115154401	167	788	1779	7	ring finger protein 180 [Source:MGI Symbol;Acc:MGI:1919066]
uc008eko.1	Fam13b	5.281672646	-2.44783594	8.380064896	0.365438032	497	290	2556	19	family with sequence similarity 13, member B [Source:MGI Symbol;Acc:MGI:2447834]
uc007rtt.1	Rnf180	4.564105854	-2.438064588	8.503715079	0.115154401	199	1858	1728	7	ring finger protein 180 [Source:MGI Symbol;Acc:MGI:1919066]
uc008ojw.2	Dido1	5.547757134	-2.423688194	5.662473719	0.691852454	577	1375	6321	14	death inducer-obliterator 1 [Source:MGI Symbol;Acc:MGI:1344352]
uc009djc.1	Rpl32	8.716815628	-2.42197282	6.754355565	0.638206285	451	47	408	3	ribosomal protein L32 [Source:MGI Symbol;Acc:MGI:98038]
uc007lrs.3	Rundc3a	3.684017699	-2.403147013	5.502024647	0.731494074	273	432	1341	11	#N/A
uc007cat.2	Hes6	3.090408447	-2.402213692	4.0514634	0.115154401				0	#N/A
uc007rts.1	Rnf180	4.849429983	-2.398873654	9.516044076	0.115154401	140	1363	1776	7	ring finger protein 180 [Source:MGI Symbol;Acc:MGI:1919066]
uc007joh.1	Rpl26	8.262374094	-2.36592444	7.894475003	0.605953388	47	41	438	3	ribosomal protein L26 [Source:MGI Symbol;Acc:MGI:106022]
uc007joi.1	Rpl26	8.262374094	-2.36592444	7.894475003	0.605953388	128	40	438	3	ribosomal protein L26 [Source:MGI Symbol;Acc:MGI:106022]
uc007lrr.3	Rundc3a	4.57825991	-2.33582081	7.289849217	0.665289328	273	432	1341	11	RUN domain containing 3A [Source:MGI Symbol;Acc:MGI:1858752]
uc007nrp.2	Rps29	7.481806023	-2.317148587	4.940035239	0.665289328	128	91	171	3	ribosomal protein S29 [Source:MGI Symbol;Acc:MGI:107681]
uc029vci.1	#N/A	5.79827763	-2.311311458	5.324198209	0.770131557				0	#N/A
uc007sra.1	Rps24	7.103277139	-2.296792262	6.132005167	0.676755153				0	#N/A
uc007bkv.2	Rpl37a	7.457118193	-2.290659839	6.946456316	0.464968196	31	248	279	4	ribosomal protein L37a [Source:MGI Symbol;Acc:MGI:98068]
uc008djw.2	Mtcl1	5.915783371	-2.283203644	6.532283322	0.452829838	405	978	5838	14	microtubule crosslinking factor 1 [Source:MGI Symbol;Acc:MGI:1915867]
uc009nue.2	Rpl13	8.4836878	-2.271422726	6.572541672	0.639042177	102	42	636	5	#N/A
uc007lrq.3	Rundc3a	4.261390466	-2.259623822	6.874905081	0.744734678	273	346	1218	11	RUN domain containing 3A [Source:MGI Symbol;Acc:MGI:1858752]
uc009gqb.2	Nr1h2	3.999758058	-2.253786691	5.810305373	0.685746322	288	368	1332	8	nuclear receptor subfamily 1, group H, member 2 [Source:MGI Symbol;Acc:MGI:1352463]
uc009gqc.2	Nr1h2	3.999758058	-2.253786691	5.810305373	0.685746322	266	350	1332	8	nuclear receptor subfamily 1, group H, member 2 [Source:MGI Symbol;Acc:MGI:1352463]
uc007bhv.1	Crygf	10.06349922	-2.247026576	4.071605892	0.811905822	20	229	345	3	crystallin, gamma F [Source:MGI Symbol;Acc:MGI:88526]
uc009juc.1	Maz	5.483754819	-2.244419011	3.914011526	0.340420048	38	879	1365	6	MYC-associated zinc finger protein (purine-binding transcription factor) [Source:MGI Symbol;Acc:MGI:1338823]
uc009kug.1	Arglu1	5.066745297	-2.242216863	3.271277041	0.685008824	204	2177	816	4	arginine and glutamate rich 1 [Source:MGI Symbol;Acc:MGI:2442985]
uc008djv.2	Mtcl1	5.833538577	-2.241641524	6.418044628	0.46393982	405	1187	5682	14	microtubule crosslinking factor 1 [Source:MGI Symbol;Acc:MGI:1915867]
uc007qro.2	Ddx41	4.249567105	-2.239656857	4.347773759	0.588617347	151	185	1869	17	DEAD (Asp-Glu-Ala-Asp) box polypeptide 41 [Source:MGI Symbol;Acc:MGI:1920185]
uc008rjd.2	Rpl34	7.151479732	-2.227512358	10.571651	0.587922453	226	44	354	4	ribosomal protein L34 [Source:MGI Symbol;Acc:MGI:1915686]
uc008rje.3	Rpl34	7.151479732	-2.227512358	10.571651	0.587922453	90	36	273	4	ribosomal protein L34 [Source:MGI Symbol;Acc:MGI:1915686]
uc033hzx.1	Rpl34	7.151479732	-2.227512358	10.571651	0.587922453	158	48	354	4	ribosomal protein L34 [Source:MGI Symbol;Acc:MGI:1915686]
uc007srb.1	Rps24	8.311615393	-2.224148047	6.768456824	0.665289328				0	#N/A
uc007src.1	Rps24	8.365009076	-2.212835383	6.752426714	0.670401107	26	103	396	5	ribosomal protein S24 [Source:MGI Symbol;Acc:MGI:98147]
uc009gpz.2	Nr1h2	4.03398964	-2.21084448	6.01312993	0.699985605	270	333	1341	8	nuclear receptor subfamily 1, group H, member 2 [Source:MGI Symbol;Acc:MGI:1352463]
uc009gqa.2	Nr1h2	4.03398964	-2.21084448	6.01312993	0.699985605	289	369	1341	8	nuclear receptor subfamily 1, group H, member 2 [Source:MGI Symbol;Acc:MGI:1352463]
uc007sre.1	Rps24	8.351299535	-2.204167168	6.749352528	0.675886096	38	1173	402	5	ribosomal protein S24 [Source:MGI Symbol;Acc:MGI:98147]
uc008xnp.2	Rpl9	7.613966138	-2.172105414	9.681172938	0.680657018	14	678	501	5	ribosomal protein L9 [Source:MGI Symbol;Acc:MGI:1298373]
uc008oju.2	Dido1	5.682483051	-2.170921562	5.371249059	0.737633154	577	2476	1845	4	death inducer-obliterator 1 [Source:MGI Symbol;Acc:MGI:1344352]
uc008ojv.2	Dido1	5.682483051	-2.170921562	5.371249059	0.737633154	277	2491	1845	4	death inducer-obliterator 1 [Source:MGI Symbol;Acc:MGI:1344352]
uc007nfs.2	Rps7	8.443373446	-2.170051547	7.637678462	0.676755153	107	262	585	6	ribosomal protein S7 [Source:MGI Symbol;Acc:MGI:1333818]
uc008kiw.2	Selenoh	3.340177472	-2.169157389	10.39190542	0.308629495	184	212	351	3	selenoprotein H [Source:MGI Symbol;Acc:MGI:1919907]
uc007srd.1	Rps24	8.743156719	-2.16509655	6.395335457	0.685746322	291	66	357	4	ribosomal protein S24 [Source:MGI Symbol;Acc:MGI:98147]
uc008jnz.1	Rpl35	8.262761544	-2.160763149	6.578906361	0.678602112	538	36	372	4	ribosomal protein L35 [Source:MGI Symbol;Acc:MGI:1913739]
uc009jdc.2	Eif3f	6.590993709	-2.146055724	7.925170301	0.464968196	15	1413	1086	8	eukaryotic translation initiation factor 3, subunit F [Source:MGI Symbol;Acc:MGI:1913335]
uc008wfd.2	Dvl1	3.715121117	-2.143930788	11.34606548	0.452829838	503	937	1918	15	#N/A
uc008aia.1	Tagap1	5.431630442	-2.143822555	8.551921679	0.452235542	27	767	1518	4	T cell activation GTPase activating protein 1 [Source:MGI Symbol;Acc:MGI:1919786]
uc009eto.2	Caprin2	5.375461379	-2.139241007	5.469779858	0.340420048					caprin family member 2 [Source:MGI Symbol;Acc:MGI:2448541]
uc033ihb.1	Rpl22	4.288115975	-2.130711868	8.949162416	0.340420048	17	1647	387	4	#N/A
uc007mfk.1	Rpl38	7.142756958	-2.117806339	5.949709358	0.665289328	203	41	213	4	ribosomal protein L38 [Source:MGI Symbol;Acc:MGI:1914921]
uc007mfl.1	Rpl38	7.142756958	-2.117806339	5.949709358	0.665289328	117	41	213	4	ribosomal protein L38 [Source:MGI Symbol;Acc:MGI:1914921]
uc029tlb.1	Six3os1	3.329908139	-2.115982184	3.890726785	0.784826993				0	#N/A
uc009kqe.2	Shank2	3.203316117	-2.11393719	5.346989378	0.722353639	391	3359	4419	16	SH3 and multiple ankyrin repeat domains 2 [Source:MGI Symbol;Acc:MGI:2671987]

uc008bzt.2	Rps28	6.572815654	-2.104120646	7.766610647	0.678602112	90	92	210	3	#N/A
uc008oir.1	Rps21	6.629704024	-2.099818711	9.473661131	0.525971465	84	58	252	5	ribosomal protein S21 [Source:MGI Symbol;Acc:MGI:1913731]
uc008ois.1	Rps21	6.629704024	-2.099818711	9.473661131	0.525971465	84	58	252	5	#N/A
uc007mbr.1	Cep112	4.090649601	-2.093212904	8.326739092	0.452829838	201	419	2865	26	centrosomal protein 112 [Source:MGI Symbol;Acc:MGI:1923673]
uc008bpi.1	Rps10	7.193369069	-2.091926187	10.15055146	0.650581019	37	20	465	4	ribosomal protein S10 [Source:MGI Symbol;Acc:MGI:1914347]
uc008bph.1	Rps10	7.650981366	-2.085562706	10.52500687	0.637961627	25	177	510	4	ribosomal protein S10 [Source:MGI Symbol;Acc:MGI:1914347]
uc008wvt.2	Cenpa	2.982297462	-2.080398055	5.01698732	0.452829838	252	809	405	4	centromere protein A [Source:MGI Symbol;Acc:MGI:88375]
uc009pdn.1	Rps25	7.515723122	-2.072522076	7.599848604	0.678493924	616	286	378	4	ribosomal protein S25 [Source:MGI Symbol;Acc:MGI:1922867]
uc008cak.1	Rps18	6.241461634	-2.067699419	7.493911493	0.665289328				0	#N/A
uc009kuh.1	Arglu1	4.572407931	-2.067250844	4.16560114	0.770074746	204	2177	816	4	arginine and glutamate rich 1 [Source:MGI Symbol;Acc:MGI:2442985]
uc009nuu.3	Vps9d1	3.560518244	-2.060120333	6.296164932	0.698842742	6	737	1953	15	VPS9 domain containing 1 [Source:MGI Symbol;Acc:MGI:1914143]
uc029qyg.1	#N/A	13.21660619	-2.058496608	2.431356963	0.827560446					#N/A
uc029wdl.1	#N/A	13.17002554	-2.051799808	2.407495015	0.827560446					#N/A
uc007meu.1	Fam104a	3.419088927	-2.04933181	7.382640474	0.305869677	70	1991	558	3	family with sequence similarity 104, member A [Source:MGI Symbol;Acc:MGI:106351]
uc008ciu.2	Ppp1r18	3.973103299	-2.049034448	6.537231628	0.464968196	178	780	1785	3	protein phosphatase 1, regulatory subunit 18 [Source:MGI Symbol;Acc:MGI:1923698]
uc008civ.2	Ppp1r18	3.973103299	-2.049034448	6.537231628	0.464968196	620	780	1785	3	protein phosphatase 1, regulatory subunit 18 [Source:MGI Symbol;Acc:MGI:1923698]
uc012ars.1	Ppp1r18	3.973103299	-2.049034448	6.537231628	0.464968196	75	676	1785	3	protein phosphatase 1, regulatory subunit 18 [Source:MGI Symbol;Acc:MGI:1923698]
uc007ufc.2	Spata13	4.463909237	-2.042803529	7.751119856	0.340420048	235	3498	3734	12	spermatogenesis associated 13 [Source:MGI Symbol;Acc:MGI:104838]
uc011zna.2	Spata13	4.463909237	-2.042803529	7.751119856	0.340420048	277	3505	3735	12	spermatogenesis associated 13 [Source:MGI Symbol;Acc:MGI:104838]
uc008fzb.1	Rps6kb2	3.071748638	-2.040759114	6.340666128	0.731494074	109	297	1458	15	ribosomal protein S6 kinase, polypeptide 2 [Source:MGI Symbol;Acc:MGI:1927343]
uc009rgv.1	Bfsp2	7.563377824	-2.036687846	10.75613547	0.676755153	194	217	1251	7	beaded filament structural protein 2, phakinin [Source:MGI Symbol;Acc:MGI:1333828]
uc008jtu.1	Baz2b	6.317756597	-2.033871905	6.683607983	0.588617347	350		2583	10	#N/A
uc008jtv.1	Baz2b	5.987638715	-2.032778542	7.259752997	0.637961627	392	120	1968	10	#N/A
uc009pdm.1	Rps25	7.352791959	-2.030074795	8.070547017	0.665289328	60	51	282	3	ribosomal protein S25 [Source:MGI Symbol;Acc:MGI:1922867]
uc007elo.1	Gje1	3.564466527	-2.028444456	10.24919318	0.313884135	66	796	618	3	gap junction protein, epsilon 1 [Source:MGI Symbol;Acc:MGI:1923993]
uc008rwn.2	Rps20	7.301350187	-2.025142444	5.379171129	0.716478694	179	3167	360	4	ribosomal protein S20 [Source:MGI Symbol;Acc:MGI:1914677]
uc007bhj.2	Crygb	10.88658527	-2.022461416	4.343484746	0.830895446	33	73	528	3	crystallin, gamma B [Source:MGI Symbol;Acc:MGI:88522]
uc009nuv.3	Vps9d1	3.744125681	-2.019197623	6.645860925	0.685008824	262	740	1950	15	VPS9 domain containing 1 [Source:MGI Symbol;Acc:MGI:1914143]
uc057awz.1	Rps15	7.367136328	-2.017845218	10.41000755	0.637961627	208	7	357	3	ribosomal protein S15 [Source:MGI Symbol;Acc:MGI:98117]
uc008ysv.2	Crybb1	10.47320603	-2.016993006	5.968660383	0.823637791	44	85	753	5	crystallin, beta B1 [Source:MGI Symbol;Acc:MGI:104992]
uc057buy.1	Crybb1	10.47320603	-2.016993006	5.968660383	0.823637791	117		710	5	crystallin, beta B1 [Source:MGI Symbol;Acc:MGI:104992]
uc057buz.1	Crybb1	10.47320603	-2.016993006	5.968660383	0.823637791	38	2	753	5	crystallin, beta B1 [Source:MGI Symbol;Acc:MGI:104992]
uc057bva.1	Crybb1	10.47320603	-2.016993006	5.968660383	0.823637791	33	85	753	5	#N/A
uc009nux.3	Vps9d1	3.477678273	-2.015392993	5.93849496	0.726767184				0	#N/A
uc009gvf.1	Ftl1	7.697509185	-2.006861688	3.592745504	0.722353639	20		483	5	ferritin light polypeptide 1 [Source:MGI Symbol;Acc:MGI:95589]
uc008bzs.2	Rps28	7.259522867	-2.002405772	9.025234024	0.665289328	90	82	210	3	#N/A
uc009tvy.2	Igbp1	2.837670168	-1.991031927	2.979887648	0.305869677				0	#N/A
uc007gea.2	Csnk1g2	5.262233403	-1.989506867	13.25229201	0.305869677	354	665	1329	10	casein kinase 1, gamma 2 [Source:MGI Symbol;Acc:MGI:1920014]
uc008upe.2	Pabpc4	4.681856672	-1.984019137	9.421069415	0.340420048	790	425	1896	13	#N/A
uc007rht.1	Adgrv1	5.68313209	-1.981689414	7.881457208	0.305869677	111	618	1851	9	adhesion G protein-coupled receptor V1 [Source:MGI Symbol;Acc:MGI:1274784]
uc007kil.3	Rpl23a	8.483667094	-1.98038215	5.758867655	0.722353639	41	48	471	5	#N/A
uc009ihl.2	Crebzf	5.129469788	-1.971167362	5.759965513	0.74977518	286	2013	1077	1	CREB/ATF bZIP transcription factor [Source:MGI Symbol;Acc:MGI:2675296]
uc008uic.1	Rps8	8.169302489	-1.970934705	7.031257365	0.685008824	182	51	627	6	ribosomal protein S8 [Source:MGI Symbol;Acc:MGI:98166]
uc008oiq.1	Rps21	5.199044592	-1.97047244	8.110142021	0.685746322	82	153	246	4	#N/A
uc008air.2	Tagap	4.569574799	-1.960673106	10.49531907	0.512008755	163	768	2145	9	T cell activation Rho GTPase activating protein [Source:MGI Symbol;Acc:MGI:3615484]
uc007geb.2	Csnk1g2	5.282416836	-1.956839995	13.69311464	0.305869677	316	261	1248	11	casein kinase 1, gamma 2 [Source:MGI Symbol;Acc:MGI:1920014]